UNIVERSITY OF CAPE TOWN
IYUNIVESITHI YASEKAPA • UNIVERSITEIT VAN KAAPSTAD

# THE STRATIGRAPHIC AND STRUCTURAL CONTROLS ON COPPER-GOLD MINERALIZATION AT CASSENHA HILL PROSPECT, WITHIN THE ARCHEAN TO PALEOPROTEROZOIC ANGOLAN SHIELD, CONGO CRATON, SOUTH WESTERN ANGOLA

by

**STELVIO VAZ SIDRE**

THESIS

Presented in fulfilment of the requirement of the degree of Master of Science

in

**ECONOMIC GEOLOGY**

in the

FACULTY OF SCIENCES

of the

UNIVERSITY OF CAPE TOWN

SOUTH AFRICA

**Supervisor: Prof. Chris Harris**

**Co-supervisor: Dr. Lynnette Greyling**

February 2020

# DECLARATION

By submitting this thesis, I declare that the entirety of the work contained therein is my own original work and that I am the sole author thereof (save to the extent explicitly stated otherwise). The reproduction and publication thereof by the University of Cape Town will not infringe any third-party rights and that I have not previously submitted it either in its entirety or in part at any university for obtaining a qualification.

Stelvio Sidre

Signed by candidate

Date

2020/02/06

Place

Cape Town, South Africa

# ABSTRACT

The Cassenha Hill copper-gold prospect is situated in the Catabola area, Huambo Province, southwestern Angola. Geologically, the prospect is part of the Angolan Central Eburnean Zone (CEZ) and consists of Paleoproterozoic metasedimentary rock sequences which have been intruded by Eburnean granitoids at ± 2.1 Ga. The prospect itself comprises an area of 180 $Km^2$ and has been intermittently explored since 2005 by Rift Valley Resources (RVR) and its associates. The Cassenha Hill prospect is characterized by the occurrence of partially altered and highly oxidized metasedimentary rocks (meta-mudstone, meta-siltstone, carbonate-rich rock, meta-sandstone, breccia, and quartzite), and altered isolated granitoids.

This study represents the first detailed study of the prospect and aims to shed light on the characteristics of the various rock types (i.e., host and barren rocks), their source/provenance, styles of alteration, and the origin and/or type of the fluid responsible for the mineralization. Techniques applied include borehole core logging, petrography, whole-rock geochemistry (XRF and ICP-MS), and stable isotope geochemistry on samples collected on the surface and from exploration boreholes drilled as part of RVR exploration program.

Overall, the petrographic and geochemical studies undertaken in the rocks of the Cassenha Hill prospect indicate the following: (1) The rocks are moderately to strongly fractured; (2) The rocks have experienced weak to moderate chemical weathering; (3) The rocks are compositionally immature and originated from felsic provenance; (4) The rocks are sulfur-poor, and lacking in sulfide minerals (5) The rocks are enriched in LREE and LILE elements and depleted in HREE and HFSE elements; (6) The mineralization is associated with chloritization alteration and predominantly occurs within and/or at the edges of quartz/chlorite-rich veins/fractures and is not restricted to any rock type.

Two ore stages could be identified, namely, hypogene ore (stage I) consisting of pyrite ± chalcopyrite ± other copper sulfides, and supergene ore (stage II) consisting of malachite ± azurite ± chrysocolla, which represents the prevalent mineralization at the prospect.

The $\delta^{18}O$ value of quartz veins range from +12.81 to +13.53‰, while the δD of chlorite minerals range from -51 to -45‰. Therefore, assuming fluid-rock interaction took place at ≈ 350°C, due to the presence of quartz, the fluid had $\delta^{18}O_{H20}$ values of about +8‰, which are typical of magmatic waters. On the other hand, at a temperature of ≈ 350°C, and with the difference between chlorite and water being -33.5‰, such fluids would have had $\delta D_{H20}$ values of about -20‰ ($\delta^{18}O_{H20}$= -4‰), which are typical of meteoric waters.

Although the various mineral phases have yielded different isotopic signatures, this study suggests that water is ultimately of meteoric origin but exchanged with hydrogen-poor magmatic rock, thus maintaining the meteoric signature.

The continuous influx of meteoric waters within the fracture system led to the development of copper oxides such as malachite, azurite and chrysocolla, which possibly originated from the in-situ oxidation of the hypogene sulfides. This signature, together with other field, petrographic and geochemical observations allows one to, tentatively, suggest that the Cassenha Hill prospect represents an extension of a polymetallic vein-type of porphyry Cu deposit that has been subjected to supergene processes at the weathering profile.

*KEYWORDS*: Cu mineralization, stable isotopes, supergene processes, polymetallic veins, chrysocolla, malachite.

# ABBREVIATIONS:

RVR: Rift Valley Resources

Qtz: Quartz

bt: Biotite

chl: Chlorite

gt: Goethite

py: Pyrite

Kfds: K- feldspar

mc: Microcline

tlc: Talc

dol: Dolomite

calc: Calcite

ser: Sericite

ms: Muscovite

hm: Hematite

lm: Limonite

FeO: Iron oxides/hydroxides

opq: Opaque

ep: Epidote

FeOx: Iron oxides/hydroxides

IOCG: Iron Oxide Copper Gold

# ACKNOWLEDGEMENTS

I would like to thank my project supervisor, Prof. Chris Harris, for his wisdom and guidance throughout the course of this research project, and for cheering me up at the setbacks of the project. I would also like to thank Dr. Lynnette Greyling for opening the doors and giving the opportunity of pursuing the Masters Degree at UCT Geological Sciences Department. Special thanks go to CIMERA and Rift Valley Resources (RVR) for their financial support (scholarship, analytical costs, conference costs, etc).

I am also deeply indebted to all technical staff of the Department of Geological Sciences (at UCT – Miss Sherissa roopnarain, Mrs Rene Van der Merwe, and Mr. Jonathan Van Rooyen) for providing technical support in anything technical-related to this project. Special thanks and huge debt of gratitude goes to Mr. Greg Cunnold and Mr. Dave Hammond for giving us access to all resources related to the Cassenha Hill prospect which made this study possible.

Special thanks to my parents, family members, friends, and everyone that believed in me, for their continuous support and guidance. I would also like to express my gratitude to Mr. Benedito Madaleno, a geologist from RVR, for his companionship and elucidation of the Cassenha Hill geology during the fieldwork and meaningful discussions.

## V. TABLE OF CONTENTS

**LIST OF FIGURES**

**LIST OF TABLES**

# 1. CHAPTER I

# INTRODUCTION

## 1.1. Introduction

Angola is known for its huge economic potential in terms of natural resources. To date, the country's economy is governed by the production of hydrocarbons and diamond mining. The country itself is considered to be the 2nd largest producer of crude oil in Africa (Pariona, 2017) and the 4th largest producer of rough diamonds in the world (Pariona, 2017). Furthermore, as these two commodities represent over than 90% of the country's export, much attention in terms of mineral exploration has been given to the exploration of additional resources of such commodities for future exploitation, leaving the remaining mineral commodities such as base and precious metals with relatively little attention. However, despite the little attention/consideration given to the exploration of precious and base metals, more specifically, to copper and gold, it is believed that the country has the geological potential to host world class-type of deposits of such mineral occurrences.

Geologically, Angola is part of the southern segment of the Congo Craton, and is termed as Angolan Shield (Begg et al., 2009). The Angolan Shield (Figs., 1 and 2) is a magmatic arc terrane that occurs above an older Archean crust (Carvalho et al., 2000). The Shield extends from the Atlantic Ocean to the eastern part of Angola at 18° E, and is bordered by the Democratic Republic of Congo and by the Republic of Namibia to the north and south, respectively. The Angolan Shield consists of a Paleoproterozoic crust at the base, which is dominated by granitoids of varying composition, and Supracrustal rocks at the top (McCourt et al., 2013).

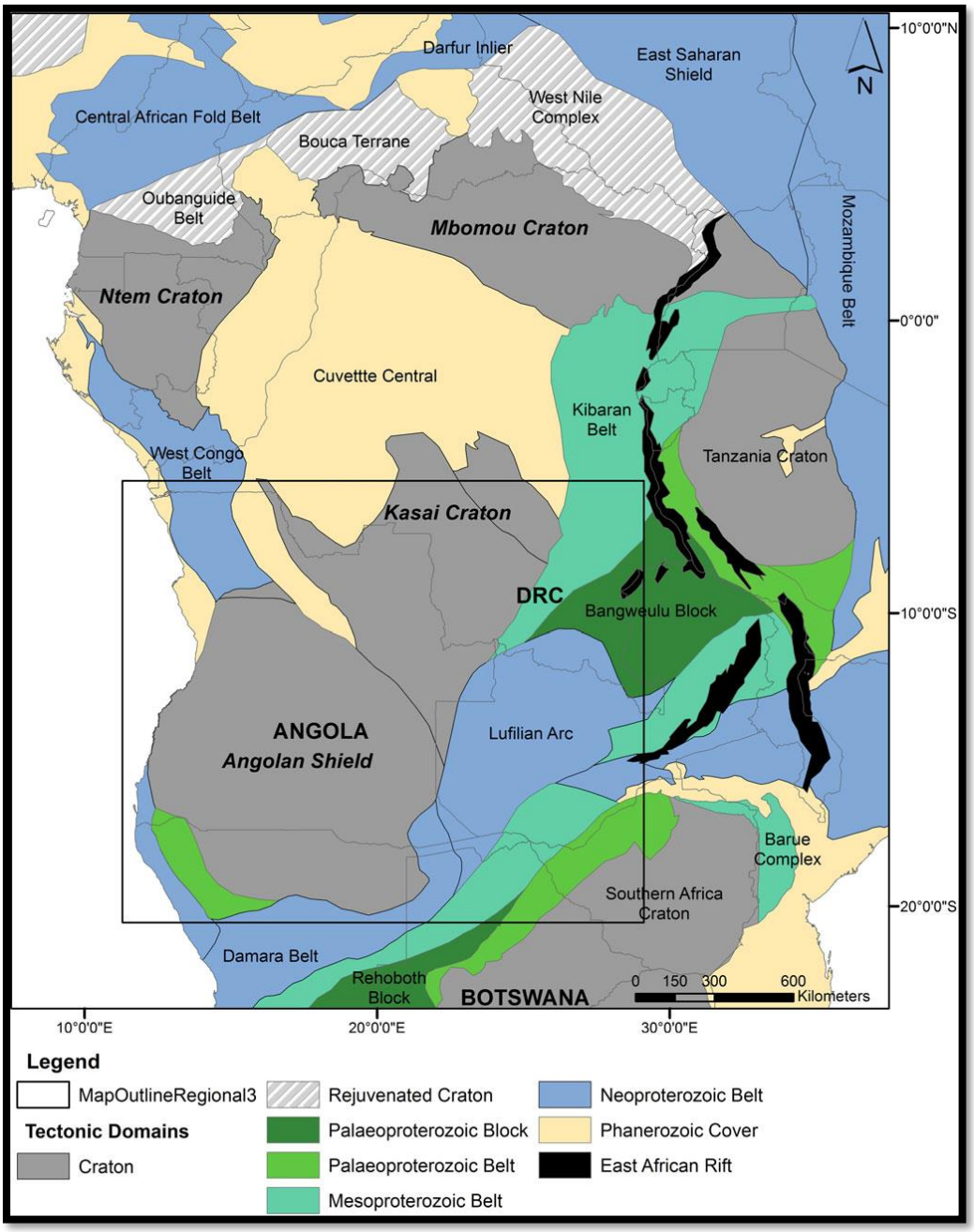


**Figure 1**: Tectonic framework of southern Africa showing the location of the Angolan Shield, Kasai Craton (south) and Angolan Shield (southwest), Ntem (Chaillu-Gabon) Craton (northwest) and Mbomou (north east of DRC) Craton (northeast) (after Jelsma et al., 2018).

The Angolan Shield has been affected by two major metamorphic events, namely, the Lunda-Cuango-Malanje event at approximately 2.9 Ga and the Malanje-Andulo event between 2.68 and 2.5 Ga (Carvalho et al., 2000). These events are argued to be contemporaneous with the Musefu charnockitisation and the Moyo episode occurring in the Republic of Congo (Carvalho et al., 2000). The Angolan Shield was then affected by three major tectonic events/cycles, namely, the Eburnean orogeny (2.2 – 1.8 Ga), the Kibaran orogeny (1.4 – 1.0 Ga), and the Pan African orogenic event (900 – 500 Ma) (Carvalho et al., 2000). The Eburnean orogenic event, which is characterized by the reworking of the cryptic Archean terrane, granitoid intrusions (Eburnean/Regional granite) and migmatization, was more pervasive and important as it affected most of the rocks of the Shield (Carvalho, 1984; Carvalho et al., 2000). Following the Eburnean orogeny, there was a period of partial stabilization of the Shield prior to the Kibaran orogenic event (Carvalho et al., 2000). The latter event affected the southernmost part of the western Angolan Shield and is characterized by the intrusion of the Kunene Basic complex and the Red granitoids (Allsopp, 1975; Carvalho et al., 2000). Although the Kibaran granitoids are predominant in the southern part of Angola, they can also be observed as orthogneissic occurrences in the northern part towards the border between Angola and the Democratic Republic of Congo (Carvalho et al., 2000). The Pan African orogenic event, where rifting processes and passive margin deposits were developed, affected the northwestern part of the Angolan Shield (Carvalho et al., 2000). This event is characterized by the occurrence of metasediments, which lie unconformably on the Eburnean metasediments. Moreover, this tectonic event was responsible for the intrusion of mafic and granitic rocks, which are alkaline and/or peralkaline in composition, causing considerable fenitization in the southwest of Angola (Carvalho et al., 2000).

Based on its tectonic characteristics the Angolan Shield can be subdivided further into four broad tectonic zones, namely: The Central Shield Zone, Cassinga Zone, the Central Eburnean zone (study area) and the Lubango zone (Fig. 2) (Carvalho et al., 2000). These zones occur in the eastern and western part of the Angolan Shield, respectively (Carvalho et al., 2000; Jelsma et al., 2011). The south/central western part of Angola consists of the Central Eburnean Zone. The latter is characterized by the occurrence of an Archean gneissic-migmatitic complex at the base overlain by the Quipungo-Kuanza Supergroup (Carvalho et al., 2000). The rock sequences of the southern part of the CEZ were later intruded by the Eburnean granitoids at approximately 2.1 Ga, whereas, the northern rock sequences were intruded by the Quibala granite at approximately 1.9 Ga (Carvalho et al., 2000).

The south/central western part of Angola has been one of the most prolific regions in the country in terms of mineral occurrences. The region hosts the Cassinga and Kissala-kitungo iron-ore deposit, in the Jamba region (the largest iron-ore deposit in Angola), the Mpopo gold deposit, the Chipindo prospect, the Longonjo REE prospect, the Bongo gold prospect, the Cassenha Hill prospect (study area) and many others.

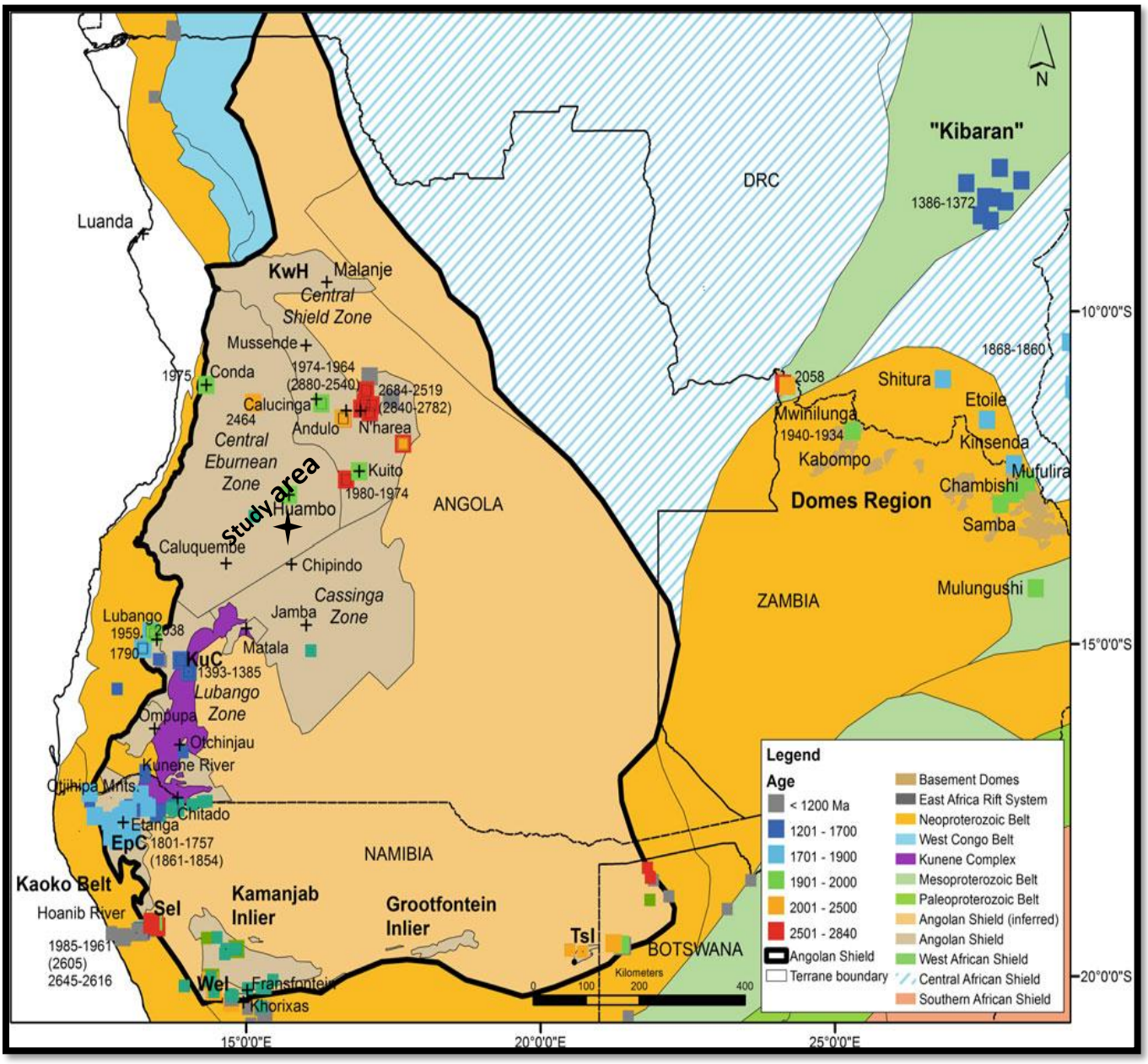


**Figure 2**: Tectonic zones of the Angolan Shield (modified after Carvalho et al., 2000; Jelsma et al., 2018).

## 1.2. Location of the study area

The Cassenha Hill copper-gold prospect (Fig. 4), in the south/central western part of Angola, is situated in the Catabola area approximately 60 km south from the Longonjo municipality and 90 km west from the Huambo province. The Cassenha Hill prospect is part of the Ozango exploration license which covers an area of 3670 km$^2$. The Ozango exploration license is owned by Ozango Minerais S.A, a wholly owned subsidiary of Rift valley Resources Ltd, and includes the Cassenha Hill prospect, the Bongo gold prospect, and the Longonjo REE resource. On its own the Cassenha Hill prospect comprises an area of approximately 180 km$^2$. The prospect site can be easily accessed by road and it takes approximately two and half hours from Huambo. The route from Huambo to Longonjo is paved, and there is approximately 60 km of gravel road from the Longonjo Municipality to the prospect site.

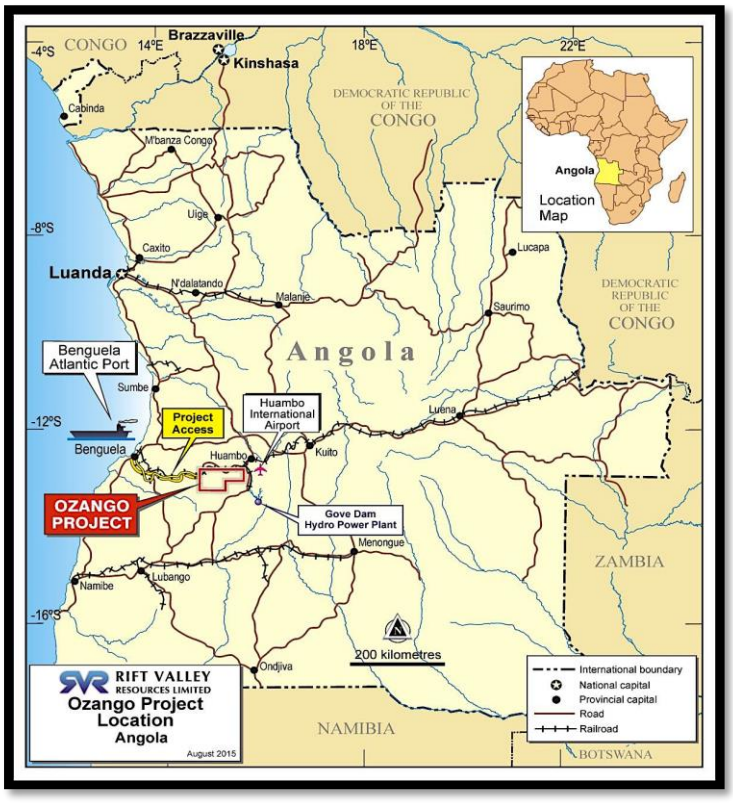


**Figure 3**: Ozango Project location map (Adapted from Rift Valley Resources).

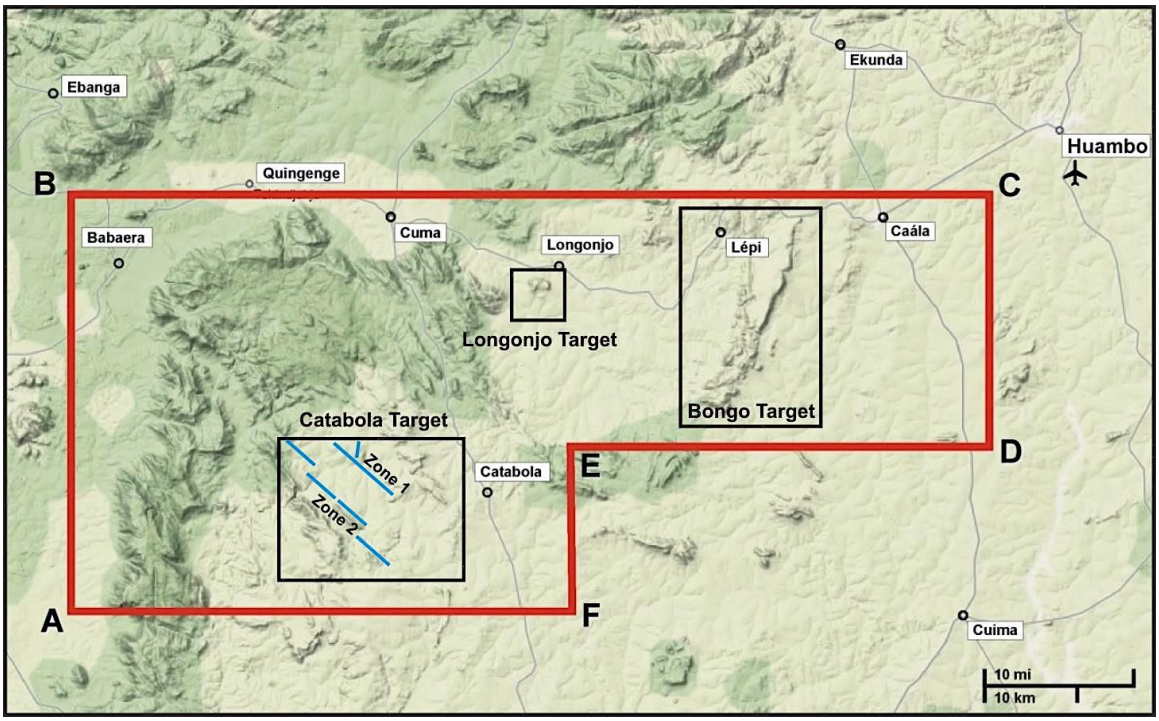


**Figure 4**: Location map of the Cassenha Hill (Catabola) prospect (Adapted from Rift Valley Resources).

The Cassenha Hill prospect (Fig. 5) consists of a low-grade metamorphic terrain surrounded by granitoids. These granitoids, which vary from granites to granodiorites and diorite, occur either as isolated plutons or intrusions into the Paleoproterozoic metasediments (Jordana, 1950). The Cassenha Hill prospect has been subdivided into two zones, namely, Zone 1 (study area) and Zone 2. Zone 1 consists of granitoids of granitic composition towards the N, SW, S and E borders of the prospect. These granitoids are, in most cases, altered and consist of secondary minerals such as epidote, zoisite, kaolinite, and limonite (Jordana, 1950). In addition to this, the granites have fractures filled with iron-rich minerals such as hematite, magnetite, and biotite (Jordana, 1950).

The metasedimentary rocks consist, from the base to the top, of sandstone/quartzite, greywackes and slate/clay, iron-rich quartzite, quartzite, and fine/coarse-grained sandstone (Jordana, 1950). Structurally, the area is characterized by the occurrence of

NNW-SSE, NW-SE, and W-E trending structures (Aurum Exploration Services, 2007). The structures consist of the following: joints, simple faults, open faults, fault gouges, mylonite zones, breccia zones, and tectonic clay (Aurum Exploration Services, 2007).

Based on its mineralization and structural characteristics the prospect has been classified as a shear-zone hosted, vein type, Cu-Au prospect, consisting of copper/gold-rich parallel quartz veins which seem to be bounded by magnetite/barite veins, within an Early-Proterozoic to Archean metasedimentary granodiorite complex (Aurum Exploration Services, 2007).

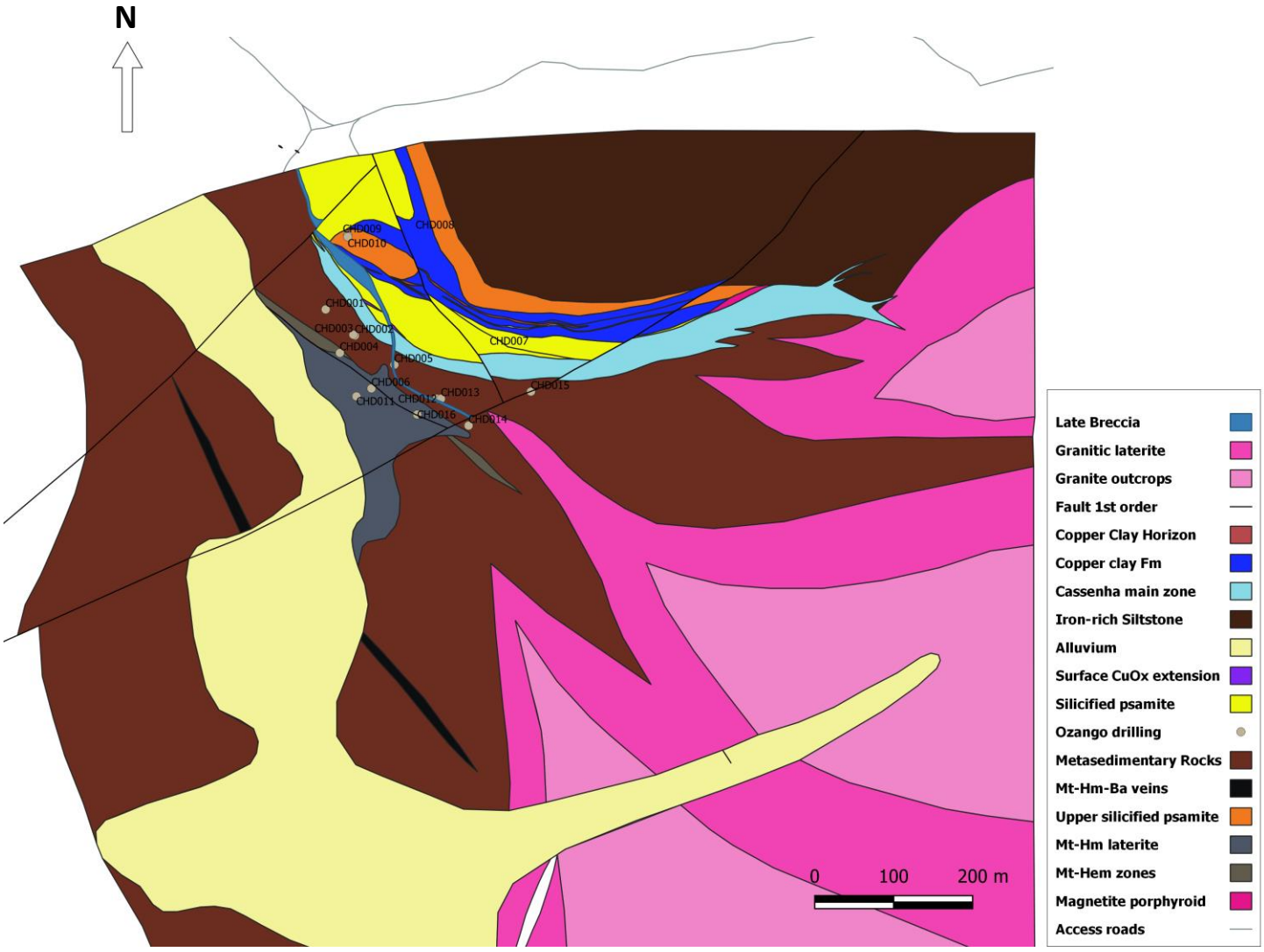


**Figure 5**: Geological map of the Cassenha Hill prospect (modified after Karel Maly (2017).

## 1.3. Exploration history of the Cassenha Hill prospect

The first documented exploration work at Cassenha Hill prospect, then referred as Caquete section, was compiled by Jordana (1950). The exploration work took place between the years of 1947 and 1950. The primary objective was to map the area and to do a ground validation on the prospective occurrence of gold mineralization as suggested by Hall (1947), a geologist employed by the Geology and Mining Services at that time. The exploration work by Jordana (1950) involved geological mapping, trenching, adit excavation and mapping, petrographic and geochemical investigation. From his exploration work, Jordana (1950) identified two closely spaced zones of distinctive mineralization and structural characteristics. He then subdivided the Cassenha Hill prospect into two zones (Fig. 4). Zone 1, in the eastern part, consisting of copper salts, which eventually led to the formation of chrysocolla, malachite, uranium salts, manganese oxides, and gold, while Zone 2, in the western part, consisting mostly of manganese and iron oxides with small amounts of pyrite and chalcopyrite (Jordana, 1950).

The exploration work did not reach the hydrostatic level/oxidation zone, it reached a total depth of 20 and 12 meters in Zone 1 and Zone 2, respectively. The work focused on the characterization of the gold, copper, and uranium occurrences and the significance of the fractures in their occurrence (Jordana, 1950). After inspecting the area, Jordana (1950) suggested that the fractures were not of deep tectonic origin, but instead the result of dynamic effects that took place at the late stage of magma cooling. He also suggested that the area comprises of a fault-seam that crosscuts the parallel vein system in Zone 1. Furthermore, as the hanging wall consisted of sedimentary rock and the footwall of granitic rock, he suggested that the area has been subjected to contact metamorphism.

From his investigations, he made the assumption that the mineralization was originated by hydrothermal fluid, which is derived from the lower granitic rocks. However, the absence of fault gouges, mirrors, visible transition of a metamorphic quartzite to hornsfels, made him realize that the difference in permeability of the rocks also played an important role. Therefore, he suggested that the area might contain minerals, which are of hydrothermal origin and others that are exclusively magmatic. In order to properly explain the genesis of the mineralization in the prospect, Jordana (1950), proposed genetic models for each of the occurrences, namely, copper, uranium, and gold.

In his genetic model for copper mineralization, Jordana (1950) proposed that pyrite and chalcopyrite were either of hydrothermal origin or were present in the magma at late stages of cooling. After having been exposed to the oxidizing zone, these sulfides were partially or completed oxidized into iron hydroxide (i.e. hematite which is insoluble), and copper sulfides. Under further oxidation, copper sulfides were transformed into copper oxides and remained in carbonate-rich solution. Some of the copper sulfides reacted in solution to produce cuprite, and other copper carbonates. Due to secondary alteration processes at shallower depth, copper carbonate produced chrysocolla.

According to Jordana (1950), this model is valid for the eastern part of the prospect (Zone 1), where copper silicate and carbonate in the form of chrysocolla and malachite are the predominant mineralization. In the western part (Zone 2), copper salts are less predominant, whereas, sulfides (i.e., pyrite and chalcopyrite) are more predominant. Therefore, he assumed that the oxidation process was lesse active in Zone 2 than Zone 1.

Based on geochemical results from rocks/soils sampled, Jordana (1950) concluded that the Cassenha Hill prospect comprised a total reserve of 221.2 Kg of gold, 419.4 Kg of silver, and 2.5% of copper. These results were based on rough resource calculations and only considered the oxidized zone. Based on these results, Jordana (1950) then concluded that the Cassenha Hill prospect/deposit was not economically viable for exploitation. He

recommended the expansion exploration area in order to be considered economically viable. From 1950 to 2004, no exploration work was documented and/or undertaken in the area.

In July 2005, Glenvale Associates Ltd (a joint venture between Petro-African Energy and CityView Corporation) was responsible for the first modern exploration work undertaken in the Cassenha Hill prospect. The exploration work consisted of three (3) different phases which took place in July 2005 (Phase 1), between November- December 2006 (Phase 2), and lastly between April – May 2007 (Phase 3).

Phase 1 involved ground validation and sample collection, where, a potential iron-oxide copper-gold deposit was recognized.

Phase 2 was a follow-up work based on the results obtained from the first phase of exploration. A total of 730 rock and soil samples were collected and geological mapping was conducted on selected areas. From this Phase, the following was established: 1) possible source of mineralization; 2) main structural features of the area; 3) the host rocks; and 4) the copper occurrence as the main mineralization in the area, followed by gold, silver, and uranium.

Phase 3 involved the collection of a further 367 samples (i.e. 170 channel samples, 77 stream sediment samples, and 120 soil samples). The exploration work focused on the precise definition of mineralization and local geology. From this Phase, the following was achieved: 1. Updated geological map; 2. Preliminary 3D model of mineralization; and 3. The definition of the type of deposit. There was a proposition and need for 3000 meters drilling campaign in order to properly understand the geology and verify the findings on the samples collected, but due to financial constraints, it was never executed.

At that stage, based on exploration work undertaken in the oxidized zone, the Cassenha Hill prospect was then defined as a "shear-zone hosted vein type Cu-Au prospect consisting of a series of copper/gold quartz veins apparently bounded by magnetite/barite veins, within a lower Proterozoic-Archean metasedimentary/granodiorite complex" (Aurum Exploration Services, 2007).

In 2015, Rift Valley Resources (RVR) took over from Glenvale Asssociates, and recommenced the exploration work at the Cassenha Hill prospect. The main target remained copper and gold occurrences. Following up the work from Glenvale Associates, Rift Valley Resources started the first drilling campaign at the Cassenha Hill prospect in 2015. The drilling campaign was carried out during three distinctive phases. Phase 1 took place from November to December 2015, phase 2 took place from January to February 2016, and Phase 3 took place from July to December 2017. A total of 1193.85 meters were drilled among sixteen (16) exploration boreholes. The boreholes intersected various mineralized zones, obtaining copper values ranging from 0.23% -1.71 % and gold values ranging from 0.48 – 3.11 g/t. In addition to diamond core drilling, other exploration techniques were employed since 2015. These include the following: Airborne magnetics geophysics, trench sampling, underground workings, stream sediment survey, and geological mapping.

## 1.4. Aims and Objectives

The occurrence of copper-gold mineralization at Cassenha Hill, Catabola area, and the subsequent uncertainty regarding the style of mineralization and geological characteristics of the prospect, represent an interesting object of scientific study and of further exploration activity. Therefore, this thesis aims to characterize and refine the understanding on the genesis and classification of the prospect by integrating diamond core logging, petrography, bedrock geochemistry, stable isotope geochemistry, and develop a meaningful compilation of these studies as a possible porphyry Cu or Supergene-enriched type of deposit.

The specific aims are the following:

- Characterize the prospect by identifying the origin of its mineralization, as well as the types and characteristics of the host and barren rocks.

- Determine the style and spatio-temporal distribution of alteration and mineralization at the prospect.

- Understand the genesis, and propose a genetic model for the prospect.

# 2. CHAPTER II

# GEOLOGY OF THE PROSPECT

## 2.1. Regional Geological Setting

The Cassenha Hill Prospect is situated in the Southwestern Angola in the vicinity of the settlement called Catabola. The area is often referred as Caquete section or Cassenha, and forms part of the Central Eburnean Zone. The Central Eburnean Zone (CEZ) is characterized by the occurrence of an Archean gneissic-migmatitic complex at the base, overlain by the Quipungo-Kuanza Supergroup, which were intruded by Eburnean granitoids, also referred to as regional granites, and by the later Quibala granite, in the southcentral/western and northern part of the CEZ, respectively (Carvalho et al., 2000; Da Silva 2005).

The Quipungo-Kuanza Supergroup, previously known as Chivanda-Negola-Utende-Cela Supergroup, consists of two groups, namely, the Chivanda-N'gola and the Quibala Groups (Korpershoek, 1984; Da Silva, 2005). Torquato and Oliveira (1977) have suggested that the Chivanda-N'gola Group, which is located in the southwestern part of the CEZ, has a continuation towards the eastern section, in the region of Chipindo, thus termed those rock sequences as Chipindo Group. However, Bassot et al. (1981) and more recently, Carvalho et al. (2000) and Da Silva (2005), defined the Chipindo Group as part of the Chivanda-N'gola Group.

### 2.1.2 Chivanda-N'gola Group

The Chivanda-N'gola Group is characterized by the occurrence of metamorphosed rock sequences with variable lithologies (Carvalho et al., 2000; Da Silva, 2005). The Chivanda-N'gola, as mentioned above, outcrops in the southern section of the CEZ (study area), and

consists, from the base to the top, of the following formations: the Cuengue, the Camenha, and the Bambi formations.

*Cuengue Formation*

The lithological sequence of the Cuengue Formation is not well constrained due to the limited occurrence of well exposed outcrops (Oliveira, 1981). The formation consists predominantly of relatively compact metagreywackes, reddish silts and pelites exhibiting schistosity and/or cross-stratification/bedding on millimeter to centimeter scale, and sericitized metavolcanics (Oliveira, 1981). According to Oliveira (1981), some of the pelites and silts have tuff-like characteristics and occur at the top of the unit as small-deformed ellipsoids of fine-grained material often referred to as lapilli. The contact between the Cuengue Formation and the eburnean granitoids is evidenced by the occurrence of the metamorphosed rock sequence of the Cuengue Formation, which grades from metagreywackes to quartzofeldspathic hornfels, schist, pelitic rocks, to mottled schist consisting of chlorite + sericite + quartz (Oliveira, 1981). In addition to this, dykes of mafic composition, metamorphosed to greenschist facies, can also be observed in the area, where the ophitic texture is still preponderant.

*Camenha Formation*

The Camenha formation consists of volcano-detritic sediments, with a northeast-southwest orientation, that tend to be lithologically distinct/variable. The formation is further subdivided into three Members, namely, the lower, middle, and the upper Members (Oliveira, 1981).

*Lower Member*

The Lower Member is characterized, from the base to the top, by the occurrence of banded iron-rich reddish/pinkish sitlstones, silicified rocks with greyish-greenish colour, often referred to as volcano-detritic sediments, black schist, whitish arenites with variable granularity exhibiting cross-bedding, ripples, and herringbone type of sedimentary structure, as well as a grade bedding structure with conglomerate sequences at the base (Oliveira, 1981). The iron-rich base is partly brecciated, which according to Oliveira (1981), suggest that these characteristics are typical of shallow marine sedimentary environment.

*Middle Member*

The Middle Member is characterized by the occurrence of a less variable lithology. According to Oliveira (1981) a continuous section could not be observed, however, it consists of well-rounded conglomerates at the base of varying sizes, followed by cross-bedded and/or rippled arenites and siltstones in an iron-oxide rich matrix. The base of the conglomerate sequence is partially eroded, the coloration of the arenites and siltstones is highly variable. They tend to be more fine-grained and lighter colored towards the east and greyish to dark colored towards the west.

*Upper Member*

The Upper Member consists of alternating bands consisting of arenite and siltstone of varying compositions grading into volcanic-detritic sediments (Oliveira, 1981). These variations, according to Oliveira (1981), are possibly due to folding and/or lateral variations in the facies. The bands have an average thickness of 65 meters. The arenites are generally light-coloured, mica- and iron-rich, with interleaving cross-bedded and/or rippled siltstones. On the other hand, the siltstones are generally whitish-pinkish grading into red pelites with cross bedding on a millimeter scale.

*Bambi Formation*

The Bambi Formation is better observed towards the north of the Bambi village and locally observed in the depression of Cassongue River (Oliveira, 1981). The formation is subdivided into two Members, namely, the black schist and volcanics, and the mafic rocks and pillow lavas.

*Black schist and volcanic rocks*

This member consists predominantly of manganese- and carbonate-rich black schist, with fine stratifications, laterally grading into laminated volcano-detritic sediments and fine-grained silica-rich rocks (Oliveira, 1981). In addition to this, reddish jasperite with pyrite, black chert, and opaque minerals can also be observed.

*Mafic rocks and pillow lavas*

This member is characterized by the occurrence of medium-grained dark-greyish coloured rocks displaying NW-SE trending structures (Oliveira, 1981). Petrographically, these rocks consist of variable mineralogical composition, however, it is mainly composed of green amphiboles, sericitized plagioclase, chlorite, quartz, prehnite, and iron oxides (Oliveira, 1981). According to Oliveira (1981) most of the amphiboles, chlorite and, prehnite minerals are of neoformation, which indicates that the rocks have been affected by greenschist facies grade of metamorphism.

### 2.1.3. Eburnean granitoids (regional granite)

The Eburnean granite intruded the rocks of the Chivanda-N'gola Group at approximately 2.1 Ga (Carvalho et al., 2000). This syn-tectonic granite was originated by anatexis processes during the peak period of the Eburnean orogeny (Torquato et al., 1979). These processes led to the granitization and migmatisation of the previously described rock sequences, as well as, the formation of the granitoid rocks of the southcentral/western Angola (Torquato et al., 1979). In general, the regional granite is characterized by being homogeneous, leucocratic, equigranular, medium-grained, porphyritic at some areas, consisting predominantly of quartz, oligoclase, microcline, biotite, and muscovite. However, at some areas it tends to exhibit a darker colouration as a result of its considerable high biotite and andalusite content (Oliveira, 1981). The contact between the granite and metasediments is characterized by the occurrence of enclaves, microgranitic dykes, quartzo-dioritic porphyries.

### 2.1.4. Quibala Group

The Quibala Group is exposed in the northern section of the CEZ, and forms part of the Cela-Cariango fold belt (Silva and Kawashita, 1978; Da Silva, 2005). Similarly, to the Chivanda-N'gola Group, it consists of metamorphosed rock sequences. The rock sequences are folded, and rest unconformably on the older Archean basement (Silva et al., 1972). The Quibala Group consists, from the base to the top, of the following Formations: Utende, Cariango, and Quissongo Formations.

*Utende Formation*

The Utende Formation consists of metapelites, metagreywackes, and metaconglomerates (Silva and Fernandes, 1978). The rocks of this Formation are generally fine-grained and have dark colouration. The rocks have been subjected to

intense recrystallization and migmatization, resulting in the poor preservation of sedimentary structures (Silva and Fernandes, 1978). In general, the rocks are composed of quartz, feldspars, muscovite, sericite, and clay and opaque minerals (Silva and Fernandes, 1978).

*Cariango Formation*

The Cariango Formation consists of quartzites, metarenites, metagreywackes, and phyllites (Silva and Fernandes, 1978). The rocks of this formation have fine to medium grain-sizes, and tend to be whitish and/or reddish in colour. The reddish colouration is due to the iron oxides present in the rocks (Silva and Fernandes, 1978). Although recrystallization and migmatization processes affected these rocks, their bedding structure is relatively better preserved when compared to the Utende Formation (Silva and Fernandes, 1978). Overall, the rocks are composed of sericite, muscovite, and biotite (Silva and Fernandes, 1978).

*Quissongo Formation*

The Quissongo Formation is characterized by the occurrence of itabirites. Microscopically, the rock is composed of alternating bands, of opaque minerals, predominantly consisting of hematite, and bands consisting of quartz, amphiboles, and apatite (Silva and Fernandes, 1978). These bands are generally folded and the overall texture resembles gneisses (Silva and Fernandes, 1978).

*Serra do Bango Formation*

The Serra do Bango Formation consists of metaconglomerates, quartzites, and metarenites (Silva and Fernandes, 1978). These rocks are commonly red. The minerals of quartz, muscovite, sericite, apatite and some opaque minerals occur as cement in the conglomerates. The transition from metaconglomerates to metarenites, to quartzite, is

gradual, and is characterized by the increase of lamination in the texture (Silva and Fernandes, 1978).

*Serra da Banga Formation*

The Serra da Banga Formation consists of porphyry and/or quartzo-feldsphatic granitoids, metamorphosed dacites, rhyolites, and metagreywackes (Silva and Fernandes, 1978). These granitoids intruded the rocks of the older Utende Formation. Microscopically, the granitoids are composed of orthoclase, microcline, perthite, quartz, biotite muscovite, sericite, and opaque minerals (Silva and Fernandes, 1978). Although the volcanic imprint can be observed in the metamorphic sequences, their matrix is partially recrystallized (Silva and Fernandes, 1978).

### 2.1.5. Quibala Granite

The Quibala granite intruded the metamorphic sequences of the Quibala Group at approximately 1.9 Ga (Carvalho et al., 2000). It is exposed in the Quibala region itself, as well as, in regions of Lubango and Quipungo (Andrade, 1954). The Quibala granite is characterized by being a coarse-grained calc-alkaline porphyritic granitoid, which its occurrence is commonly spatially related to the older Eburnean granitoid. According to Da Silva (2005), the Quibala Granite is a metasomatic type of granite, which has been subjected to long periods of genetic evolution culminating in periods of intense potassic alteration at the time of its rehomogenization between 1800 and 1700 Ma. On the other hand, Silva and Fernandes (1978) suggested that the Quibala granite is originated from the remobilization of the Eburnean granitoids (regional granite). Petrographically, the Quibala granite is composed of K-feldspars, quartz, oligoclase, biotite, titanite, opaque minerals, sericite, epidote, and apatite (Silva and Fernandes, 1978). It is highly fractured, and according to Silva and Fernandes (1978), the presence of epidote indicates that the Quibala granite has been subjected to compressive tectonic forces.

### 2.1.6. Structure

The Quipungo-Kwanza Supergroup has been affected by three main phases of deformations (Oliveira, 1981). From these events, the deformation event 1 and 2 ($D_1$ and $D_2$), are responsible for the development of folding structures, and the deformation event 3 ($D_3$), is responsible for the development of several faults and fractures overprinting the pre-existing folding system.

*Folding ($D_1$ and $D_2$)*

The area is characterized by the occurrence of anticlinal and synclinal folding structures dipping towards the west. The rocks of the Camenha formation are a representation of a possible 180$^o$ rotation structure. Oliveira (1981) suggested that the Camenha formation should be interpreted as a large anticlinorium, at which the southern part is compressed and laminated. Towards the southern region, a synclinal structure can be observed which has been affected by a reverse fault. Furthermore, the folding structures seem to not be accompanied by pervasive schistosity, however, they are present and generally displaying an E-W orientation.

According to Oliveira (1981), the $D_1$ structures originated as a result from a period of eperiogenic movements followed by subduction, thus allowing the deposition of black schists as well as the development of a submarine volcanism. Thereafter, the $D_2$ deformation event, which is interpreted as the main folding event, overprinted the pre-existing structures, developing metric folding structures with cleavage and axial plane oriented towards the northern quadrant at deeper levels. At shallower levels, the cleavage is less pervasive and quartz –filled diaclases/fractures are more predominant.

*Faults ($D_3$)*

The $D_3$ deformation phase is characterized by the development of shallow penetrating normal and reverse faults as well as fractures (Oliveira, 1981). Field evidences suggest that the entire Chivanda-N'gola Group has been affected by this phase of deformation. As general characteristics, the fracture zones are normally brecciated, the host rock is surrounded by quartz veins, which, in most cases, occur as filling bodies within the fractures. These fractures tend to display a WNW-ESE orientation, and a less predominant N-S orientation. In addition to this, the general orientation of the mafic dykes, which are mostly metamorphosed to greenschist facies, tend to have similar orientation to that of the main fault/fracture system (Oliveira, 1981).

## 2.2. Geology of the Cassenha Hill prospect

The Cassenha hill prospect (Figs. 4 and 5) can be subdivided into two zones, namely, Zone 1 (study area) and Zone 2.

*Zone 1*

Zone 1 is characterized by the occurrence of granitoids and metasedimentary rocks. The granitoids border the prospect along the N, SW, S, and E boundaries, and have intruded the metasedimentary rocks in some areas (Jordana, 1950). The granitoid intrusions have been classified as granites, which are generally, dark, grey, or pink, with a porphyritic texture, and the metasedimentary sequence consists of rocks grading from sandstones/quartzites to slates/claystones. Moreover, in general, these granites tend to be altered, forming secondary minerals such as epidote, zoisite, kaolinite, and limonite (Jordana, 1950). Ferromagnesian minerals such as biotite, magnetite and hematite, are also predominant in the granite.

Towards the southeastern boundary, iron-oxide-rich granitic occurrences can be observed with small pyrite inclusions. Similarly, to the other granitic rocks, these occurrences tend to be altered resulting in the formation of epidote and kaolinite (Jordana, 1950). In fact, this seems to be characteristic at the boundaries of the prospect.

The metasedimentary sequence, consists, from the base to the top, of the following series:

| | |
|---|---|
| Lower Series: | Conglomerate |
| | Sandstone/quatzite and feldspar |
| | Greywackes and slate/claystone |
| Upper Series: | Highly ferruginous quartzite |
| | Quartzite |
| | Fine-coarse-grained sandstone |

The silica-rich sandstones and quartzites form the base of the sedimentation at Cassenha prospect. The sandstones are generally fine-grained, silica-cemented, with colour varying from greyish to pinkish, composed of quartz nodes, fragments of biotite, epidote, and relatively low feldspar content. However, at some locations, these sandstones tend to be highly ferruginous, thus containing high amount of mica minerals, magnetite and/or hematite.

The clay material occurs as well compacted rock and has been defined as argillite. The argillite is characterized by having a light red to brick red coloration, which is dependent on the iron content. Moreover, this argillite, which has a slate-like composition and texture, exhibits foliations parallel to the stratification.

According to Jordana (1950), brecciated conglomerates can be observed near the feldspar sandstone consisting of angular fragments of siliceous sandstone, quartz, and limonite, joined by clay cement. It has then been classified as silico-ferruginous breccia.

*Zone 2*

This area is located towards the south from the Tahiaio River, and is characterized by the occurrence of granitoid islands similar to those found in Zone 1. The occurrence of silica-rich rocks is restricted to the southernmost part of the zone, and consists of sandstone-conglomerate association, which is overlain by highly ferruginous argillite.

### 2.2.1. Structure

Structurally, the area is characterized by the occurrence of NNW-SSE, NW-SE, and W-E trending structures. According to Aurum Exploration Services (2007), these structures are related to the regional shear zone orientation, which trends NW-SE. Two main tectonic zones can be observed in the area, namely, the main vein zone, and the roxi vein zone, which trend NW-SE and W-E, respectively. The structures include the following: joints, simple faults, open faults, fault gouges, mylonite zones, breccia zones, and tectonic clay. Overall, according to Aurum Exploration Services (2007), many of the tectonic structures exhibit characteristics that indicate periods of reactivations, contemporaneous or later than the crystallization of hydrothermal minerals. These reactivations led to the generation/development of brecciated and mylonitized quartz veins with saccharoidal textures.

### 2.2.2. Mineralization

The Cassenha Hill prospect has been classified as a shear-zone hosted vein-type Cu-Au prospect consisting of a series of copper/gold quartz veins apparently bounded by magnetite/barite veins, within an Early Proterozoic-Archean metasedimentary/granodiorite complex (Aurum Exploration Services, 2007).

The two zones of the Cassenha hill prospect (Fig. 4) are characterized by having distinct mineralization. The mineralization in Zone 1 (study area) is characterized by the occurrence of a variety of copper salts leading to the formation of chrysocolla, malachite, and the occurrence of gold, manganese oxides, and uranium salts. On the other hand, in Zone 2, the mineralization consists of manganese, iron oxides, and relatively small amount of sulfides such as pyrite and chalcopyrite. The two zones are also distinctive in terms of their gangue minerals, with Zone 1 being characterized by the occurrence of quartz ore together with calcite in the gold-bearing parts, and by the absence of barite, while, zone 2 the quartz occurs as gangue together with considerable amount of iron salts. Although the two zones seem to be interlinked both spatially and geologically, this study will only focus on the features of the zone 1.

The mineralization in zone 1 (Fig. 4) is characterized by the occurrence of three vein bodies known as the Cassenha hill shear structure (Fig. 5), with an average thickness of 25 meters and extending to over 330 meters, which are relatively parallel to each other, and filled with fragmented quartz material. These mineralized veins display an overall NW-SE trend, which is believed to be in response to the NNW-SSE regional tectonic movement (Jordana, 1950).

# 3. CHAPTER III

## ANALYTICAL METHODS

### 3.1. Types of data collected

The initial step of this research involved core logging, examination, and sampling of exploration boreholes at the Cassenha Hill prospect, Catabola area, in Huambo Province. Core logging was undertaken in January 2018 for a period of 2 weeks. A total of eight (8) exploration boreholes were logged, from of which three (3) were used to collect core samples at the prospect site. The three exploration boreholes used for sampling are CHD008, CHD009, and CHD013. The sample selection was based on lithology, texture, alterations and the presence of ores. Core logging was based on (1) changes in grain size, (2) fabrics or textures, (3) colour, (4) lithological variation (5) alteration, and (6) mineralization. Each core sample collected was stored in a well-marked sample bag to prevent possible contamination from the surrounding lithologies. The samples were sent to the University of Cape Town, from which twenty (20) polished thin sections were prepared for petrographic study, and thirteen (13) were selected and prepared for X-Ray fluorescence spectrometry (XRF), and carbon, hydrogen and oxygen isotope analyses.

### 3.2. Petrography

A total of twenty (20) polished thin sections slides were prepared from core samples collected from boreholes CHD008, CHD009 and CHD013, and examined using a binocular microscope with transmitted and reflected light at the University of Cape Town. The standards of the microscope used as well as the physical working conditions are described in Raith et al. (2012). The mineral abundances were estimated based on their field of view occurrence on the thin-sections, and by using the approximate predominance of each mineral grain/crystal in volume percentage (vol. %).

### 3.3. X-Ray fluorescence spectrometry (XRF)

The major- and trace-elements concentrations were determined on bulk rock samples using XRF analysis.

For the major elements, the sample preparation and analysis were based on the methodology devised by Willis and Duncan (2008). Samples were crushed and milled according to the geochemical sample preparation standard. Approximately 2 grams of powered samples were taken, dried at 110$^{o}$C and ashed overnight at 950$^{o}$C in order to determine the loss on ignition (LOI) and allow for all the Fe to be oxidized to $Fe^{3+.}$ After completion, the ashed samples were mixed with LiT-LiM flux (on a 57:43 ratio), where LiBr was used as a releasing agent, and fused in a claisse gas burner to make fusion disks. The data was calibrated by employing the same methods on natural standards from the USGS and SARM, while the matrix was corrected using the fundamental parameter method as suggested by Rosseau et al. (1996); Willis and Duncan (2008).

The major element concentrations were measured from the fusion disks using the Panalytical Axios wavelength-dispersive x-ray fluorescence (XRF) spectrometer with a sample-changer (56 sample capacity) and rhodium end-window X-ray tube. The intensity data was processed with SuperQ software. The XRF instrument detection limits were calculated based on the sample matrix and the specific analytical conditions used for the analysis. The detection limits were between 0.003 wt. % and 0.016 wt. %. The analytical uncertainties for the major elements were in the order of 1-2 %.

For the trace elements, the samples were analyzed as powder briquettes. A flux bound of approximately 6 grams of whole-rock powder, which was supported in a boric acid base and prepared using a ten-ton hydraulic cold press. The trace element concentrations were also measured with the same equipment used for the major elements, and the data were refined using SuperQ software. The lower limits of detection for the trace elements were

between 1 ppm and 5 ppm for all the trace elements, except for S (10 ppm) and F (40 ppm).

## 3.4. Oxygen Isotope analysis

### *3.4.1. Bulk Rock*

A total of thirteen (13) samples were analyzed for oxygen isotopes at the Stable Isotope Laboratory at the University of Cape Town. Data were obtained on whole-rock samples by using the conventional methods devised by Harris and Erlank (1992), where approximately 10 mg of each sample was made to react with $ClF_3$ at 550$^{o}$C for 3 hours to release the oxygen gas from the silicate samples. The released $O_2$ was later converted to $CO_2$ using a hot platinized carbon rod which was stored in break seal tubes. Duplicate splits of quartz standard MQ were run to monitor the analytical precision and convert the raw data to the SMOW scale using the $\delta^{18}O$ value of 10.1‰ for MQ. The MQ gave a 2d error of 0.16‰.

A Finnigan Mat Delta XP mass spectrometer in dual inlet mode measured the oxygen ratios in the samples. All data were reported in the standard δ-notation relative to Standard Mean Ocean Water (SMOW): $\delta = ((R_{sample}/R_{standard}) - 1) \times 1000$, with R is the measured ratio; i.e. $^{18}O/^{16}O$.

### *3.4.2. Quartz veins*

Three (3) quartz vein-rich samples were analyzed for oxygen isotopes by using the laser fluorination method, devised by Sharp (1991) and Harris and Vogeli (2010), at the stable isotope laboratory at the University of Cape Town. The material was disaggregated using the jaw crusher, and approximately 1 to 3 mg of quartz grains were selected by using tweezers and analyzed for oxygen isotopes. The samples and standards were loaded into

a highly polished pure Ni sample holder. The Ni sample holder was then placed in an oven at 110$^{o}$C for not less than an hour, and posteriorly the samples were moved to the reaction chamber. After pumping for more than 2 hours, approximately 10 kPa of $BrF_5$ was expanded into the reaction chamber for 30 s and then removed cryogenically. Following additional pumping for approx. 30 min, a second load of 10 kPa $BrF_5$ was expanded into the reaction chamber and remained inside the chamber overnight before oxygen extraction from the samples was attempted. Each sample was reacted in the presence of approximately 10 kPa $BrF_5$. On finalization of reaction, the surplus $BrF_5$, and the free Br formed by dissociation, were frozen into a cold finger, and the remaining gases were permitted to pass through a KCl trap maintained at approximately 200$^{o}$C, so that any $F_2$ produced could be removed. The gasses were subsequently expanded into a stainless-steel double-U trap submerged in liquid nitrogen and the purified $O_2$ was collected onto 5 Å molecular sieve contained in glass storage bottles. Prior to the attempt of sample extraction, a blank was run and the amount of gas measured. The blank pressure was in the orders of < 1/200 of the sample volume of a 1 mg sample. Following the extraction, the samples were then analyzed off-line.

### *3.4.3. Carbonates*

The carbonates were analyzed for oxygen isotopes by using the method devised by McCrea (1950), which involves the extraction of $CO_2$ from carbonates by reacting them with 100% phosphoric acid. The sample was reacted at approximately 50$^{o}$C and a fractionation factor of 1.009 for $CO_2$-calcite was used to correct the raw data. In general, the carbonate sample contain both dolomite and calcite, and the $\delta^{18}O$ value obtained represents a mixture derived from both calcite and dolomite. However, the use of a wrong fractionation factor has a minimal implication in the data. The total carbonate content was estimated by comparing the pressure of gas produced for weighed aliquots of the sample and standards during the extraction of $CO_2$.

## 3.5. Hydrogen Isotopes analysis

The hydrogen isotopes were determined by using the method devised by Vennemann and O'Neil (1993) and Harris and Ashwal (2002). Isotopic ratios were measured by Finnigan MAT DeltaXP mass spectrometer in dual-inlet mode at the University of Cape Town. NBS28 standard was used for silicates, NM for carbonates, and CTMP for the hydrogen. The average values obtained for NBS28, NM, and CTMP were used to normalize the raw data in each run to the SMOW or PDB scale.

# 4. CHAPTER IV

# PETROGRAPHY

## 4.1. Introduction

Petrography was conducted on 20 sections prepared from core samples collected from boreholes CHD008, CHD009 and CHD013 to identify and/or classify the rocks which were subjected to metamorphism and hydrothermal alteration, and provide the foundation for sample selection for geochemical studies.

This study included the identification of rock-forming minerals, ores, textures, crystal shape and habit, alteration, fabric and micro-scale deformation, as well as the determination of the modal abundance. The mineral abundances were visually estimated based on their areal proportions in the thin-sections.

Overall, the lithologies present in the boreholes may be classified into two groups. These are: Igneous (Granites) and meta-sedimentary (i.e., variably altered and metamorphosed sandstone, siltstone, carbonate-rich rock, mudstone and breccia) rocks. The following paragraphs provide the detailed petrographic description of the rock types from the two groups.

### *4.2. Granite*

The thin sections cut from granite, which occurs as isolated granitoid plutons in the study area, show that the rocks are composed of K-feldspars (microcline/perthite) (20 – 35 vol. %), quartz (15 – 25 vol. %), plagioclase (10 – 12 vol. %), chlorite (5 – 10 vol. %), biotite (3 – 5 vol. %), hematite/limonite (3 – 5 vol. %), orthoclase (2 – 5% vol. %) and opaque minerals (1 – 2 vol. %). Epidote, muscovite and zircon occur in minor amounts. In general, these granites are medium-grained, with grain sizes varying from 1 to 5 mm, with an equigranular to seriate/hiatal relative grain size, anhedral to subhedral crystal shapes, thus having fabric varying from hypidiomorphic to allotriomorphic granular, non-foliated, moderately to highly fractured, characterized by the intergrowth and overgrowth of quartz and K-feldspar minerals. The grain boundaries are generally infiltrated by iron oxides, possibly hematite and/or limonite.

Microcline/perthite are subhedral to anhedral and exhibit tartan twinning/multiple twinning with grain sizes ranging from 2 to 4 mm. Furthermore, numerous quartz grains, biotite, and muscovite inclusions can be observed on the face of the crystals, as well as, iron oxide filled fractures cross-cutting the face. Among the inclusions, quartz seems to be more predominant and the crystals have well-developed irregular and elongated shapes. Plagioclase crystals are mostly exsolved from original alkali feldspar (Fig. 6) and occur either as interstitial crystals at boundaries between quartz and microcline/perthite crystals or as interstitial crystals interlocked between quartz grains, or as inclusions in quartz. Plagioclase is albitized to some extent. The crystals have subhedral to anhedral shapes and also have inclusions which consist of quartz and muscovite.

Quartz crystals have grain size that ranges from 1 to 3 mm. They are mostly hexagonal with euhedral to subhedral crystal shapes, have low relief and are moderately to highly fractured. In addition to the presence of crosscutting iron oxide-filled fractures, various

mineral inclusions, predominantly consisting of K-feldspars, plagioclase, muscovite, apatite, and chlorite/biotite, can be observed in some crystals. Hematite/limonite occur either in the form of filled-veins/fractures crosscutting the mineral grains or as cement at grain boundaries. They are dark brown in color and have bladed crystal shape.

Chlorites have anhedral crystal shapes, which do not follow any specific pattern of occurrence. They typically occur as replacements of biotite. Overall, chlorites are medium- to coarse-grained and their grain sizes range from 1 to 3.5 mm. Although they are randomly distributed throughout the rock, they mostly occur at the boundaries/edges of quartz and K-feldspar crystals or also as inclusions in other minerals in the rock. Furthermore, numerous inclusions and/or growth of muscovite, biotite, and opaque minerals, can be observed in the face of some crystals. Biotite crystals typically occur either as inclusions in other mineral grains (predominantly in quartz grains), or as replacing product during chloritization. The crystals grains tend to exhibit a subhedral to anhedral/tabular crystal shape.

Three types of alteration were observed in the rocks, namely, sericitization, chloritization, and albitization.

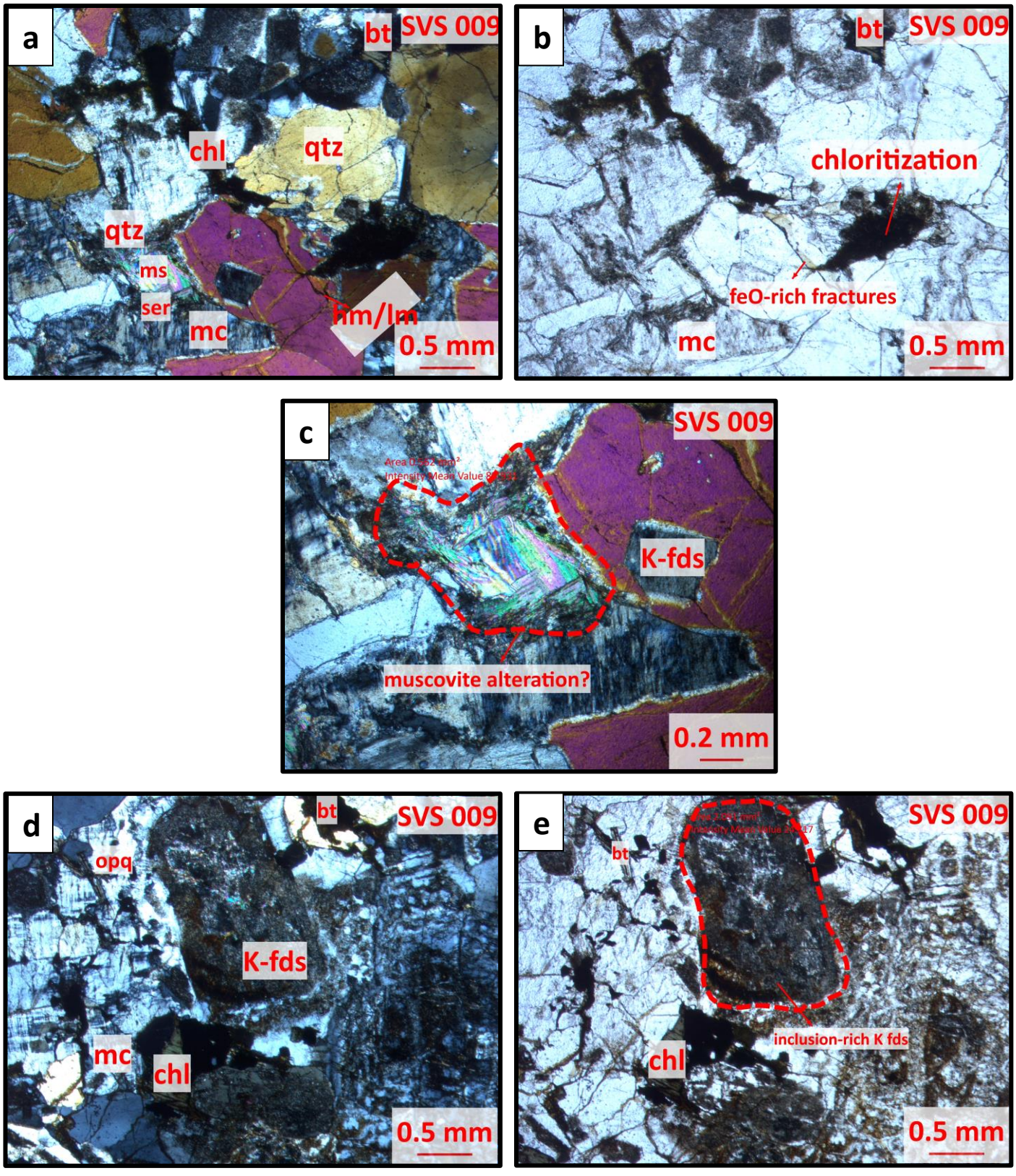
a
bt
SVS 009
chl
qtz
qtz
ms
ser
mc
hm/lm
0.5 mm
b
bt
SVS 009
chloritization
feO-rich fractures
mc
0.5 mm
c
SVS 009
K-fds
muscovite alteration?
0.2 mm
d
bt
SVS 009
opq
K-fds
mc
chl
0.5 mm
e
SVS 009
bt
inclusion-rich K fds
chl
0.5 mm

**Figure 6:** Photomicrographs of the granitic rock occurring at Cassenha Hill prospect. Note intergrowth relationship between crystals and the absence of primary plagioclase in thin section **(a). (b)** Denotes the replacement of biotite by chlorite (chloritization). Note the iron-rich fractures occurring throughout the rock. **(c)** Denotes the replacement of K-feldspars by fine mica. **(d)** and **(e)** Shows the inclusion rich K-feldspar. The inclusion minerals include: muscovite, biotite, quartz, and Fe-Oxides. Two alteration minerals can be observed in the photos (b) and (c): (1) biotite to chlorite and (2) K-feldspar to sericite.

### 4.3. Meta-sedimentary rocks

There are five (5) meta-sedimentary rocks types identified in the three boreholes of interest. These rocks, which are meta-sandstone, meta-siltstone, carbonate-rich rock, meta-mudstone and breccias, are variably metamorphosed and altered. Based on the degree of alteration and deformation, the rocks were termed as least to highly altered and fractured to non-fractured, respectively.

***Meta-sandstone***

Microscopically, various types of meta-sandstone were identified. They vary from weakly to highly hydrothermally altered and from weakly to strongly deformed/fractured (Figs. 7, 8a, and 8d). Overall, the meta-sandstones in the study area are composed, in order of decreasing abundance, of quartz (45 – 65 vol.%), chlorite (15 - 25 vol.%), calcite (10 - 15 vol.%), muscovite (10 - 12 vol.%), epidote (5 - 10 vol.%), and accessory minerals. In general, these rocks consist of relatively well-developed, sub-angular to sub-rounded quartz grains, cemented together by calcite and/or chlorite, the rock is medium- to coarse-grained, consisting of two clearly distinct quartz grain sizes, one being fine and the other considerably coarser. The quartz crystals have sub-angular to sub-rounded crystal shapes, have numerous inclusions and/or overgrowth of opaque minerals, muscovite,

and/or calcite, are weakly to moderately fractured, and have an intergrown relationship with calcite and muscovite. The chlorite and calcite minerals also occur as cement.

Three (3) types alteration can be observed, which consist of: chloritization, chlorite-sericite, and carbonate alteration behaviors.

The undeformed/ non-fractured fresh sandstones (Figs. 8c and 8d) are characterized by the occurrence of relatively well-developed, sub-angular to sub-rounded quartz grains, cemented together by calcite and/or chlorite. The quartz grains have varying grain sizes, which range from fine- to medium-/coarse grained, are characterized by being corroded, with radiating growth of calcite at the edges. The rock is neither foliated nor lineated, absent of any micro-scale deformation, and quartz clots are predominant. The two types of cement occur interchangeably throughout the rock and do not follow a specific pattern. The muscovite crystals occur at the calcite cement, lamellar crystal shape and have sizes less than 1mm.

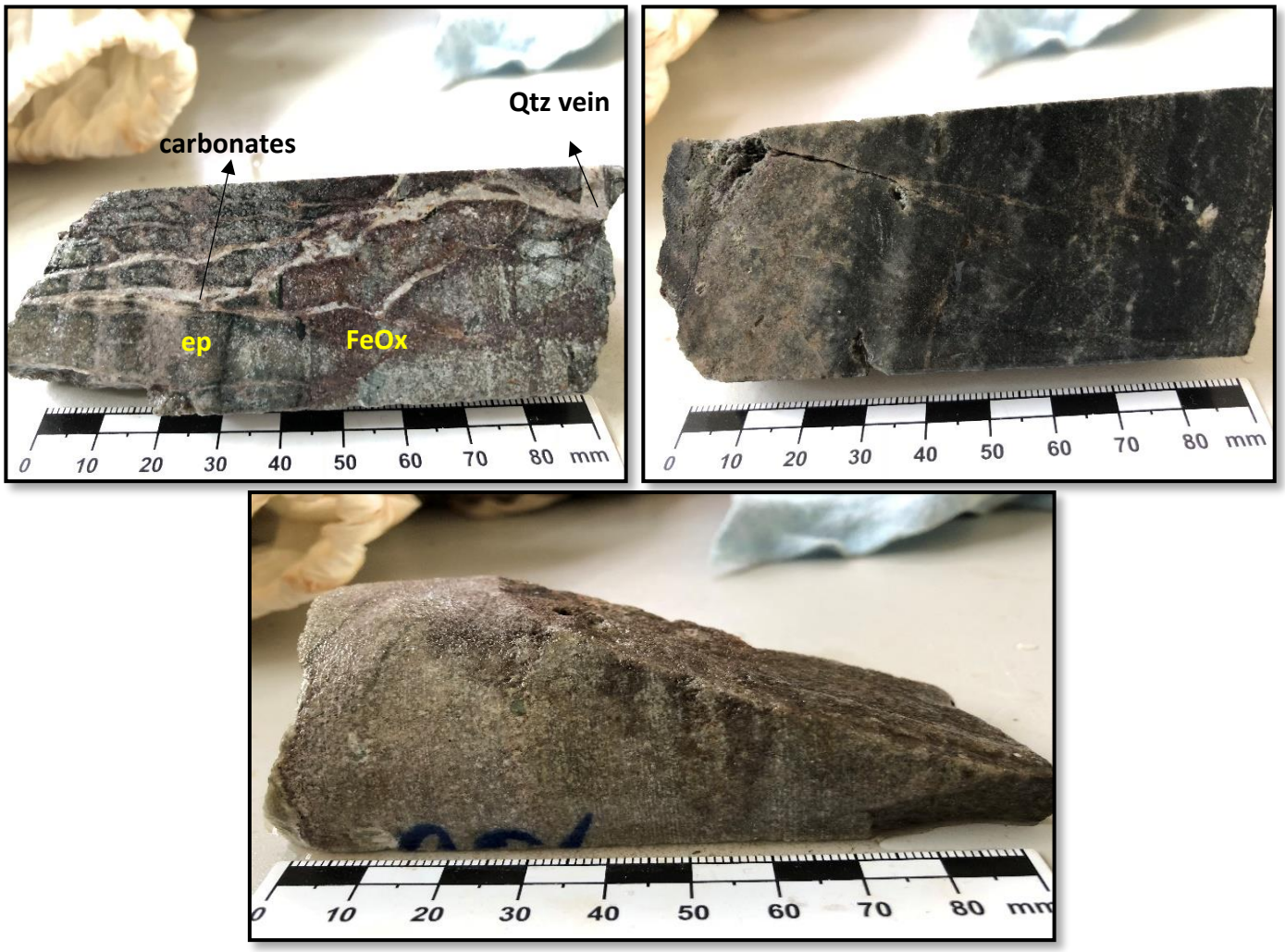


**Figure 7:** Photographs of core showing the various types of meta-sandstone occurring at the Cassenha Hill prospect. (a) Denotes the highly altered and vein-rich meta- sandstone. (b) Denotes the partly altered and moderately fractured meta- sandstone. (c) Denotes the fresh and relatively undeformed sandstone.

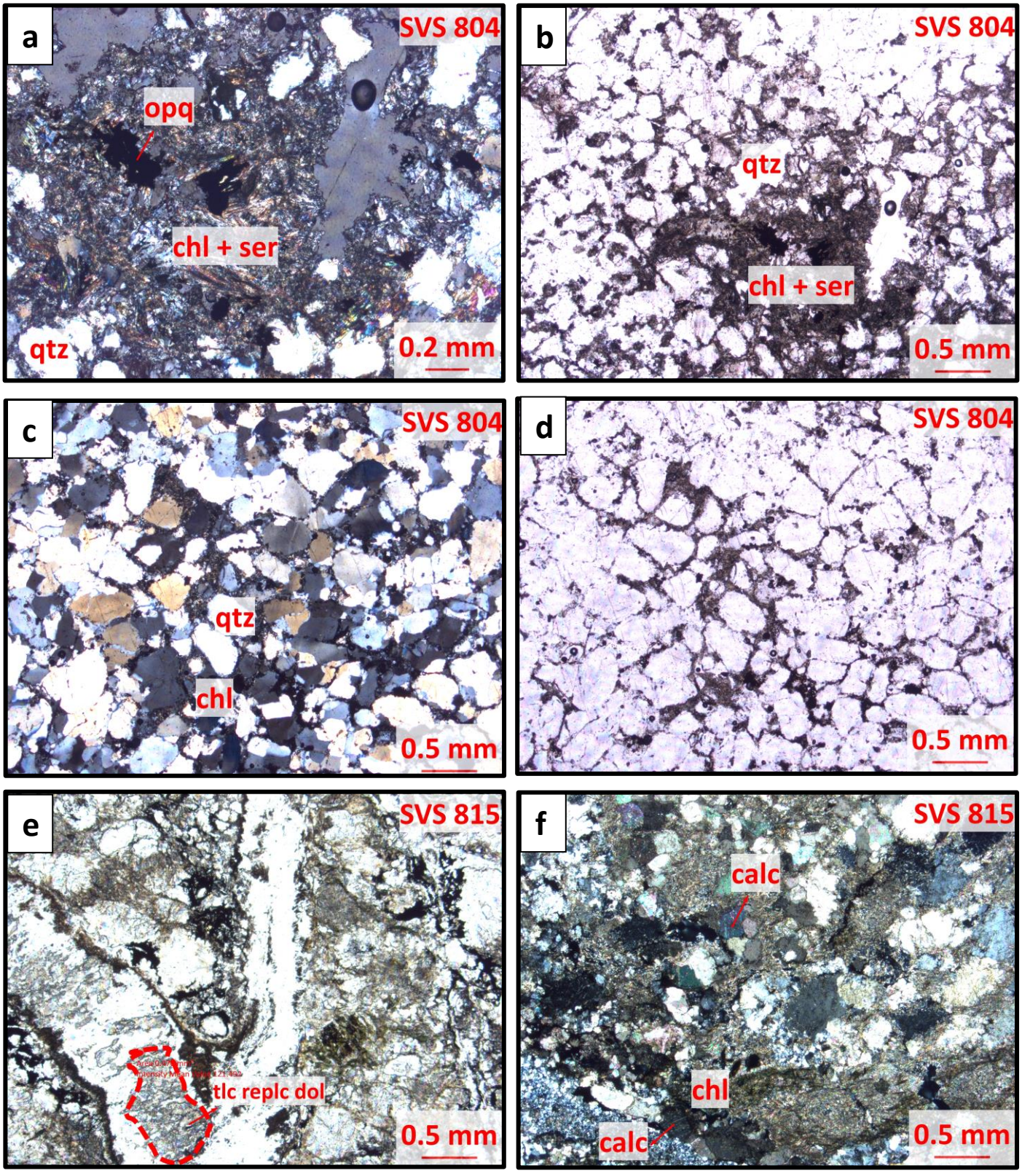
a
SVS 804
opq
chl + ser
qtz
0.2 mm
b
SVS 804
qtz
chl + ser
0.5 mm
c
SVS 804
qtz
chl
0.5 mm
d
SVS 804
0.5 mm
e
SVS 815
tlc replc dol
0.5 mm
f
SVS 815
calc
chl
calc
0.5 mm

**Figure 8:** Photomicrographs of the various types of sandstone occurring at Cassenha Hill prospect. **(a)** and **(b)** denote the weakly to moderately fractured meta-sandstone in XPL and PL, respectively. Note the consumption of feldspars by chlorite-sericite alteration. **(c)** and **(d)** denote the fresh sandstone in XPL and PL, respectively. Note the occurrence of preferred oriented fractures on the quartz grains in thin section (c) and (d). **(e)** and **(f)** denote the strongly fractured and vein-rich sandstones. Note the replacement of dolomite by talc within the quartz + carbonates-rich veins in thin section (e).

***Meta-siltstone***

The meta-siltstone rocks occurring in the study area are composed, in order of decreasing abundance, of quartz (40 - 60 vol.%), fine-grained matrix (calcite?) (10 - 20 vol.%), chlorite (10 - 15 vol.%), muscovite (3 - 8 vol.%), opaque minerals (2 - 3 vol.%), and accessory minerals. In general, this rock is fine-grained, moderately altered and weakly fractured. Two horizontally and/or obliquely oriented distinct bands (Fig. 10c and 10d) can be observed in some of the samples, of which, one is composed of micaceous minerals with inclusions of chlorite, muscovite, and opaque minerals, and the other one is composed predominantly of quartz together with interstitial chlorite crystals. Moreover, the crystals exhibit a specific pattern of occurrence from the edge of one band to the edge of another, which consists of, chlorite-rich, quartz-rich, chlorite-rich, and quartz-rich bands. The opaque minerals, which are possibly iron oxides, occur throughout the rock, however, they predominantly occur as crystals aligned preferably at the edges or at the center of the micaceous banding. Epidote and actinolite occur in minor amounts.

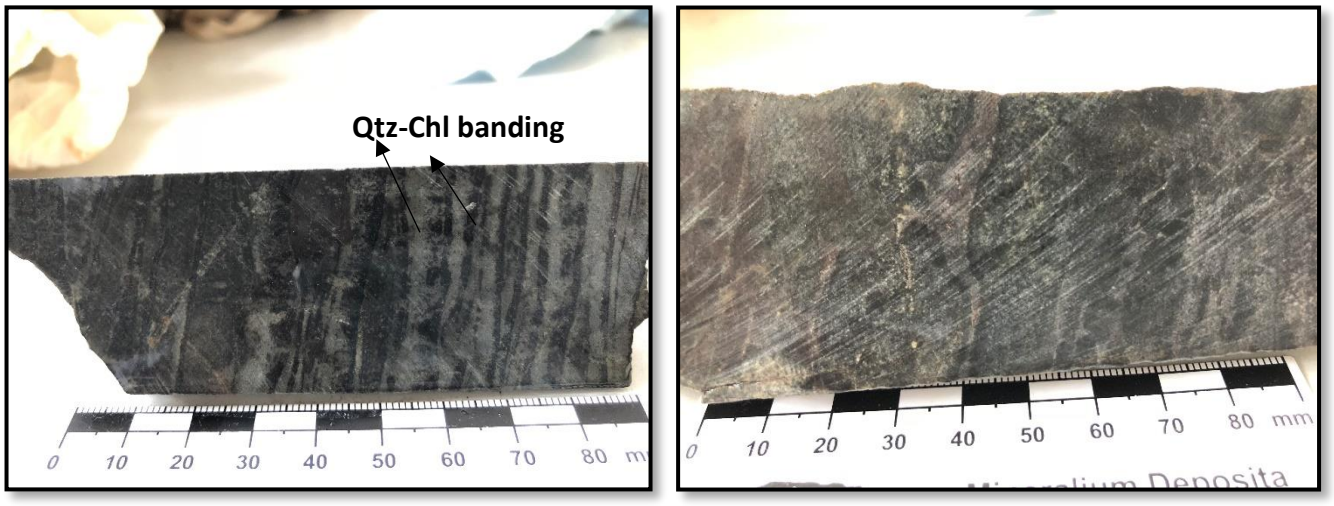


**Figure 9:** Photographs of the core showing the meta-siltstone rocks occurring at Cassenha Hill prospect. See the photomicrographs below for more detail.

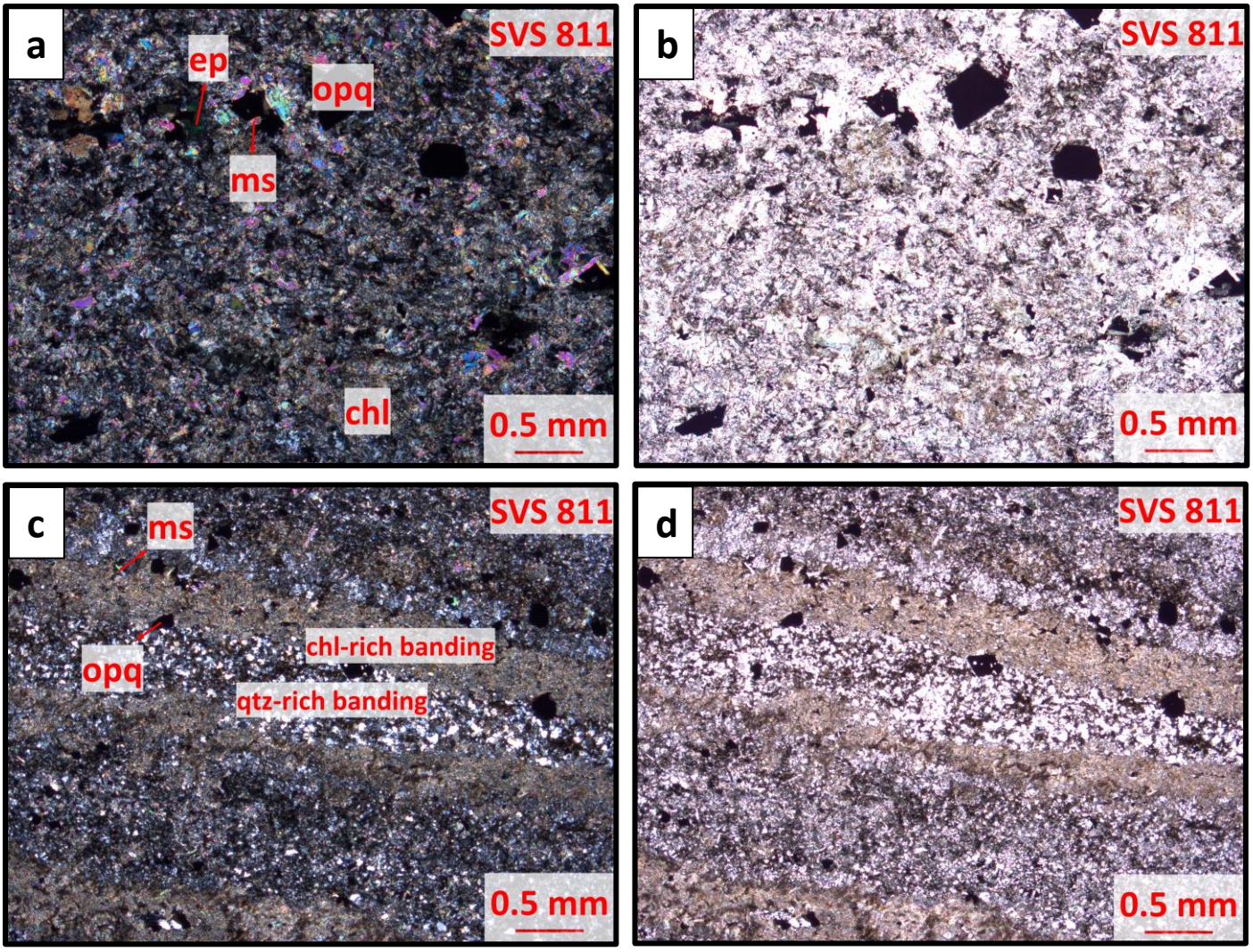


**Figure 10:** Photomicrographs of the various types of meta- siltstones occurring at Cassenha Hill prospect. **(a)** and **(b)** denote the undeformed/non-fractured meta- siltstone in XPL and PL, respectively. **(c)** and **(d)** denote the quartz-chlorite banded meta- siltstone in XPL and PL, respectively. Note the low-temperature metamorphism in thin section (a) and (b).

***Meta-mudstone***

Thin sections cut from the meta-mudstone rock show that they are composed, commonly, in order of decreasing abundance, of quartz (20 – 40 vol.%), chlorite (15 - 25 vol.%), unidentified mineral (10 – 15 vol.%), goethite (3 – 10 vol.%), magnetite (3 – 5 vol.%), muscovite (1 – 3 vol.%), and accessory minerals. The quartz crystals have sub-angular to sub-rounded crystal shapes, are inclusion-free when not associated with the veining, and inclusion-rich when associated with the veining. The inclusion minerals include: muscovite, chlorite, and iron oxides. Chlorite crystals occur throughout the rock, in some crystal faces a non-preferred oriented cleavage can be observed. Chlorites are associated with every feature in the rock. Which includes, the quartz veins, fractures, and goethite minerals. Goethite occurs as a replacement of earlier sulfides (i.e., pyrite), exhibits a dark brown coloration, which seems to be overprinting a yellowish earlier colored mineral, and tend to occur within and/or at edge of chlorite-quartz-rich veins. In general, the rock is characterized by being fine-grained, highly fractured, and moderately to highly altered. The fractures do not follow a specific pattern/orientation and displacements can be observed (Fig. 12c). These fractures are chlorite-rich, and often associated with opaque minerals and iron oxides. Furthermore, various quartz-rich veins can be observed, they generally occur as standalone features or associated with chlorite-rich veins. Chloritization and/or propylitic is the predominant type of alteration.

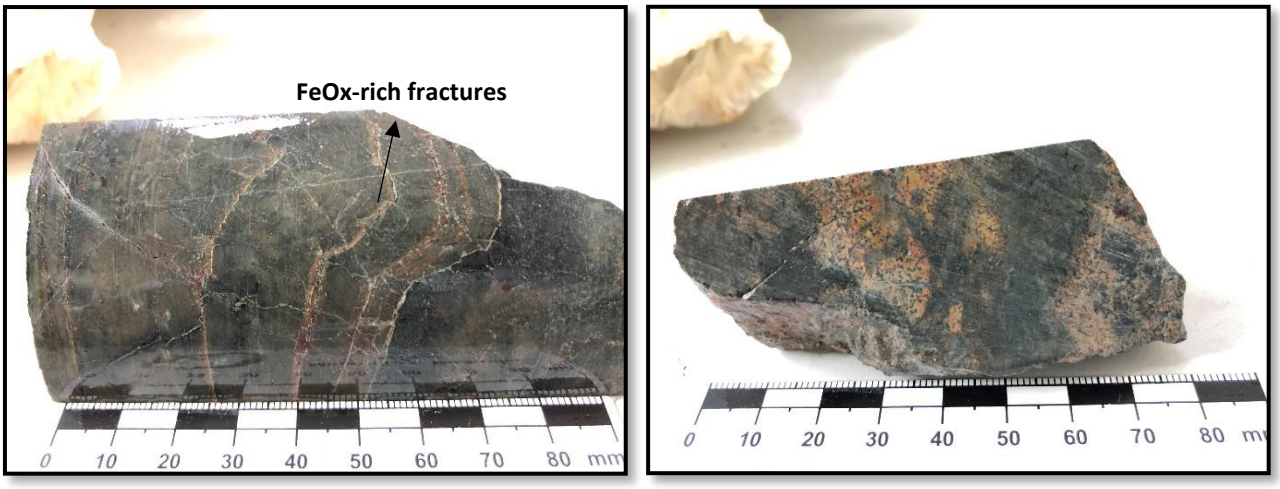


**Figure 11:** Core photographs of the meta-mudstone occurring at Cassenha Hill prospect. Note brittle behavior of the rock characterized by the occurrence of fractures which are infilled by the iron oxides.

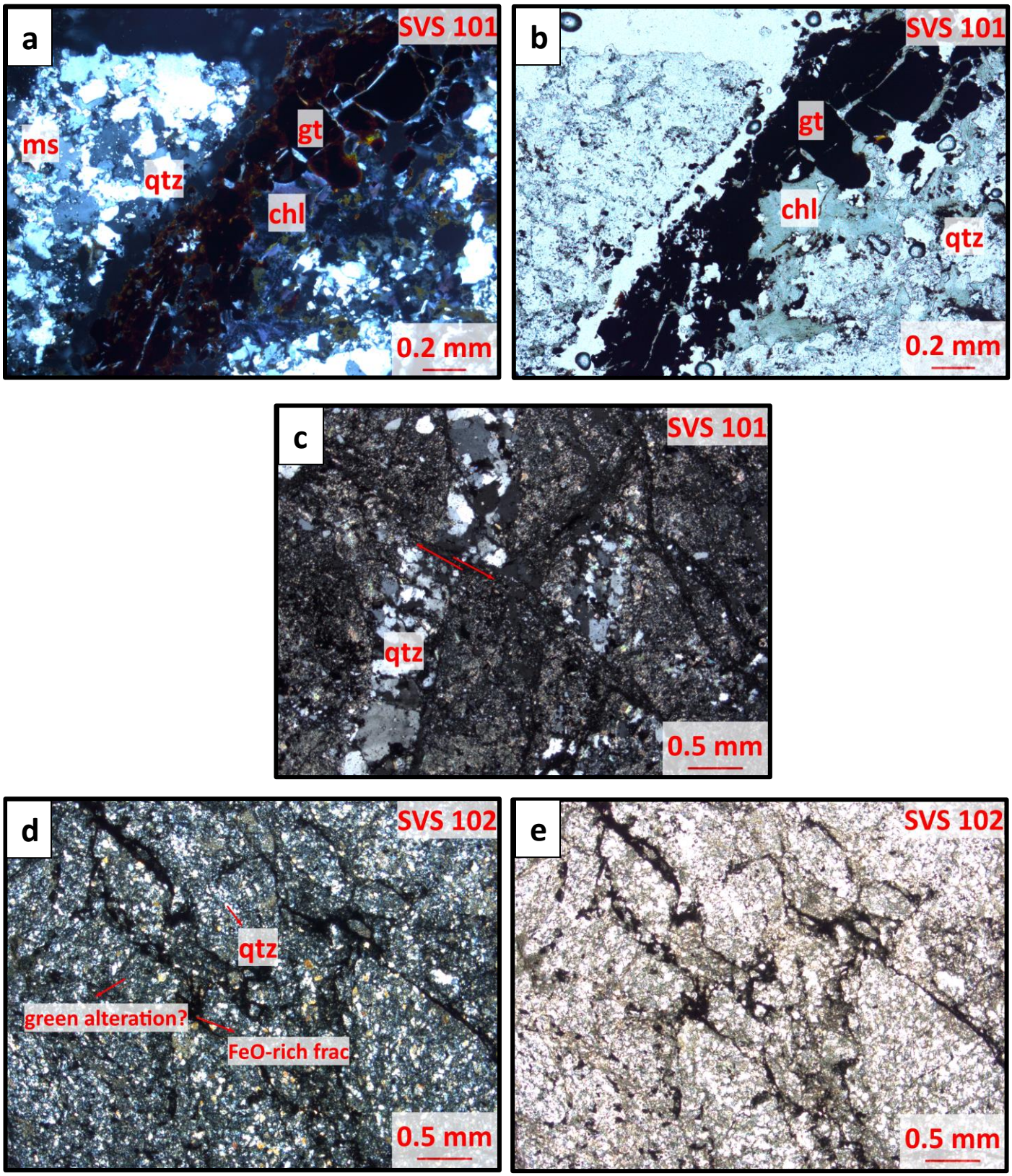
a
SVS 101
ms
qtz
gt
chl
0.2 mm
b
SVS 101
gt
chl
qtz
0.2 mm
c
SVS 101
qtz
0.5 mm
d
SVS 102
qtz
green alteration?
FeO-rich frac
0.5 mm
e
SVS 102
0.5 mm

**Figure 12:** Photomicrographs of the meta-mudstone occurring at Cassenha Hill prospect. Note the replacement of pyrite by pseudomorph goethite and their association with chlorite in **(a)** and **(b)** in XPL and PL, respectively. Note the various fractures and the displacement in thin section **(c). (d)** and **(e)** denote a chlorite-epidote-rich meta-mudstone. Note the predominance of an unidentified dark green mineral at the edges of the fractures and the overall green coloration in thin section **(d).**

***Carbonate-rich Rock***

This carbonate-rich metasedimentary rock is composed, in order of decreasing abundance, of a fine-grained matrix consisting of dolomite (15 - 30 vol.%), calcite (10 – 25 vol.%), talc (12 – 25 vol.%), quartz (10 – 20 vol.%) opaque minerals (3 – 10 vol.%), and accessory minerals. In general, the rock consists of talc-rich bands, which obliquely and/or horizontally crosscut the matrix. These talc-rich bands are commonly enriched in opaque minerals. The opaque minerals occur either at the core or at the edges of the bands, and, in most cases, overgrow the talc crystals. Although to a lesser extent, the opaque minerals also occur in the dolomitic matrix, however, always associated with the occurrence of talc crystals. The matrix itself is fine-grained and rich in talc and opaque minerals. The talc crystals occur throughout the rock, and have sub-angular to sub-rounded crystal shapes. The grain size is highly variable, and ranges from fine to coarse grains. The fine grain crystals typically occur in the bands and the coarser grains occur as individual grains in the dolomitic matrix. These individual grains are, in most cases, rich in opaque mineral inclusions. Overall, the rock is moderately fractured and highly altered. Carbonate and/or talc alteration are the main types of alteration.

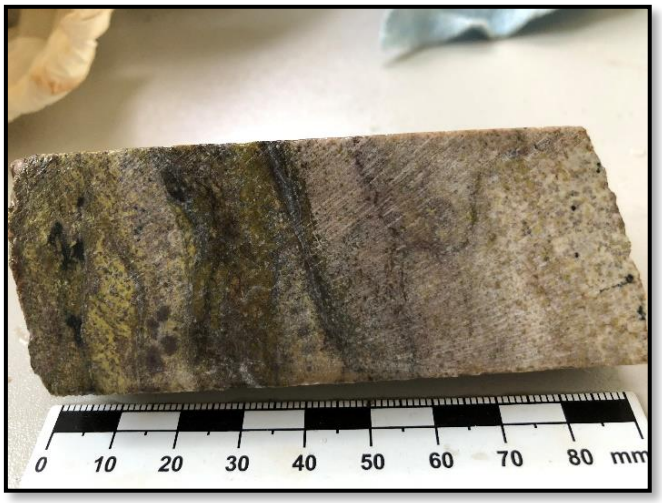


**Figure 13:** Photograph of the carbonate-rich rock occurring at the Cassenha Hill prospect

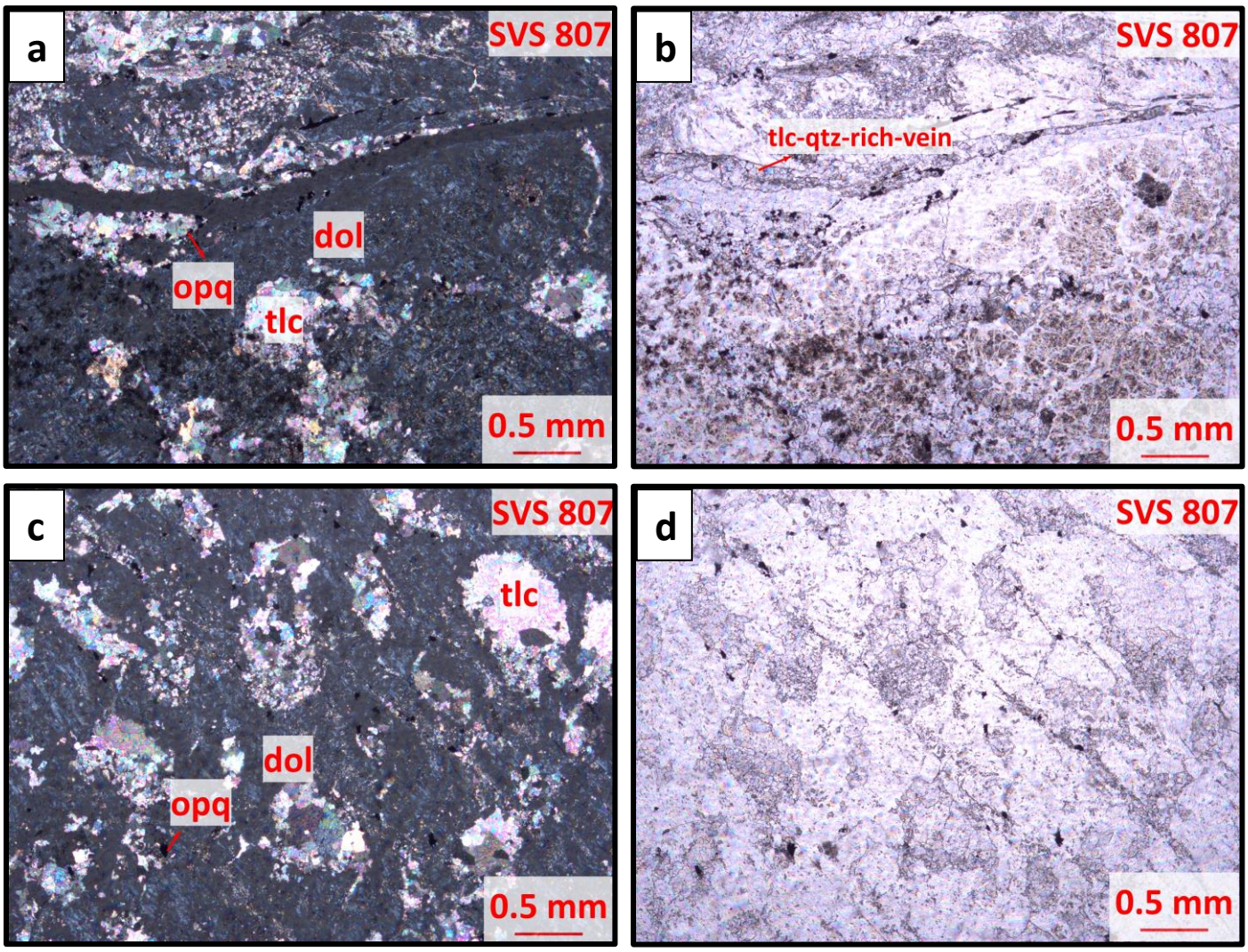


**Figure 14:** Photomicrographs of the carbonate-rich rocks occurring at Cassenha Hill prospect. Note the replacement of carbonates (dolomite and calcite) by talc in thin section (c) in XPL.

***Breccia***

The thin sections cut from the breccia shows that the rock is composed, in order of decreasing abundance, of quartz (20 – 40 vol.%), chlorite (10 -20 vol.%), unidentified green mineral (7 – 15 vol.%), biotite (5 – 10 vol.%), goethite (5 – 7 vol.%), (< 5 vol.%) of magnetite, and accessory minerals. In general, the rock is highly fractured, matrix-supported, and consists of fine-grained, sub-angular to angular quartz crystals, which occur interchangeably with other features in the rock. The size of quartz grains is similar and not much irregular. The cement predominantly consists of quartz, chlorite, and calcite material. The fractures occur throughout the rock and do not follow a specific pattern. These fractures are in most cases filled by disseminated unidentified dark green mineral as well as with iron oxides (goethite and rare hematite). Furthermore, goethite crystals, which have crystal shapes ranging from anhedral to cubic, are also found within the veins as inclusions and/or later occurrences. Replacement of biotite by chlorite (Fig. 16e) is the main alteration behavior, and can be observed throughout the rock. Four compositionally distinct veins can be observed, consisting of (1) quartz, (2) quartz + chlorite + iron oxides, (3) iron oxides (goethite), and (4) chlorite + unidentified dark green mineral. These veins have a branch-like type of shape, crosscut each other, and have thickness ranging from 0.1 to 0.5 mm.

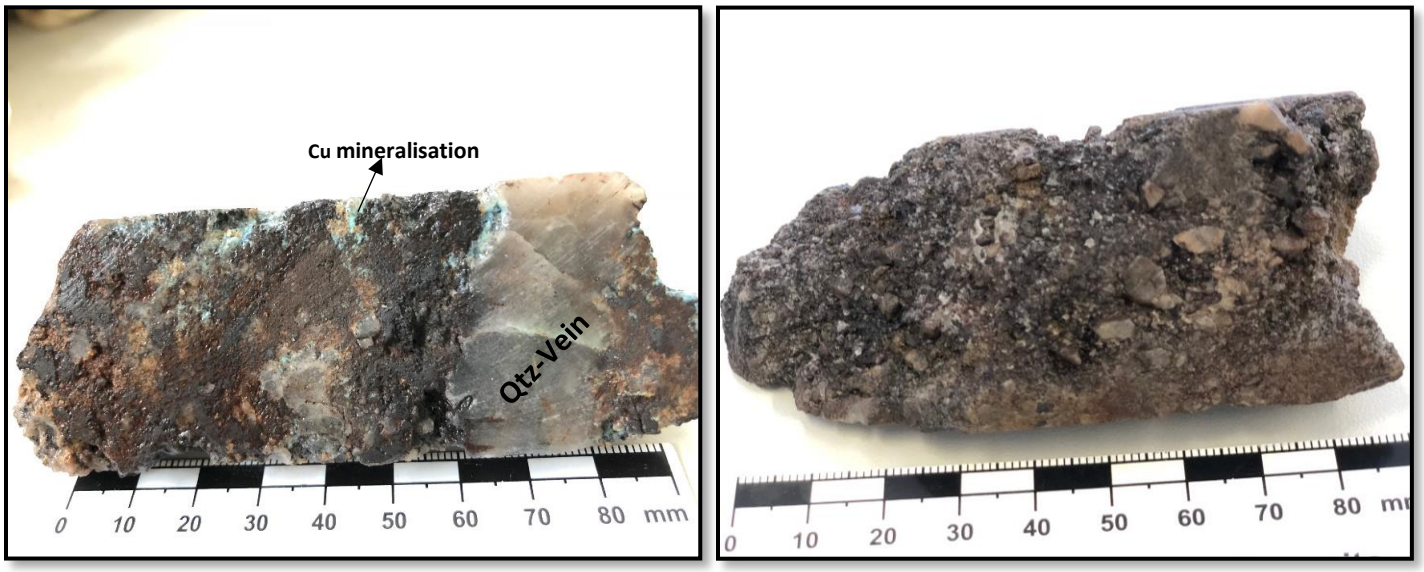


**Figure 15:** Core photograph of the brecciated quartz rock occurring at the Cassenha Hill prospect. Note the occurrence of Cu mineralization staining and magnetite-quartz veins.

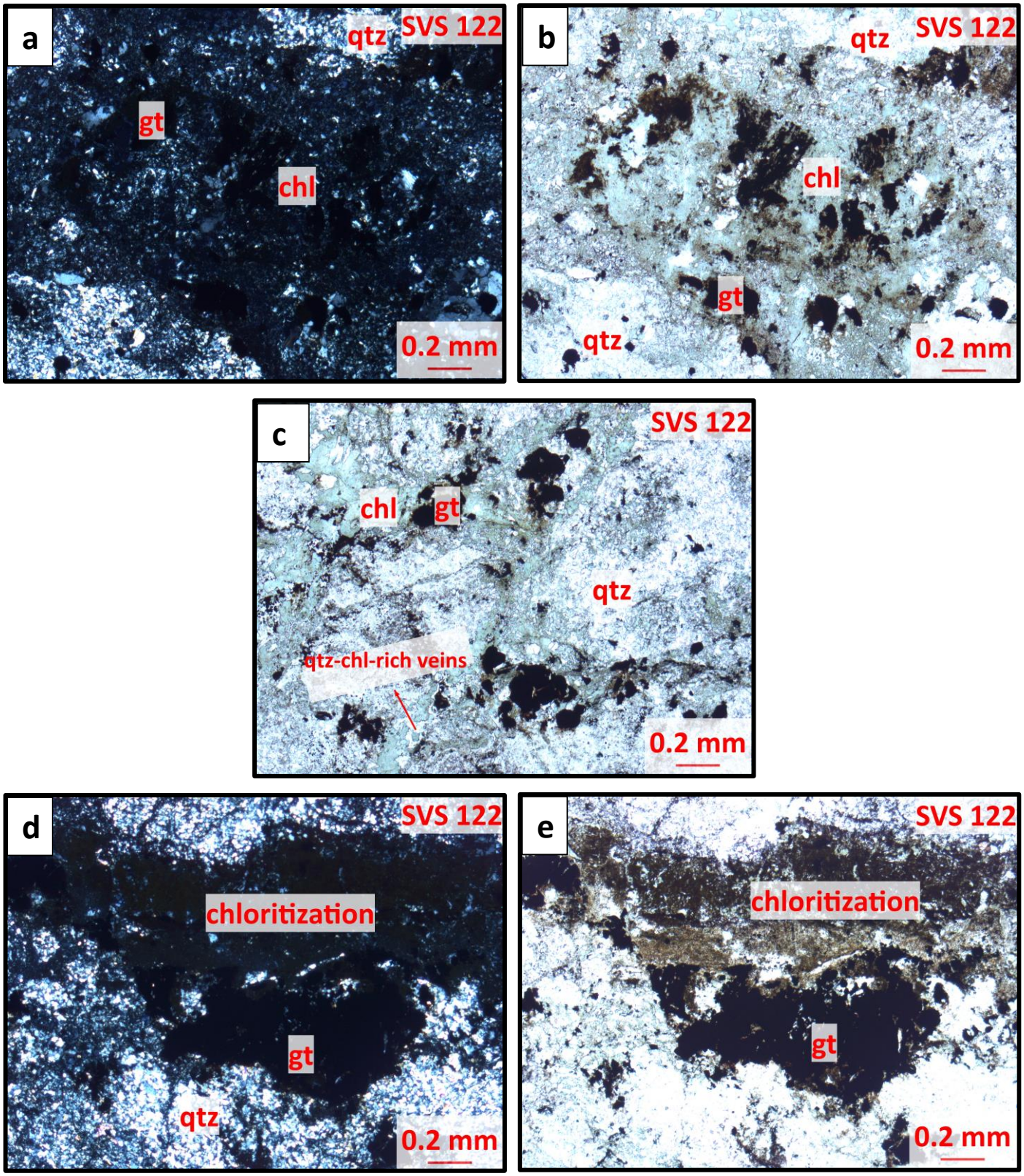
a
qtz
SVS 122
gt
chl
0.2 mm
b
qtz
SVS 122
chl
gt
qtz
0.2 mm
c
SVS 122
chl
gt
qtz
qtz-chl-rich veins
0.2 mm
d
SVS 122
chloritization
gt
qtz
0.2 mm
e
SVS 122
chloritization
gt
0.2 mm

**Figure 16:** Photomicrographs of the brecciated rock occurring at Cassenha Hill prospect. Note the high degree of chlorite alteration and the spatial relationship between chlorite and goethite. Note the occurrence of chlorite-quartz-rich veins and their association with goethite. Goethite tends to occur as replacement of sulfide minerals (i.e., pyrite and chalcopyrite).

### 4.4. Summary of the Petrographic characteristics

The petrographic study enabled the identification of two rock groups (i.e., igneous and metasedimentary rocks) in which six (6) litho-types were identified, namely, granites, meta-sandstone, meta-siltstone, meta-mudstone, breccia and the carbonate-rich rock. Overall, the granites exhibit a hypidiomorphic to allotriomorphic type of texture, are moderately fractured, do not exhibit major microscale deformation, and are composed of minerals which vary from strictly magmatic origin such as plagioclase and some of the K-feldspars, and minerals of hydrothermal origin such as limonite, chlorite, and sericite. Replacement textures could be observed and are characterized by the replacement of K-feldspars by fine mica (i.e., muscovite and/or sericite), replacement of Na-rich by K-rich feldspars, and magmatic biotite by hydrothermal chlorite. On the other hand, the metasedimentary rocks tend to exhibit textures characteristic of a very low-grade metamorphic facies, where, the clastic and sedimentary nature of the rocks is still preserved. In terms of mineral composition, the metasedimentary rocks are mostly composed of quartz, carbonates, chlorite, fine micas, and iron oxides. Replacement of biotite by chlorite represents the most common alteration as it occurs in all of the examined rocks. Other observed replacements include: dolomite by talc (Fig. 8e), calcite by quartz (Fig. 8d) and pyrite by goethite (Figs. 12a and 16e). The rocks are strongly fractured, with the exception of the siltstone and some of the meta-sandstones that grade into moderately to non-fractured. Evidences of microscale displacement could be observed in the mudstone (Fig. 12c), however, no other major microscale deformation could be observed. The main alteration minerals are: chlorite, sericite, talc, and

carbonates, and such minerals, mainly, chlorite, tend to be associated with the occurrence of brittle features of the rocks. The mineralization is associated with the brittle features of the rock and tend to occur within and/or at the edges of the veins as later occurrences.

**Table 1**: Summary of the petrographic characteristics of the selected rocks of the Cassenha Hill prospect.

| Rock type | Texture | Grain size | Deformation | Alteration | Mineralogy | Mineral abundance |
|---|---|---|---|---|---|---|
| Granite | Varying from hypidiomorphic to allotriomorphic granular | Medium-grained equigranular matrix | Weakly to moderately fractured | Chloritization, sericitization, and K-alteration | K-feldspars, quartz, plagioclase, chlorite, biotite, orthoclase and hematite/limonite, opaque minerals | 20-35 vol.% K-feldspars, 15-25 vol.% quartz,10-12 vol.% plagioclase, 5-10 vol.% chlorite, 3-5 vol.% biotite, 3-5 vol.% hematite/limonite, 2-5 vol% orthoclase, and 1-2 vol% opaque minerals |
| Meta-sandstone | Clastic | Medium- to Coarse grained | Non-fractured, to weakly to moderately fractured | Chloritization. Carbonate, and Chlorite-sericite | Quartz, chlorite, calcite, muscovite, epidote, and accessory minerals | 45-65 vol.% quartz, 15-25 vol.% of chlorite, 10-15 vol.% calcite, 10-12 vol.% muscovite, 5-10 vol.% epidote |
| Meta-mudstone | Clastic | Very fine-grained | Strongly fractured | Chloritization | Quartz, unidentified mineral, chlorite, opaque minerals, muscovite, and accessory minerals | 20-40 vol.% quartz, 20-30 vol.% unidentified mineral, 15-25 vol.% chlorite, 3-10 vol.% opaque minerals, 3-5 vol.% muscovite |
| Meta-Siltstone | Clastic | Fine-grained | Weakly fractured | Chloritization, Silicification | Quartz, calcite?, chlorite, muscovite, opaque and accessory minerals | 40-60 vol.% quartz, 10-20 vol.% calcite?, 10-15 vol.% chlorite, 3-8 vol.% muscovite, 2-3 vol.% opaque minerals |
| Carbonate-rich rock | Clastic | Fine-grained matrix with medium- to coarse grained crystals | Strongly fractured | Carbonate | Dolomite, calcite, talc, quartz, opaque minerals, and accessory minerals | 15-25 vol.% dolomite, 10-30 vol.% calcite, 10-25 vol.% talc, 10-35 vol.% quartz, 3-10 vol.% opaque minerals |
| Breccia | Clastic | Fine grained | Strongly fractured | Chloritization, Silicification | Quartz, chlorite, unidentified dark green mineral, biotite, magnetite, hematite, and accessory minerals | 20-40 vol.% quartz, 10-20 vol.% chlorite, 7-15 vol.% of unidentified dark green mineral, 5-10 vol.% biotite, 5-7 vol.% magnetite, <5 vol.% hematite |

# 5. CHAPTER V

## BULK ROCK COMPOSITION

Geochemistry of the Cassenha Hill prospect was characterized through the analyses and interpretation of 13 samples selected from the exploration boreholes logged as part of this study, as well as from the interpretation of ICP-MS (Inductively Coupled Plasma Mass Spectrometry) trace element data from boreholes CHD008, CHD009, CHD011, and CHD013 drilled and analyzed by Rift Valley Resources (RVR) as part of their exploration program. In order to properly describe the geochemical characteristics of the Cassenha Hill prospect, the XRF and ICP-MS data were used together to discriminate and classify the rocks of the prospect and infer their tectonic provenance. Furthermore, for diagrams which the data required was not obtained as part of this study (i.e., REE diagrams, spider plots, and tectonic setting discriminant diagrams) the ICP-MS data from RVR was used as the primary data source. Lastly, for the oxygen isotope study, the 13 samples selected and analyzed in this study were used to determine the source of the fluid thus inferring the possible system of origin.

The primary objective of this chapter is to provide an insight on the geochemical characteristics of the various rock types observed at the Cassenha Hill prospect, thus enabling the identification of the host rock, classification of the various rock types, and infer their origin/provenance as well as their protoliths.

## 5.1. General classification

The use of whole-rock geochemistry is well documented in the literature and has proved to be a valuable tool in the classification of various rock types (i.e., sedimentary, igneous, and low-grade metasedimentary rocks) as well as in determining their provenance/source and tectonic setting (Bhatia, 1983; Lima et al., 2014). Due to their relative low mobility and high resistance to weathering, elements such as Ti, Zr, and Al, are generally used to classify the major rock types. This is achieved by using the Al-Ti-Zr ternary diagram developed by Garcia et al. (1991). For sedimentary rocks, the interpretation from this diagram is based on the assumption that during sedimentation, processes such as weathering, transport, mixing and sorting take place (Sawyer, 1986; Khider and McQueen, 2005). During the first three processes, the proportion of insoluble elements such as Ti, Zr, and Al may be affected by some degree of leaching, however, their bulk proportion suffers relatively low modification (Khider and McQueen, 2005), whereas, the ratio of $Al_2O_3/TiO_2$ in igneous rocks is strongly influenced by differentiation processes which contrasts with the weak Al/Ti fractionation in sedimentary rocks. This disparity is generally used to identify igneous rocks of unknown origin (Moine et al., 1982; Garcia et al., 1994). Therefore, although the diagram was primarily developed for the classification of sedimentary (sandstone-shale fractionaction) and low-grade metasedimentary rocks, it proves to be a useful distinguishing tool between igneous and sedimentary samples as they plot in specific fields of the diagram (Khider and McQueen, 2005). This technique was applied in the Cassenha Hill drill cores as they are, in most cases, highly oxidized which makes their macroscopic classification difficult to constrain.

**Figure 17**: Rock classification discriminant diagrams after Garcia et al. (1994) for low-grade metasedimentary and granitic samples collected from the Cassenha Hill prospect. The diagrams confirm the classification suggested in the petrographic study. The samples plot in three distinctive groups on the diagram. The fine-grained metasediments, which include meta-mudstone, meta-siltstone, and carbonate-rich rock plot in the shale

compositional field, while, the coarse-grained metasediments, which include, meta-sandstone and quartzite, plot on the sandstone compositional field. The brecciated rock also plots in the shale compositional field. The granite plots in the granite compositional field. (**Top center**): The Al-Ti-Zr diagram (wt.%) modified after Garcia et al. (1994), where SPG is strongly peraluminous granite and CAS is calc-alkaline suites (Khider and McQueen, 2005). (**Bottom left and right**): Al-Ti-Zr diagram of the samples collected in the Cassenha Hill prospect.

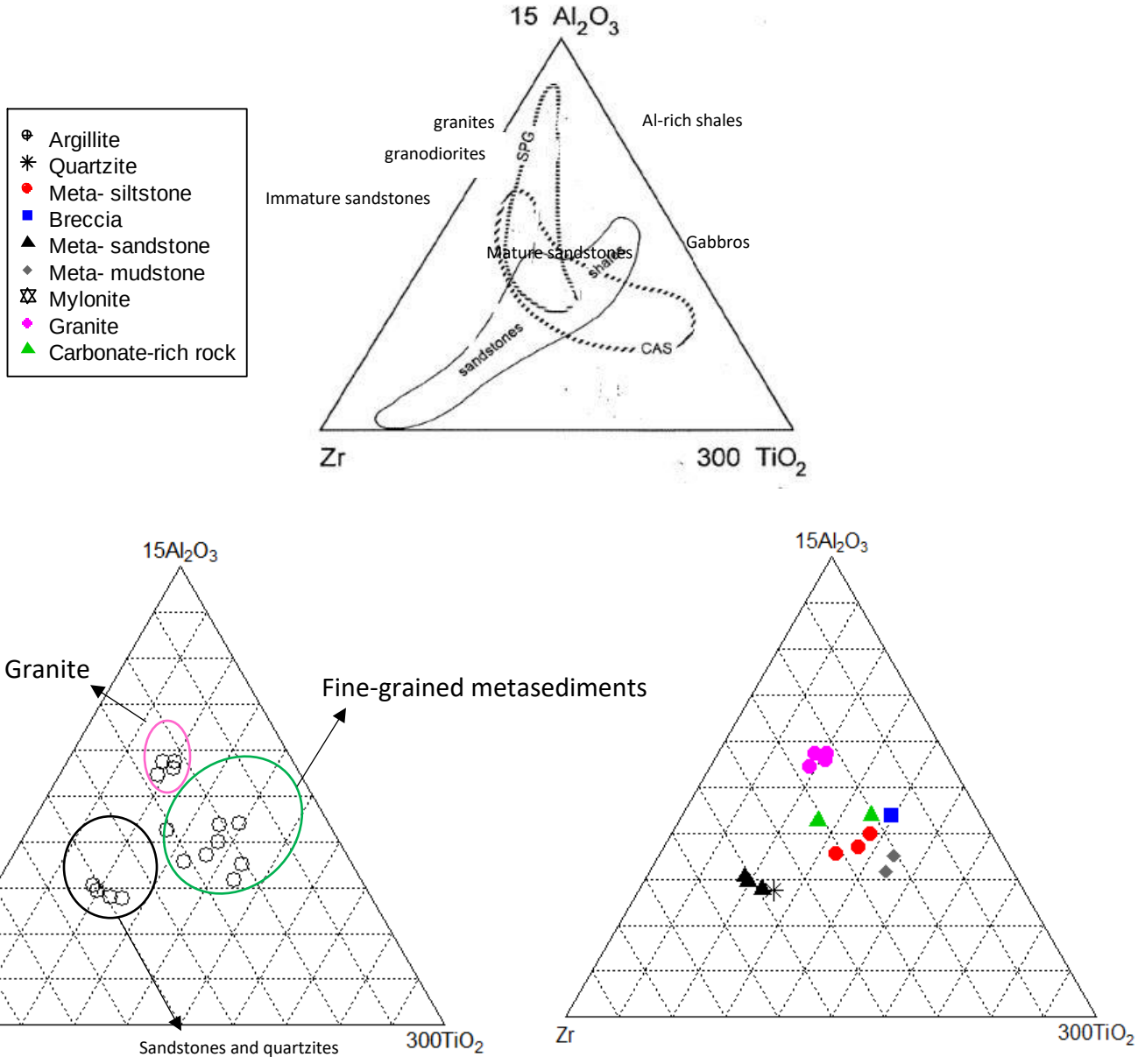

The various rock types examined, namely the granite, breccia, meta- mudstone, meta-siltstone, carbonate-rich rock, meta- sandstone, and quartzite are characterized by having high $SiO_2$ (9.84 to 96.16 wt.%) and relatively low $TiO_2$, MnO, $Na_2O$, $P_2O_5$, $SO_3$, $Cr_2O_3$, NiO, and H2O- content (Table 2). However, different lithologies tend to have characteristic concentration of $Fe_2O_3$, $Al_2O_3$, MgO, CaO, and $K_2O$ (Table 2). For a better and more concise description of the observed geochemical characteristics, each rock group will be discussed separately.

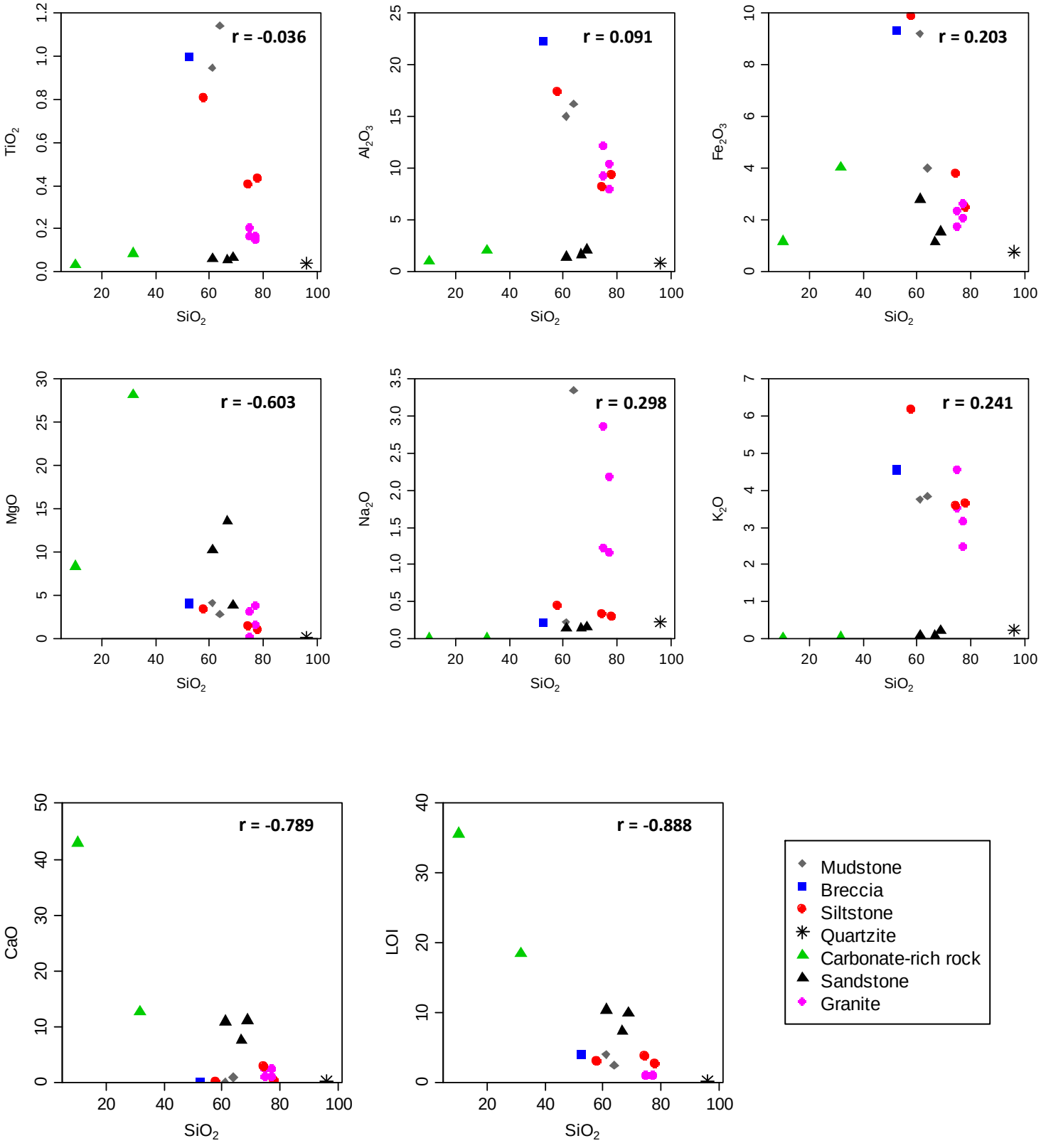


**Figure 18:** Harker diagrams of major oxides (Wt.%) plotted against $SiO_2$ in Wt.%. Note the characteristic poor correlation among the various samples. r: Correlation coefficient.

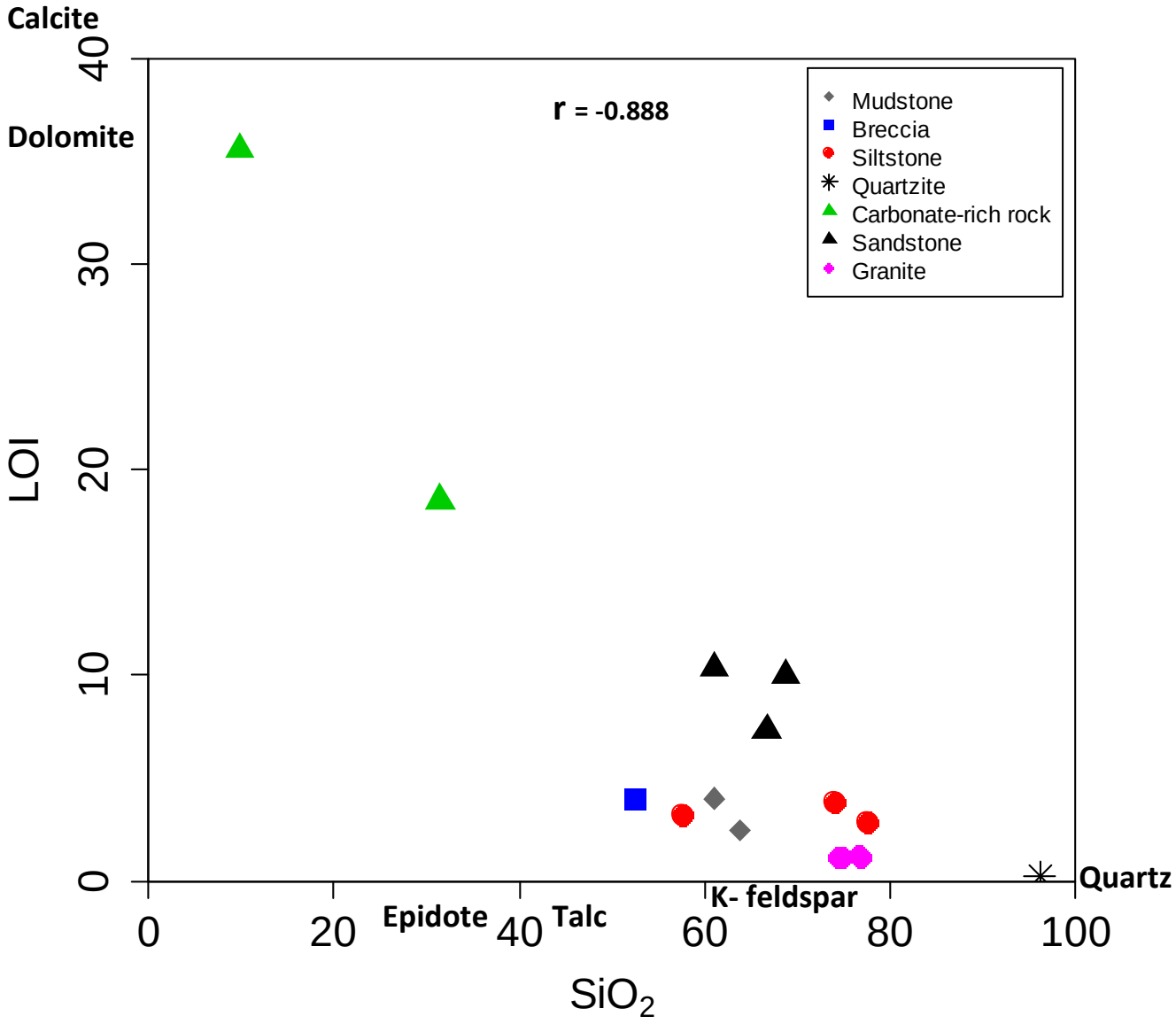


**Figure 19:** Bivariate plot of LOI versus $SiO_2$ in Wt.%. Note the overall negative correlation between $SiO_2$ and LOI. The carbonate-rich rock plots towards the composition of calcite, dolomite, epidote, and talc content as observed in the petrographic study. The sandstones tend to be also relatively enriched in carbonates (> 8 wt.%) when compared to other metasedimentary rocks, this is evidenced by the calcite-rich cement observed in the petrographic study. The breakdown of feldspars and the generation of muscovite, biotite, chlorite, and/or kaolin-group of minerals (i.e., illite, smectite) possibly resulted in the depletion of Ca, Na, and Sr in breccia, mudstone, siltstone, quartzite, and granite.

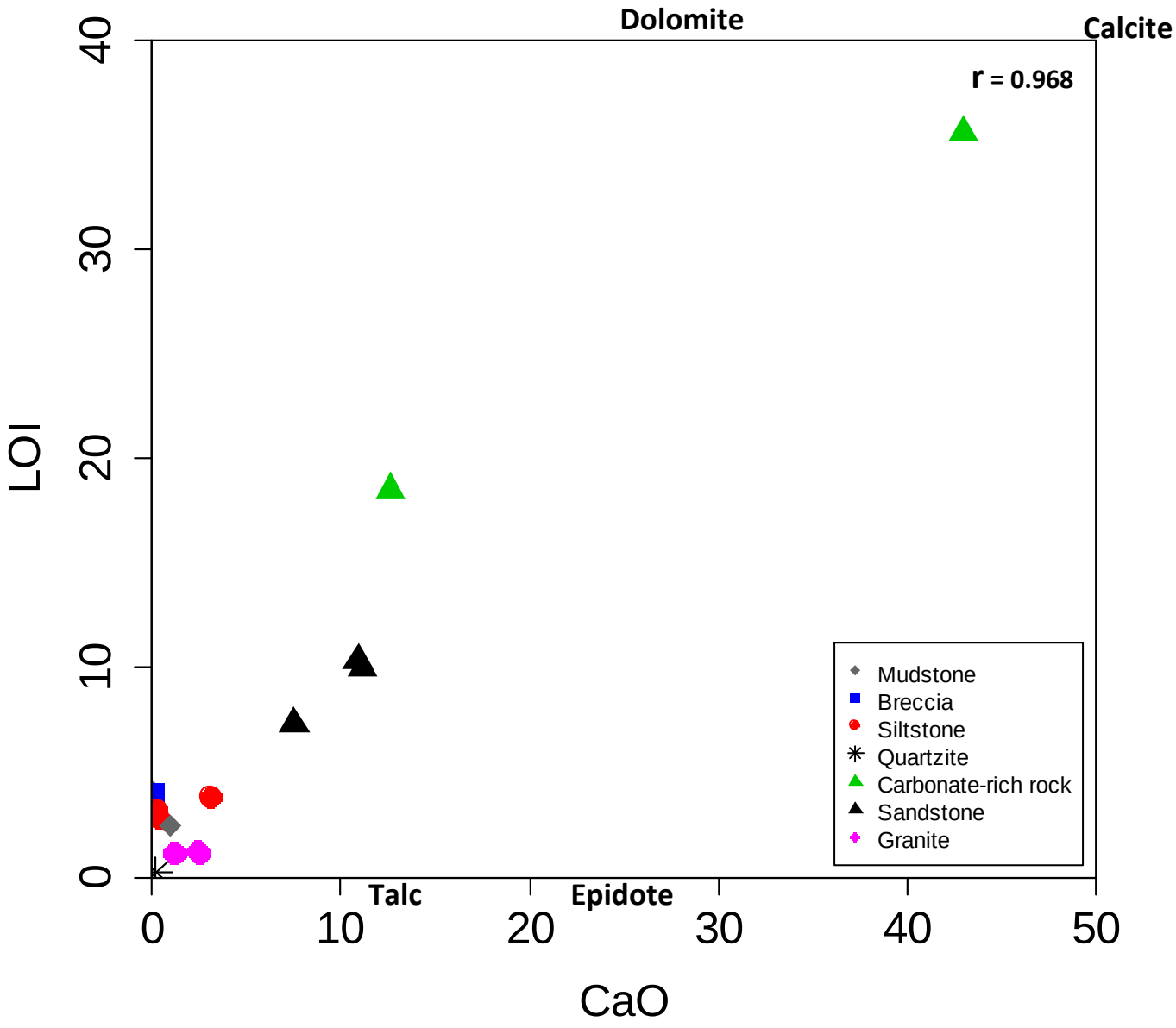


**Figure 20:** Bivariate plot of LOI versus CaO in Wt.%. Note the strong positive correlation between LOI and CaO in the samples as a whole, and the relatively low content of calcium and $CO_2$ in the granite, breccia, mudstone, siltstones, and quartzites.

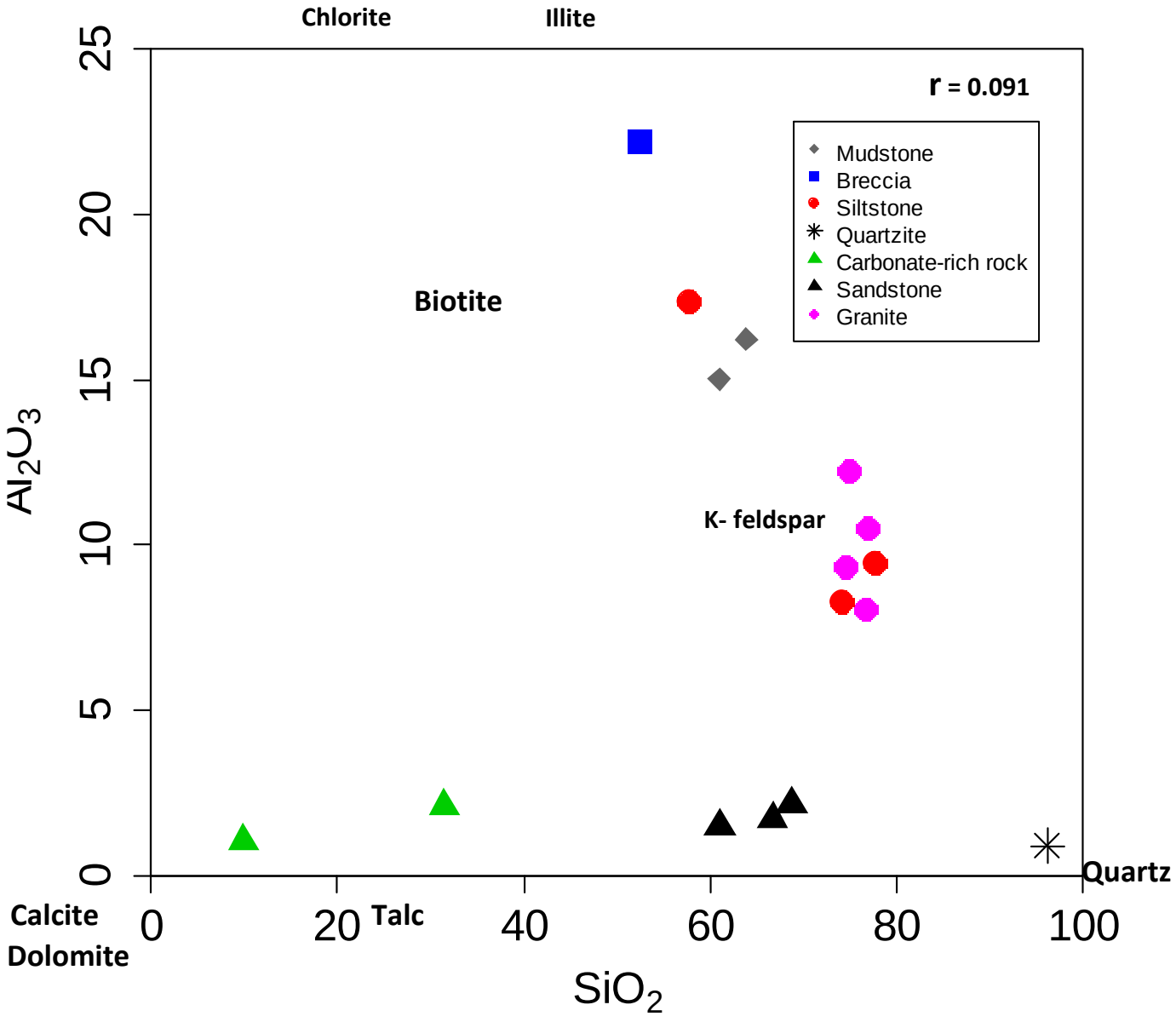


**Figure 21:** Bivariate plot of $Al_2O_3$ versus $SiO_2$ in Wt.%. Note the trend towards the chlorite-illite compositional field.

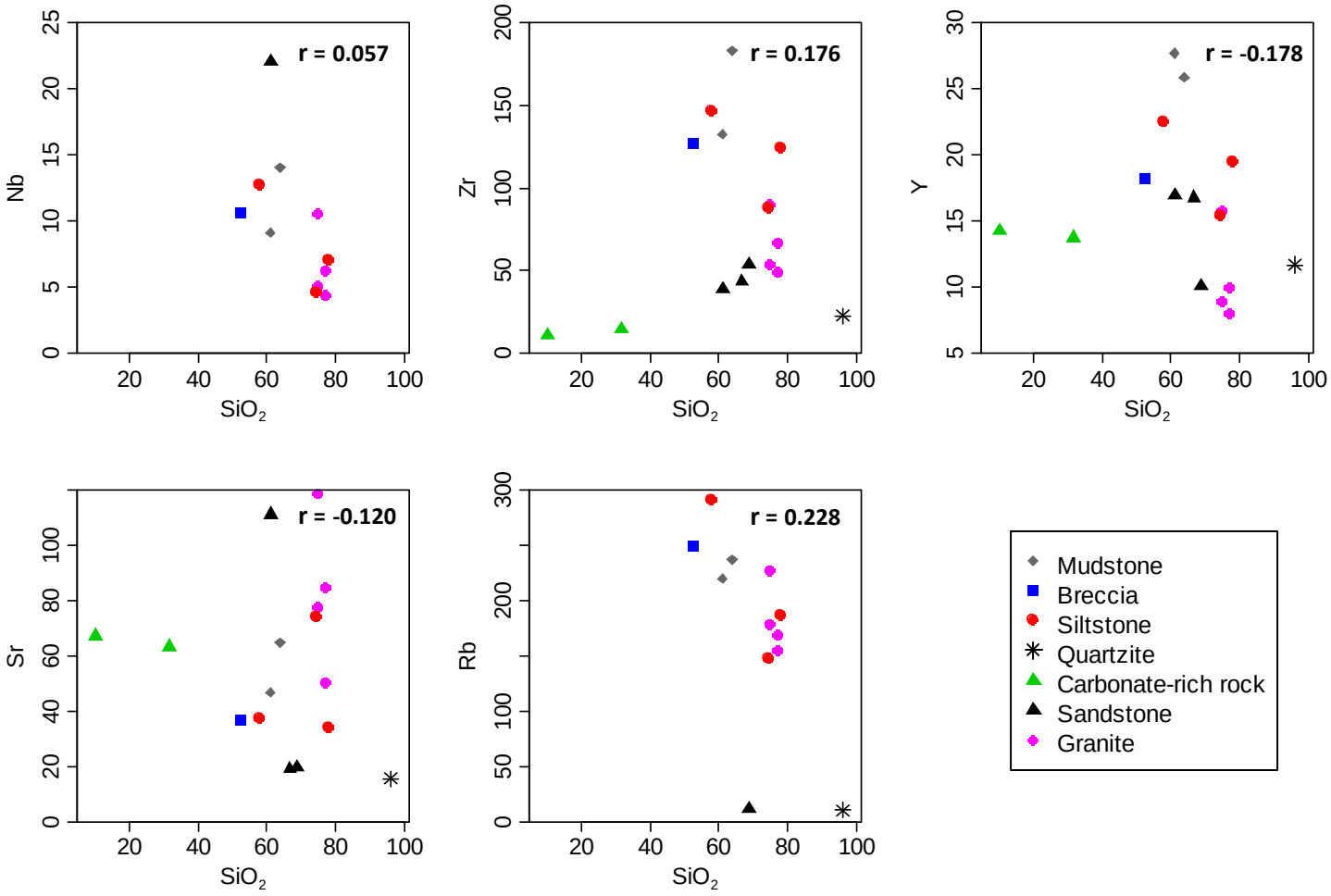


**Figure 22**: Harker diagrams of trace elements (Nb, Zr, Y, Sr, and Rb) in ppm comprising the major rock types versus $SiO_2$ in wt.%.

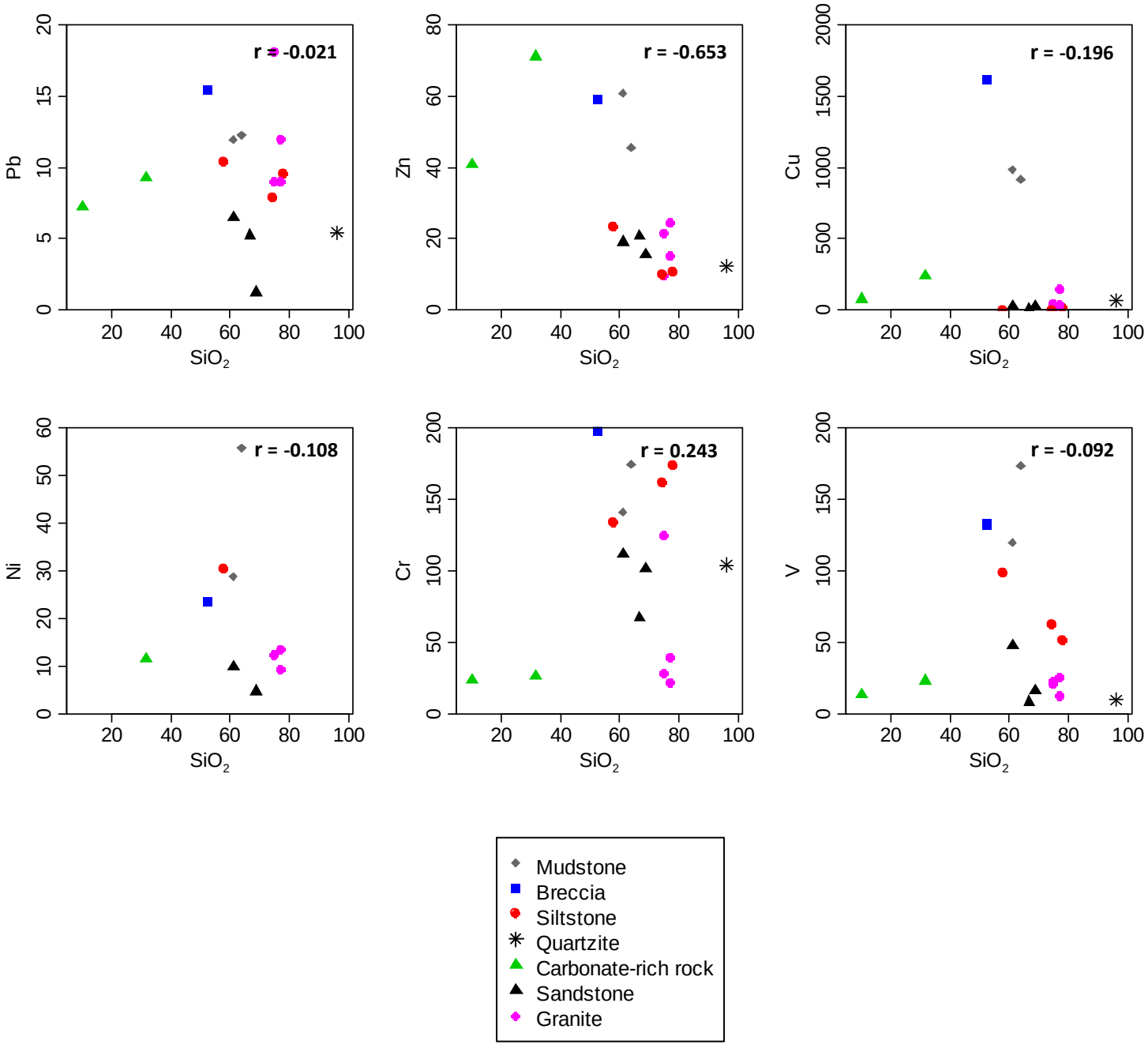


**Figure 23:** Harker diagrams of trace elements (Pb, Zn, Cu, Ni, Cr, and V) in ppm comprising the major rock types plotted against $SiO_2$ in wt.%. Note the poor correlation among the samples.

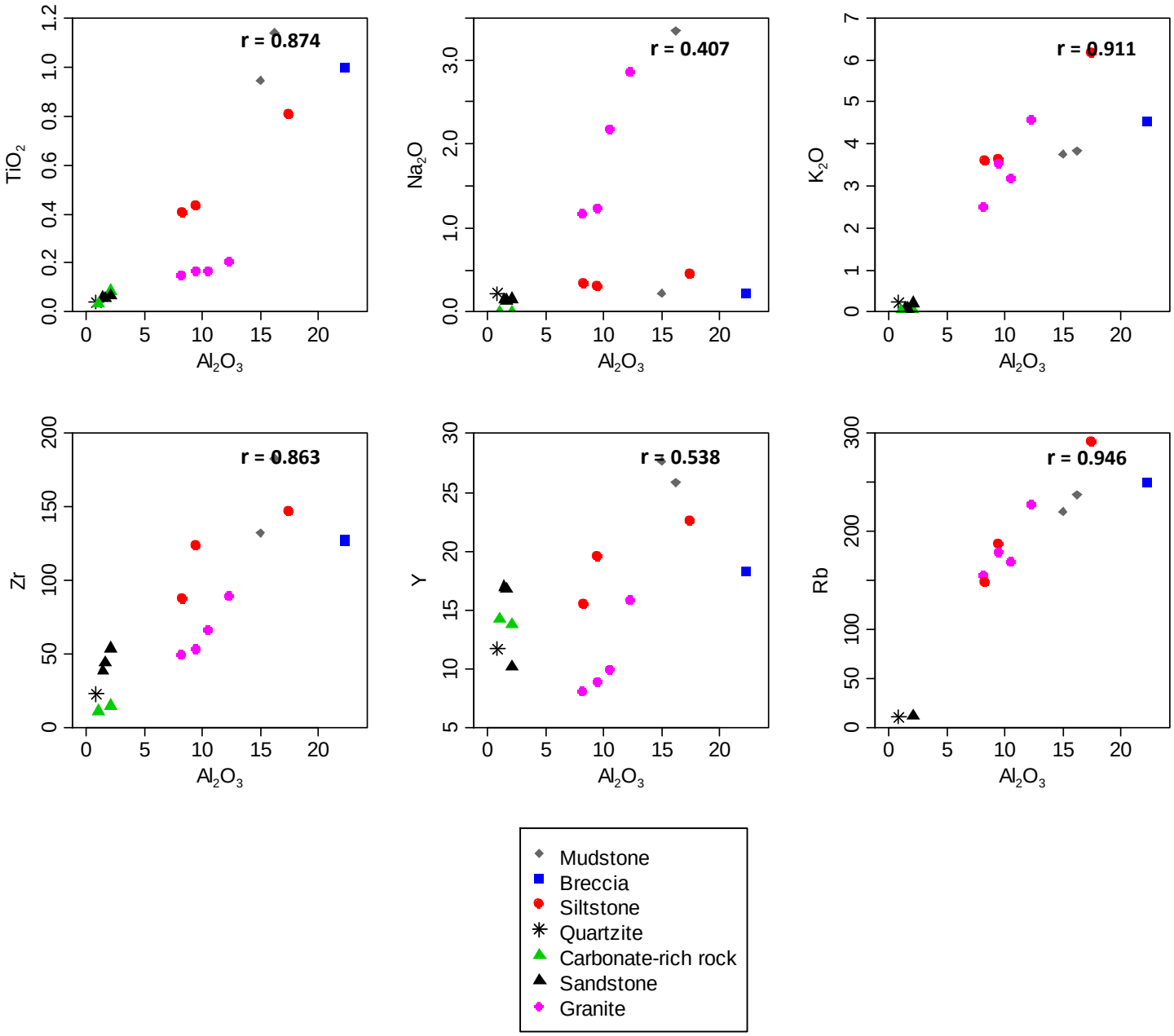


**Figure 24:** Harker diagrams of selected major oxides ($TiO_2$, $Na_2O$, $K_2O$) in Wt.% and selected trace elements (Zr, Y, and Rb) in ppm comprising the major rock types plotted against $Al_2O_3$ wt.%. Note the good correlation between $Al_2O_3$ and $TiO_2$, $K_2O$, Zr, and Rb. This collective trend supports the Al, Ti, and Zr conservative behavior in all rock types. It further suggests that K-enrichment together with depletion of Ca and Na (Figs. 18 and 19) possibly accompanied the fluidization in the rocks.

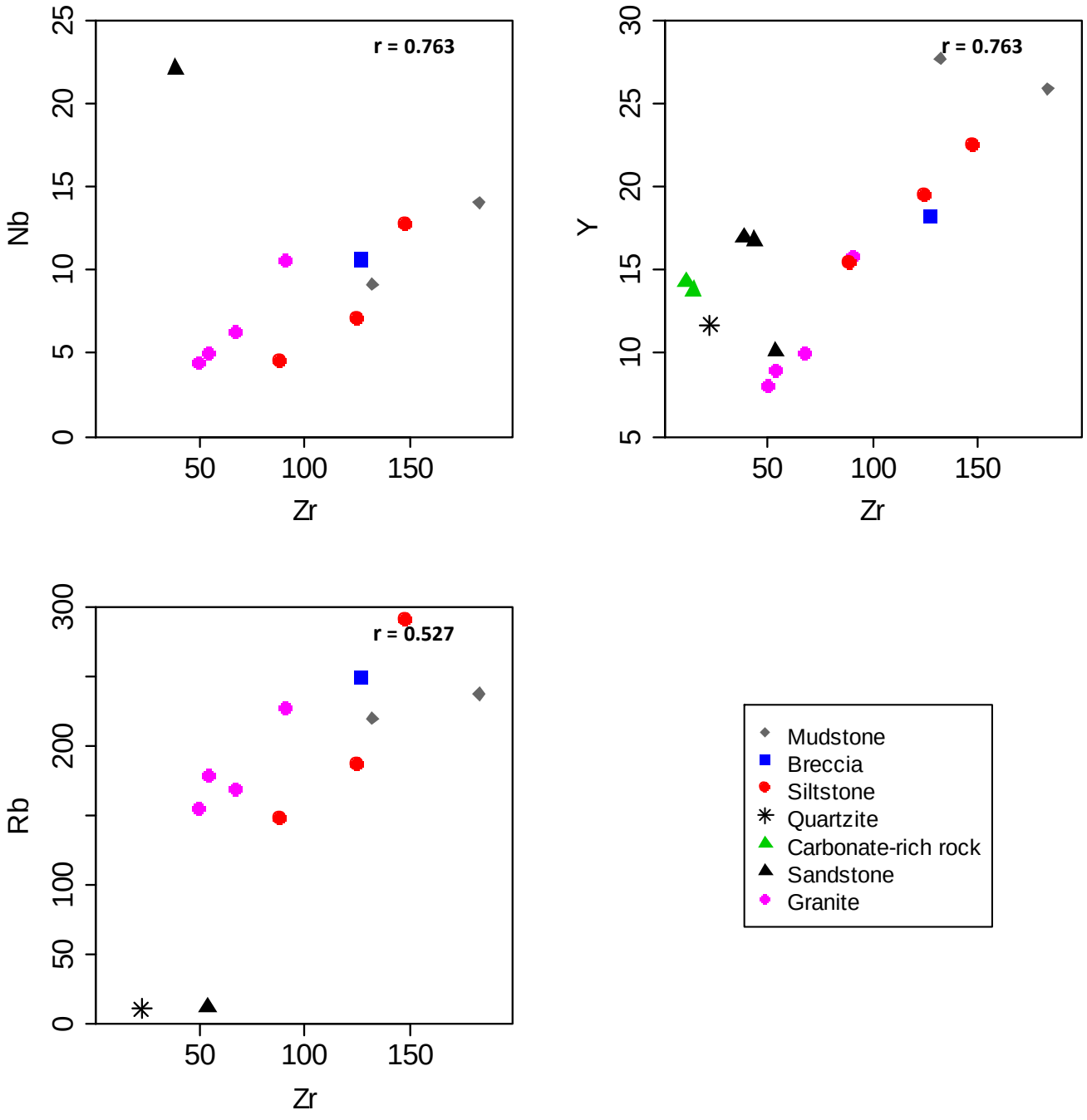


**Figure 25:** Bivariate plots of trace elements (Nb, Y, and Rb) comprising the major rock types versus Zr in ppm. Note the good correlation between the elements.

## 5.2. *Granite*

Granitic rocks of the study area are characterized by having typical silica, magnesium, iron, and calcium values (range: 74.42 – 76.77 wt%, ave. 75.69 wt.% $SiO_2$; range: 0.34 – 3.96 wt.%, ave. 2.27 wt.% MgO; range: 1.79 – 2.67 wt.%, ave. 2.24 wt.% $Fe_2O_3$; range: 1.18 – 2.53 wt.%, ave. 1.87 wt.% CaO), intermediate values of aluminum, titanium, manganese (range: 8.07 – 12.26 wt.%, ave. 10.5 wt.% $Al_2O_3$; range: 0.17 – 0.21 wt.%, ave. 0.17 wt.% $TiO_2$; range: 0.03 – 0.10 wt.%, ave. 0.06 wt.% MnO), and very low average values of potassium and sodium (range: 2.51 – 4.58 wt.%, ave. 1.87 wt.% $K_2O$; range: 1.17 – 2.87 wt.%, ave. 3.45 wt.% $Na_2O$) when compared to typical granitic rock composition as proposed by Piispanen (1977). In terms of trace element composition, the analysed granitic rocks comprise Rb (183 ppm), Sr (83 ppm), Pb (12ppm), (416 ppm), Zr (65 ppm), Ni (11.9 ppm), Y (10.74 ppm), Co (9 ppm), Sc (7 ppm), Nb (6.63 ppm) of Mn (497 ppm), V (21 ppm), and Cu (18 ppm).

The Cassenha Hill granitic samples (Figs. 18 and 24) show linear positive correlation between $Al_2O_3$ and $Na_2O$, $K_2O$, $TiO_2$, Zr, Y, and Rb on the Harker diagrams. On the contrary, the same oxides tend to display poor correlation with SiO2. This characteristic linear positive correlation between $Al_2O_3$ and $TiO_2$, Zr, Y, and between Zr vs Y, Rb, and Nb (Fig. 25) suggest that these elements were relatively immobile during chloritization processes and/or during hydrothermal alteration, and that the analyzed granites were originated from the same source and are the result of fractional crystallization. Moreover, positive correlation between $Al_2O_3$ , $K_2O$ and $Na_2O$ and the poor correlation between $Al_2O_3$ and CaO, indicates that these granitic rocks contain Na-rich feldspars (albite) and K-rich feldspars (microcline and orthoclase) and that they are possibly generated from the breakdown of primary plagioclase as observed in thin-sections (Fig. 6).Furthermore, with continuous hydrolysis reactions and/or interaction with fluids the K-rich feldspar gave rise to micaceous minerals (i.e., muscovite) and clay minerals such as illite. In contrast,

the poor correlation between $SiO_2$ and $Al_2O_3$ suggests that Al was retained during weathering while Si was consumed.

In summary, the 4 (four) granitic rocks analyzed show some degree of variation in terms of chemical composition. Two characteristic patterns could be observed, one being relatively richer in $Al_2O_3$, MgO, CaO, and the other one relatively poorer in the same oxides. No major differences were observed in the trace element composition.

Commonly, S-type granites originate from the partial melting of mainly sedimentary rocks giving rise to granites of adamellitic to granitic composition (Table 2). I-type granites are derived from the partial melting of predominantly igneous rocks, giving rise, in most cases, to granites of tonalitic to granodioritic composition. Moreover, I-type granites are relatively more oxidized and, in most cases, associated with porphyry Cu-Mo mineralization (Fig. 27), on the other hand, S-type granites are more reduced and are generally associated with Sn-W mineralization (Table 2 and Fig. 27). Lastly, A-type (anorogenic) granites tend to manifest characteristics of the other two groups. In order to differentiate between S- type and I-type granites, Chappell and White (1974) suggested that granitic rocks with molecular (Al)/(Na+K+Ca) ratio greater than 1.1 are considered to be S-type, while rocks with (Al)/(Na+K+Ca) ratio less than 1.1 originated from the partial melting of predominantly igneous rocks (I-type). The granitic samples from the Cassenha Hill prospect have yielded (Al)/(Na+K+Ca) ratios ranging from 1.14 to 1.28, with an average value of 1.18. These results suggest that the Cassenha Hill granites are in fact originated from the partial melting of mainly sedimentary rocks (S-type). This is further supported by the CIPW norm calculation, which enabled the identification of normative corundum (> 1%) in the four granitic samples, which is generally associated with S-type granites (Table 2).

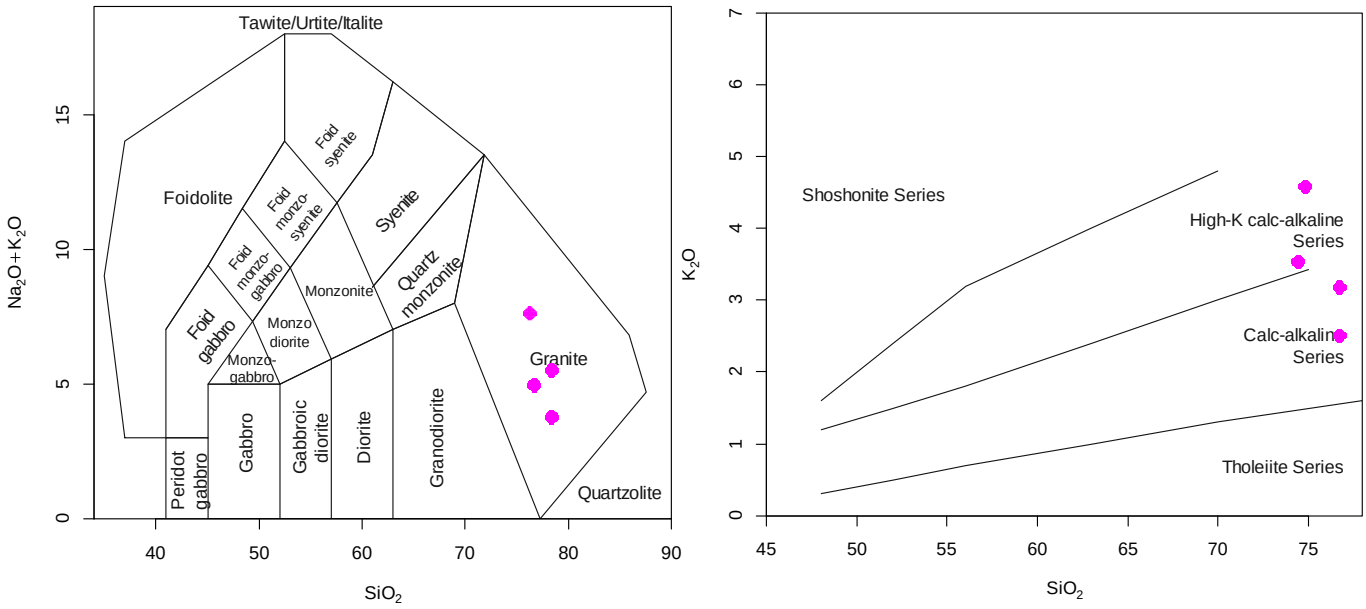


**Figure 26**: Compositional classification diagrams for granitic rocks. (**Top left**): TAS classification diagram for granitic rocks (after Middlemost, 1994). (**Top right**): $SiO_2$ vs $K_2O$ classification diagram (after Peccerillo and Taylor, 1976).

Based on the diagrams above (Fig. 26), the granitic samples of the Cassenha Hill prospect have a typical “granite” composition, their alkalinity ranges from Calc-alkaline to high K-Calc-alkaline series, and are meta-peraluminous.

**Table 2**: Characteristics S-type, I-type, and A-type granites (after Chappell and White, 1974).

| GRANITE TYPE | TECTONIC ENVIRONMENT | CHEMICAL SIGNATURE | TYPICAL MINERALS | ACCESSORY MINERALS |
|---|---|---|---|---|
| **S-TYPE** | Orogenic | Metaluminous to strongly peraluminous, high 18O/18O, 87Sr/86Sr | muscovite, cordierite, tourmaline | garnet |
| **I-TYPE** | Orogenic | Metaluminous | Biotite, hornblende | |
| **A-TYPE** | Anorogenic/ rift related | Metaluminous to moderatedly peralkaline, Fe-enriched | Fe-biotite, Na-pyroxene, titatine, hedenbergite | fayalite, Na-amphibole |

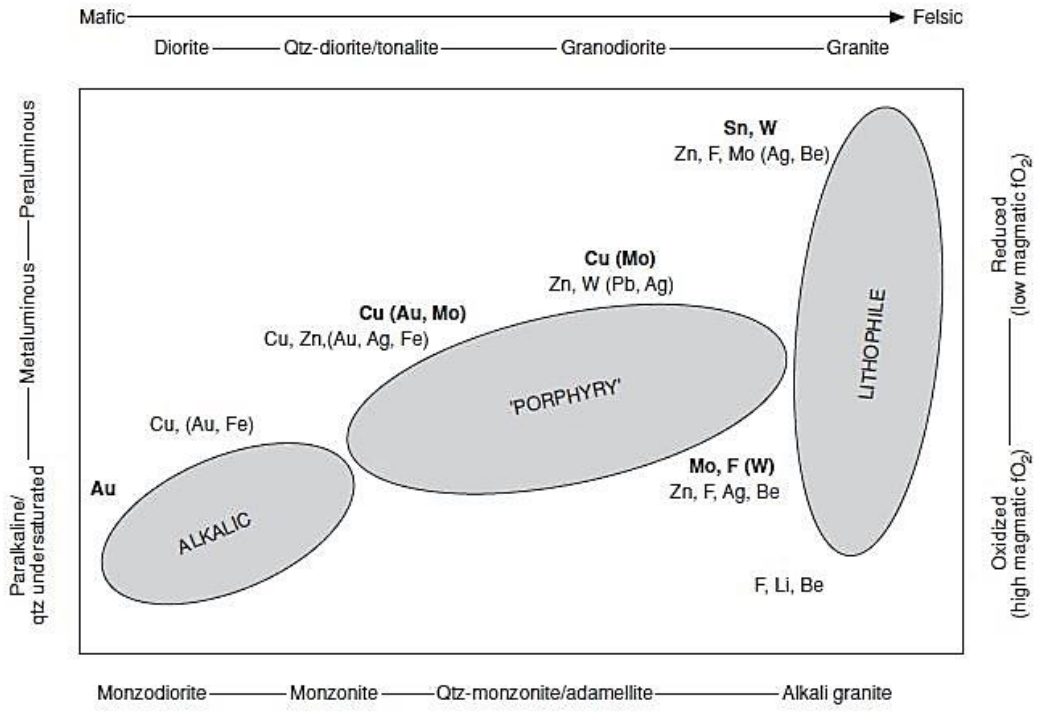


**Figure 27**: Generalized schematic diagram displaying the relationship between granitic compositions, magmatic oxidation state and their respective metal association and intrusion-related ore deposit types ( Robb, 2005).

## 5.3. *Metasedimentary rocks*

The investigated low-grade metasedimentary rocks of the Cassenha Hill prospect were geochemically characterized based on the analysis of the chemical composition of 12 samples collected at Cassenha Hill prospect. The metasedimentary succession consists of rocks with partially preserved sedimentary characteristics although metamorphically altered to some extent, and have been classified as breccia, quartzite, meta-sandstone, meta-siltstone and meta-mudstone (Fig. 17). These rocks represent the majority of the rock types outcropping in the Cassenha hill prospect and are believed to be the host of the Cu-Au mineralization.

*Major elements*

The metasedimentary rocks show some degree of variability in their major element composition. The bivariate plots (Figs. 18 and 24) indicate that the quartzites have the highest $SiO_2$ content with a value of 96.16 wt.%, while, the carbonate-rich rocks have the lowest $SiO_2$ with an average value of 20.66 wt.%. The meta-siltstones have an average $SiO_2$ content of 69.80 wt.% and a range from 57.66 to 77.66 wt.%, which is slightly higher than the $SiO_2$ content of the meta-sandstone and meta-mudstone samples. The meta-sandstones average $SiO_2$ content is 65.49 wt.% and ranges from 61.06 to 68.70 wt.%, while, the meta-mudstone average $SiO_2$ content is 62.38 wt.% and ranges from 60.96 to 63.81 wt.%. Lastly, the breccia rock has a $SiO_2$ content value of 52.52 wt.%. The various lithologies are also characterized by having accentuated variabilities in their $Al_2O_3$ content, suggesting that they have experienced weathering/alteration at varying proportions. Breccia has the highest $Al_2O_3$ content with a value of 22.21 wt.%, followed by meta-mudstones with an average value of 15.60 wt.% and ranges from 15.00 to 16.21 wt.%, which is then followed by the meta-siltstones with an average value of 11.70 wt.% and ranges from 8.28 to 17.39 wt.%. Meta-sandstone, carbonate-rich rock, and quartzite have extremely low average values of $Al_2O_3$ (1.56 wt.%; 1.76 wt.%; and 0.89 wt.%,

respectively). The average $Fe_2O_3$ values are relatively higher in the breccia, meta-mudstone, and meta-siltstone (9.33 wt.%; 6.6 wt.%; 5.42 wt.%, respectively) than in the other lithologies. Carbonate-rich rocks have the highest average value of CaO (27.78 wt.%), followed by meta-sandstone (9.85 wt.%). The remainder of metasedimentary rocks have average CaO values of < 1.24 wt.%. The carbonate-rich rock and sandstones have the highest loss of ignition (LOI) values (27.09 and 9.24 wt.%, respectively). The relatively higher LOI values obtained in the carbonate-rich rocks and sandstones are in agreement with the petrographic study, where, these rocks exhibit carbonates (i.e., calcite and dolomite) modal abundance values of > 10 vol.%. Moreover, the strong correlation between LOI and CaO (Fig. 20) suggests that calcite is the most influential among carbonates.

*Trace elements*

The metasedimentary rocks also show some degree of variation in their trace element composition. The breccia and meta-mudstones are enriched in Cu by a factor of 29 and 16, respectively, while the other rocks are relatively poorer in Cu, containing Cu values of less than 78 ppm (Table 4). The content of high field strength elements (HFSE) Y, and Nb is extremely low in all rock types, while Zr is relatively enriched in breccia, meta-mudstone and meta- siltstone, but, yet poor in meta-sandstone, quartzite and carbonate-rich rock (Table 4). Furthermore, all metasedimentary rocks are characterized by having low values of siderophile elements Ni, Co (i.e., <56 ppm), and have intermediate to extremely high values of Mn (Table 4). The carbonate-rich rocks have the highest Mn content with average value of 7315 ppm, followed by the breccia (4908 ppm), mudstones (3131 ppm), sandstone (1679 ppm), siltstone (1521 ppm), and lastly by quartzite (359 ppm). The content of lithophile elements Cr, V, F, S, Cl, Sc, and Sr, do not exhibit much variation, while, Ba and Rb contents are significantly higher in breccia (1908 ppm), mudstones (1217 ppm) and siltstones (810 ppm) and relatively lower in other lithologies (ave. < 450 ppm).

*Harker diagrams*

Overall, the major and trace elements Harker diagrams tend to display distinct relationships when plotting $Al_2O_3$ and $SiO_2$ as abscissa against all the other major oxides and trace elements comprising the metasedimentary rocks (Figs. 18 and 24). The various rock types tend to display poor or no correlation between the major oxides. $TiO_2$ and $K_2O$ are the only major oxide exhibiting some degree of positive correlation with $Al_2O_3$ in all rock types, while, bivariate plots with $SiO_2$ as abscissa only show positive correlation with specific rock types. Carbonate-rich rocks show some degree of linear positive correlation when plotting $SiO_2$ as abscissa versus $TiO_2$, $Al_2O_3$, $Fe_2O_3$, MgO, Zr, Pb, Zn, Cu, and V, contrarily, they tend to show linear negative correlations when plotting $SiO_2$ versus CaO, LOI, Y, Sr, and no or poor correlation when plotted against $Na_2O$ and $K_2O$. This trend accounts to the absence of alkali feldspars and presence of calcite, dolomite and talc minerals. meta-siltstones tend to display negative and/or poor linear correlation in bivariate plots with $SiO_2$ as abscissa. Contrarily, meta-siltstones exhibit some degree of positive linear relationship when plotting $Al_2O_3$ versus $TiO_2$, MgO, $Na_2O$, $K_2O$, Nb, Zr, Rb, Pb, and Ba, and are poorly correlated with Cu. Meta-mudstones are also better discriminated using $Al_2O_3$ as abscissa. They display positive correlation when plotting $Al_2O_3$ versus $TiO_2$, $SiO_2$, $K_2O$, Nb, Zr, Sr, Rb, Pb, and V, and are negatively correlated with, LOI, MgO, Y, Zn. The collective trend observed in meta-mudstones and meta-siltstones is due to the presence of K-feldspars, muscovite, chlorite and Kaolin-group of minerals, and it further indicates that Al and Si were retained in the weathering profile. Sandstones exhibit poor and/or no correlation in bivariate plots with $SiO_2$ or $Al_2O_3$ as abscissa.

**Table 3**: Major element composition of the selected samples of the Cassenha Hill prospect.

| | Mudstone | | Breccia | Carbonate-rich rock | | Sandstone | | | Siltstone | | | Quartzite | | Granite | | |
|---|---|---|---|---|---|---|---|---|---|---|---|---|---|---|---|---|
| **Wt.%** | SVS-101 | SVS-102 | SVS-122 | SVS-807 | SVS-808 | SVS-809-810 | SVS-812-813 | SVS-814-815 | SVS-805-806 | SVS-811 | SVS-801-802 | SVS-803 | SVS-009 | CHD013_81* | CHD013_82* | CHD013_83* |
| $SiO_2$ | 60.96 | 63.81 | 52.52 | 31.44 | 9.89 | 66.70 | 68.70 | 61.06 | 74.08 | 57.66 | 77.66 | 96.16 | 74.82 | 74.42 | 76.77 | 76.74 |
| $TiO_2$ | 0.94 | 1.14 | 1.00 | 0.09 | 0.03 | 0.06 | 0.07 | 0.06 | 0.41 | 0.81 | 0.44 | 0.04 | 0.21 | 0.17 | 0.17 | 0.15 |
| $Al_2O_3$ | 15.00 | 16.21 | 22.21 | 2.09 | 1.03 | 1.68 | 2.15 | 1.47 | 8.28 | 17.39 | 9.44 | 0.89 | 12.26 | 9.35 | 10.51 | 8.07 |
| $Fe_2O_3$ | 9.19 | 4.01 | 9.33 | 4.04 | 1.18 | 1.16 | 1.56 | 2.80 | 3.80 | 9.91 | 2.55 | 0.78 | 1.79 | 2.40 | 2.09 | 2.67 |
| MnO | 0.57 | 0.12 | 0.57 | 0.96 | 0.61 | 0.14 | 0.18 | 0.21 | 0.05 | 0.12 | 0.32 | 0.04 | 0.03 | 0.08 | 0.05 | 0.10 |
| MgO | 4.15 | 2.84 | 4.04 | 28.21 | 8.38 | 13.60 | 3.86 | 10.28 | 1.52 | 3.52 | 1.08 | 0.19 | 0.34 | 3.13 | 1.64 | 3.96 |
| CaO | 0.09 | 0.93 | 0.02 | 12.62 | 42.95 | 7.52 | 11.12 | 10.92 | 3.11 | 0.24 | 0.39 | 0.22 | 1.18 | 2.53 | 1.26 | 2.49 |
| $Na_2O$ | 0.22 | 3.35 | 0.22 | 0.003 | 0.001 | 0.14 | 0.16 | 0.14 | 0.34 | 0.45 | 0.31 | 0.22 | 2.87 | 1.24 | 2.18 | 1.17 |
| $K_2O$ | 3.75 | 3.84 | 4.54 | 0.03 | 0.01 | 0.08 | 0.21 | 0.08 | 3.61 | 6.19 | 3.67 | 0.23 | 4.58 | 3.54 | 3.18 | 2.51 |
| $P_2O_5$ | 0.07 | 0.19 | 0.07 | 0.10 | 0.04 | 0.09 | 0.06 | 0.13 | 0.09 | 0.13 | 0.07 | 0.02 | 0.06 | 0.16 | 0.18 | 0.14 |
| $SO_3$ | 0.01 | 0.00 | 0.00 | 0.03 | 0.11 | 0.01 | 0.07 | 0.09 | 0.05 | 0.01 | 0.01 | 0.00 | 0.02 | 0.01 | 0.02 | 0.00 |
| $Cr_2O_3$ | 0.02 | 0.02 | 0.02 | 0.00 | 0.00 | 0.00 | 0.01 | 0.00 | 0.02 | 0.03 | 0.02 | 0.01 | 0.01 | 0.00 | 0.00 | 0.01 |
| NiO | 0.02 | 0.02 | 0.01 | 0.01 | 0.01 | 0.01 | 0.01 | 0.01 | 0.01 | 0.01 | 0.01 | 0.01 | 0.01 | bdl | bdl | bdl |
| $H_2O^-$ | 0.24 | 0.04 | 0.54 | 1.07 | 0.03 | 0.31 | 1.20 | 1.37 | 0.03 | 0.04 | 0.27 | 0.10 | 0.02 | bdl | bdl | bdl |
| LOI | 4.02 | 2.49 | 4.01 | 18.54 | 35.64 | 7.36 | 10.00 | 10.38 | 3.80 | 3.16 | 2.78 | 0.20 | 1.16 | 1.15 | 1.15 | 1.20 |
| **Total** | 99.27 | 99.01 | 99.10 | 99.24 | 99.92 | 98.85 | 99.34 | 99.01 | 99.20 | 99.68 | 98.99 | 99.12 | 99.37 | 98.20 | 99.20 | 99.20 |
| CIA | 78.69 | 66.63 | 82.28 | 14.20 | 2.35 | 17.87 | 15.75 | 11.62 | 53.94 | 71.63 | 68.37 | 56.91 | 58.68 | 56.12 | 61.33 | 56.67 |
| WIP | 45.59 | 73.67 | 41.08 | 110.22 | 132.65 | 58.58 | 42.17 | 58.16 | 45.98 | 67.08 | 37.96 | 5.12 | 69.33 | 56.60 | 54.88 | 49.36 |
| VIR | 4.20 | 2.81 | 6.25 | 0.05 | 0.02 | 0.08 | 0.16 | 0.07 | 2.39 | 5.60 | 7.37 | 1.77 | 3.84 | 1.87 | 2.69 | 1.39 |
| ICV | 1.22 | 0.99 | 0.86 | 21.49 | 50.80 | 13.39 | 7.90 | 16.58 | 1.55 | 1.21 | 0.89 | 1.90 | 0.90 | 1.39 | 1.00 | 1.61 |
| $Al_2O_3/K_2O$ | 4.00 | 4.22 | 4.89 | 65.23 | 75.90 | 21.04 | 10.31 | 17.52 | 2.29 | 2.81 | 2.58 | 3.81 | 2.67 | 2.64 | 3.30 | 3.22 |
| $Al_2O_3/TiO_2$ | 15.90 | 14.21 | 22.30 | 24.46 | 32.53 | 29.80 | 32.93 | 23.96 | 20.37 | 21.45 | 21.69 | 21.83 | 58.17 | 56.06 | 62.97 | 57.74 |
| $K_2O/Al_2O_3$ | 0.25 | 0.24 | 0.20 | 0.02 | 0.01 | 0.05 | 0.10 | 0.06 | 0.44 | 0.36 | 0.39 | 0.26 | 0.37 | 0.38 | 0.30 | 0.31 |

* ICP-MS data extracted from Rift Valley Resources database was used for classification and comparative purposes.

bdl – Below detection limit.

**Table 4**: Trace element composition of the selected samples of Cassenha Hill Prospect.

| | Mudstone | | Breccia | Carbonate-rich rock | | Sandstone | | | Siltstone | | | Quartzite | | Granite | | |
|---|---|---|---|---|---|---|---|---|---|---|---|---|---|---|---|---|
| **PPM** | SVS-101 | SVS-102 | SVS-122 | SVS-807 | SVS-808 | SVS-809-810 | SVS-812-813 | SVS-814-815 | SVS-805-806 | SVS-811 | SVS-801-802 | SVS-803 | SVS-009 | CHD013_81* | CHD013_82* | CHD013_83* |
| Nb | 9 | 14 | 11 | bdl | bdl | bdl | bdl | 22 | 5 | 13 | 7 | bdl | 11 | 5.1 | 6.3 | 4.5 |
| Zr | 132 | 183 | 127 | 15 | 11 | 44 | 54 | 39 | 88 | 147 | 125 | 23 | 90 | 54 | 67.2 | 49.8 |
| Y | 28 | 26 | 18 | 14 | 14 | 17 | 10 | 17 | 16 | 23 | 20 | 12 | 16 | 9 | 10 | 8.1 |
| Sr | 47 | 65 | 37 | 64 | 67 | 19 | 20 | 111 | 75 | 38 | 34 | 16 | 119 | 78.1 | 85 | 50.6 |
| Rb | 220 | 238 | 249 | bdl | bdl | bdl | 12 | bdl | 149 | 292 | 187 | 11 | 229 | 179 | 170 | 156 |
| Pb | 12 | 12 | 15 | 9 | 7 | 5 | 1 | 7 | 8 | 10 | 10 | 5 | 18 | 9 | 12 | 9 |
| Zn | 61 | 46 | 59 | 71 | 41 | 21 | 16 | 19 | 10 | 24 | 11 | 12 | 10 | 21.6 | 15.5 | 24.7 |
| Cu | 985 | 917 | 1610 | 238 | 78 | 6 | 27 | 28 | 2 | 6 | 19 | 68 | 2 | 53.7 | 36.5 | 148 |
| Ni | 29 | 56 | 24 | 12 | bdl | bdl | 5 | 10 | bdl | 31 | bdl | bdl | bdl | 12.6 | 9.4 | 13.7 |
| Co | 20 | 45 | 32 | 16 | bdl | 10 | bdl | 5 | bdl | 18 | bdl | bdl | bdl | 8.7 | 5.9 | 11.4 |
| Cr | 141 | 175 | 199 | 27 | 24 | 67 | 101 | 112 | 162 | 134 | 174 | 104 | 125 | 29.1 | 22.1 | 39.5 |
| V | 120 | 174 | 133 | 23 | 14 | 8 | 17 | 48 | 63 | 99 | 52 | 10 | 23 | 21.1 | 25.8 | 13 |
| F | 829 | 648 | 548 | 895 | 471 | 534 | 833 | 706 | 492 | 612 | 632 | 319 | 598 | bdl | bdl | bdl |
| S | 269 | 268 | 268 | 296 | 491 | 284 | 316 | 325 | 354 | 278 | 290 | 277 | 299 | bdl | bdl | bdl |
| Cl | 104 | 109 | 148 | 147 | 143 | 109 | 119 | 103 | 107 | 114 | 113 | 103 | 105 | bdl | bdl | bdl |
| Sc | 21 | 22 | 27 | 15 | 33 | 11 | 15 | 14 | 13 | 21 | 9 | 2 | 9 | 6.9 | 6.6 | 5.1 |
| Ba | 1685 | 749 | 1908 | 991 | 4 | 4 | 48 | 870 | 288 | 810 | 491 | 16 | 693 | 346 | 400 | 224 |

* ICP-MS data extracted from Rift Valley Resources database was used for classification and comparative purposes.

bdl – below detection limit.

## 5.4. *Weathering in the Source area*

The chemical and mineralogical composition of siliciclastic-sediments or rocks is hugely affected by the weathering processes taking place at the source area (Taylor and McLennan, 1985). The depletion of alkali and alkali earth elements, and the consequent enrichment of other elements, especially $Al_2O_3$, observed in the chemistry of some siliciclastic sediments are often used as indicators of weathering in the source area (Harnois, 1988). The degree of depletion and enrichment of such elements can be quantified by using two parameters, which are calculated using molar proportions, one developed by Nesbitt et al. (1980), namely, the chemical index of alteration (CIA) and the other one developed by Parker (1970), namely, the Weathering Index of Parker (WIP).

(1) Chemical Index of Alteration (CIA) = $100[Al_2O_3/ (Al_2O_3+CaO^*+ Na_2O + K_2O)]$,

(2) Weathering Index of Parker (WIP) = $(100) \times [2Na_2O/0.35) + (MgO/0.9) + (2K_2O/0.25) + (CaO/0.7)$,

Where CaO* is the amount of CaO contributed by silicate minerals in the system (Nesbitt and Young 1984). CIA values are calculated using molar proportions. A CIA index >92 indicates intensive weathering, resulting in feldspars transformation into clay minerals (Potter et al., 2005; Gonzalez et al., 2017). CIA values between 60 and 80 indicate intermediate weathering, and CIA <60 indicates very low intensity of weathering (Fedo et al., 1995; Gonzalez et al., 2017). In general, fresh basalts have CIA values ranging from 30 to 45, while fresh granites and granodiorites tend to have CIA values ranging from 45 to 55 (Nesbitt and Young, 1984; Fedo et al., 1995; Gonzalez et al., 2017). Lastly, kaolinites represent the highest degree of weathering and have CIA values of 100 (Gonzalez et al., 2017). On the other hand, the WIP takes into account the mobility of the major alkali and alkaline earth elements in respect to the strength of their bonding with oxygen. This is done by assessing the degree of transformation of feldspars into clay minerals (Parker,

1970; Gonzalez et al., 2017). As a general standard, the WIP values range from 0 to ≥ 100. In contrast with CIA values, low WIP values indicate high degree of weathering (Gonzalez et al., 2017).

Therefore, for comparative purposes the CIA and WIP values (Table 3) are often used together as indicators of the intensity of chemical weathering at the source area (Gonzalez et al., 2017). The chemistry of the rocks analyzed in this study show some variability in intensity of chemical weathering to which they have been subjected. This is evidenced by the disparity in the CIA values obtained from each of the analyzed rocks. For example, the breccia rock, with a CIA value of 82, represents the most altered/weathered rock in the collected samples, while the carbonate-rich rock with an average CIA value of 8.28 (14.20- 2.35), represents the least altered rock. Meta-mudstones have average CIA value of 72.66 (78.66-66.63), these values correspond to moderately to highly weathered/altered rocks. Meta-siltstones, granites and quartzites tend to be low to moderately altered, with average CIA values of 64.64, 58.71, and 56.91, respectively. Lastly, the meta-sandstones yielded CIA values ranging from 11.62 to 17.87 which are characteristic of siliciclastic rocks that have experienced weathering of relatively low intensity. The obtained WIP values are consistent with the CIA values, mainly for the breccia and carbonate-rich rocks. With average WIP values of 41.08 and 121.44, the breccia and carbonate-rich rocks represent the most and least altered rock from the analyzed samples. For the remaining lithologies, the WIP is somehow consistent and the values obtained are suggestive of moderate amounts of weathering at the source area.

The maturity of the Cassenha Hill rocks is also investigated in this study. This was achieved by using the Index of Compositional Variability (ICV) which was proposed by Cox et al. (1995). This index uses the estimation of abundance of alumina content compared to other major cations in siliciclastic rocks or sediments. In general, immature pelitic rocks, which are comprised of high content of non-clayey silicate minerals, tend to occur in active tectonic settings such as arc settings and/or rifting basins (Van de Kamp and Lake, 1985; Bokana, 2015), and have ICV values equal or greater than 1 ($\geq 1$) (Cox et al., 1995). On the other hand, mature pelitic rocks are often enriched in clay minerals, and are associated to relatively quiescent and/or cratonic enviroments (Weaver, 1989; Bokana, 2015), where sediment recycling and weathering are predominant. Such rocks tend to have ICV values much lower than 1 (<<1) (Cox et., 1995). The majority of the rocks analyzed in this study, have ICV values greater than 1 (>1). However, rocks such as meta-sandstones and carbonate-rich rocks have considerable higher average ICV values (36.15 and 12.62, respectively) when compared to other lithologies. Therefore, the ICV values suggest that the rocks of the Cassenha are immature and are derived from an active tectonic setting.

Overall, the analyzed metasedimentary rocks have experienced weak to intermediate chemical weathering, with a weathering trend towards the illite-muscovite composition that is characteristic of K-metasomatism, and are immature. The samples from borehole CHD013, which were used for comparative purposes, yielded similar results to the ones obtained from the samples collected in this study as shown in Figure 28.

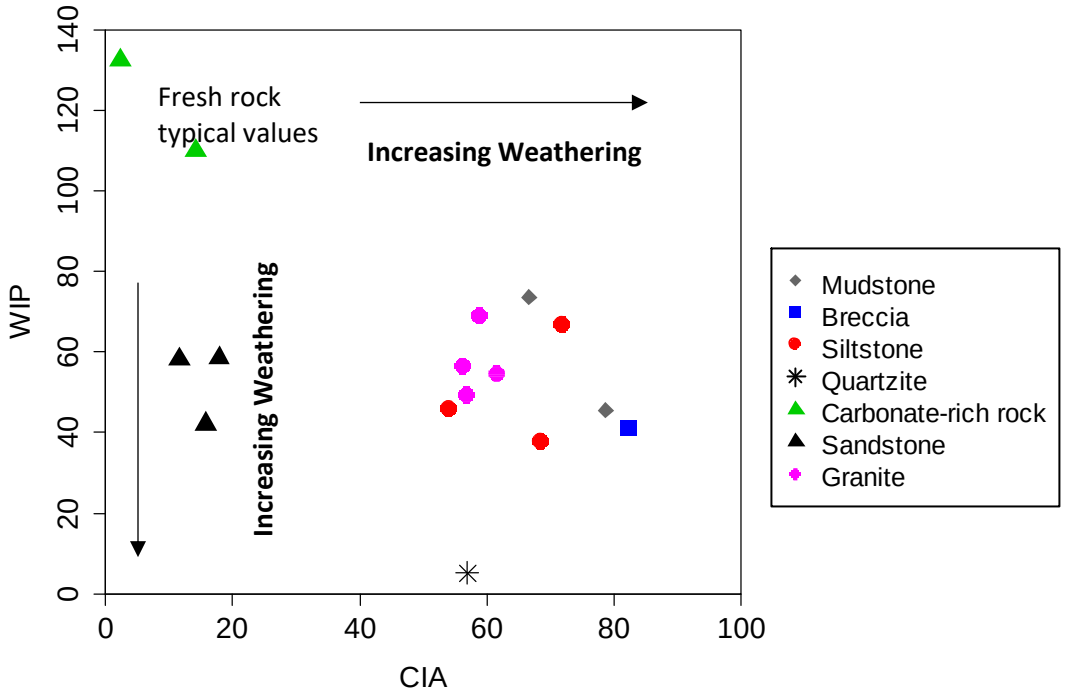
Fresh rock
typical values
Increasing Weathering
Increasing Weathering
WIP
CIA
0
20
40
60
80
100
120
140
0
20
40
60
80
100
Mudstone
Breccia
Siltstone
Quartzite
Carbonate-rich rock
Sandstone
Granite

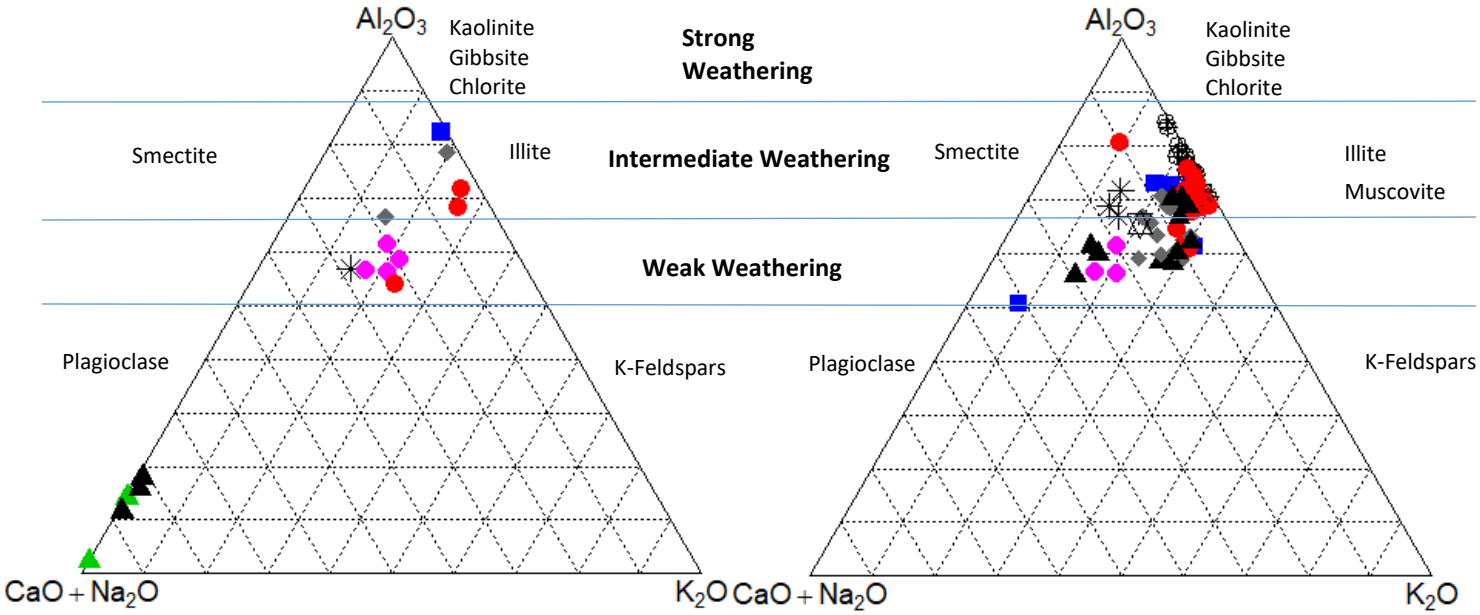
$Al_2O_3$
Kaolinite
Gibbsite
Chlorite
Strong
Weathering
Smectite
Illite
Intermediate Weathering
Weak Weathering
Plagioclase
K-Feldspars
$CaO + Na_2O$
$K_2O$
$Al_2O_3$
Kaolinite
Gibbsite
Chlorite
Smectite
Illite
Muscovite
Plagioclase
K-Feldspars
$CaO + Na_2O$
$K_2O$

**Figure 28**: **Top center**: Binary diagram displaying the relationship between two weathering indexes, WIP (Parker, 1970) and CIA (Nesbitt and Young, 1984) for the metasedimentary rocks collected from the Cassenha Hill Prospect. **Bottom Left**: A-CN-K diagram (after Fedo et al., 1995) for the samples collected at the Cassenha Hill prospect. **Bottom Right**: A-CN-K diagram (after Fedo et al., 1995) for the rocks from borehole CHD013 analyzed as part of RVR exploration program. Note the characteristic weathering trend towards the illite-muscovite composition.

### *5.4.1. Provenance*

The major and trace element composition of siliciclastic rocks can be used to infer the tectonic setting and the source rock/area composition (i.e., mafic and/or felsic source) from which the rocks are/were derived. A number of discriminant ratios and diagrams have been proposed for such purposes. Cox et al. (1995) $Al_2O_3/K_2O$ ratio is widely used as provenance indicator. This ratio takes into account the amount of clay minerals ($Al_2O_3/K_2O$ < 0.3) relative to the alkali feldspars ($Al_2O_3/K_2O$ = 0.4-10) in the rocks. Furthermore, Cox et al. (1995) suggested that rocks with $Al_2O_3/K_2O$ > 0.5 indicate maximum contribution of feldspars in the source area, while, $Al_2O_3/K_2O$ < 0.5 indicate slight contribution of feldspars in the provenance. The majority of the samples collected in this study have $Al_2O_3/K_2O$ values ranging from 2.29 to 4.89, which are suggestive of relatively maximum contribution of alkali feldspars in the source area. The carbonate-rich rocks and meta-sandstones, however, exhibit extremely high values of $Al_2O_3/K_2O$ (i.e., ranging from 65.23 to 75.90 in carbonate-rich rocks; and 10.1 to 21.04 in meta-sandstones), which suggest that alkali feldspar heavily contributed in their origin. The rocks of CHD013 yielded average $Al_2O_3/K_2O$ values of 3.12, thus indicating maximum contribution of alkali feldspars in their provenance, which are supportive to the results obtained from the rocks sampled in this study.

In order to determine the provenance of pelitic rocks, Girty et al. (1996) proposed the $Al_2O_3/TiO_2$ ratio. By using this ratio, Girty et al. (1996) were able to discriminate sediments derived from mafic igneous rocks ($Al_2O_3/TiO_2$ < 14) to the ones derived from the intermediate to felsic igneous precursors ($Al_2O_3/TiO_2$ = 19-28) (Bokana, 2015). The examined rocks have a collective $Al_2O_3/TiO_2$ ranging from 14.21 to 32.93 with an average of 23.57. These values suggest that the sampled rocks are likely to be originated from a source of felsic to intermediate composition. The rocks of CHD013 yielded average $Al_2O_3/TiO_2$ values of 24.04, thus indicating that the Cassenha Hill rocks are/were originated from a source with a dominant felsic to intermediate composition, which is also supportive to the results obtained from the rocks sampled in this study.

The trace element data obtained in this study have some limitation in the number of analyzed elements (i.e., Th, Sc, La, Hf). Therefore, for the use of discriminant ratios that predominantly use such trace elements, the ICP-MS data from exploration borehole CHD013 will be used. The Th/Co and La/Sc ratios (after Cullers, 2002) are often used to discriminate between a mafic and a felsic source for siliciclastic rocks. In general, rocks that yield Th/Co values of > 0.3 and La/Sc > 0.7 are predominantly derived from a source of felsic composition, while, rocks with La/Sc < 0.4 are often associated with mafic sources (Gonzalez et al., 2017). The examined rocks have average Th/Co and La/Sc values of 0.55 and 3.25 respectively, which suggest that these rocks are derived from a source with a dominant felsic composition. These results are in agreement to the ones obtained from the major elements ratios, which also supported a felsic provenance.

## 5.5. *Rare earth elements*

The rare earth elements (REE) composition of the Cassenha Hill prospect was characterized using the ICP-MS trace element data of boreholes CHD008, CHD009, CHD011, and CHD013, generated by the RVR exploration program. The samples were first plotted by rock type for borehole CHD013, which is the only borehole logged in this study that successfully intersected granitic rocks (Figs. 29 and 30), and posterior as a whole rock group (plotted as the REE composition of a sample collected at a specific borehole depth) versus REE atomic number for boreholes CHD008, CHD009, and CHD011 (Fig. 30).

The chondrite-normalized patterns of the granitic rocks of the Cassenha Hill prospect are shown in Fig. 29. The granitic rocks are characterized by having predominant light REE (LREE) enrichment and heavy REE (HREE) depletion and relatively uniform REE fractionation with $\sum LREE_N$ values ranging from 49.87 to 74.72 (ave. = 65.65), $\sum HREE_N$ values ranging from 14.06 to 15.94 (ave.= 15.85), and $\sum LREE_N / \sum HREE_N$ of 4.14. Furthermore, the rocks tend to exhibit small negative Eu anomalies and small variation in the REE profile. The Chondrite-normalized LREE enrichment is evidenced by ($La_N/Yb_N$ ratio = 12.19 – 17.22, ave. = 13.63), and the HREE depletion is expressed by ($Gd_N/Yb_N$ ratio = 1.88 – 2.66, ave. = 2.19). In addition to this the granitic rocks have $La_N/Lu_N$ average values of 12.76. These results support the evidence of an intermediate to felsic composition precursor, which was obtained from the major and trace element data results. Although at relatively lower concentration, the REE elements in the granitic rock tend to display similar patterns to the metasedimentary counterparts (Fig. 29).

The Chondrite-normalized REE patterns of the metasedimentary rocks occurring in the Cassenha Hill prospect are shown in Figs. 29 and 30. The rocks are LREE enriched, and exhibit negative and positive Eu anomalies. The Gd and Ho anomalies might be due to analytical error, however, they are taken into account in this study. The negative Eu and Ho anomalies are observed in some of the rocks of boreholes CHD008 and CHD011 and are accompanied by positive Gd anomalies, meanwhile, rocks of the boreholes CHD009

and CHD013 tend to display positive Eu anomalies. The rocks of boreholes CHD008 and CHD011 exhibit a relatively uniform REE fractionation when comparing to the rocks in boreholes CHD009 and CHD013. Furthermore, three (3) distinct set of rocks can be observed in the diagrams, (1) Typical LREE enriched and HREE depleted rocks, which represent the majority of the samples; (2) Rocks which are characteristically depleted in both LREE and HREE; and (3) rocks which are characteristically enriched in both LREE and HREE when compared to the average rock types.

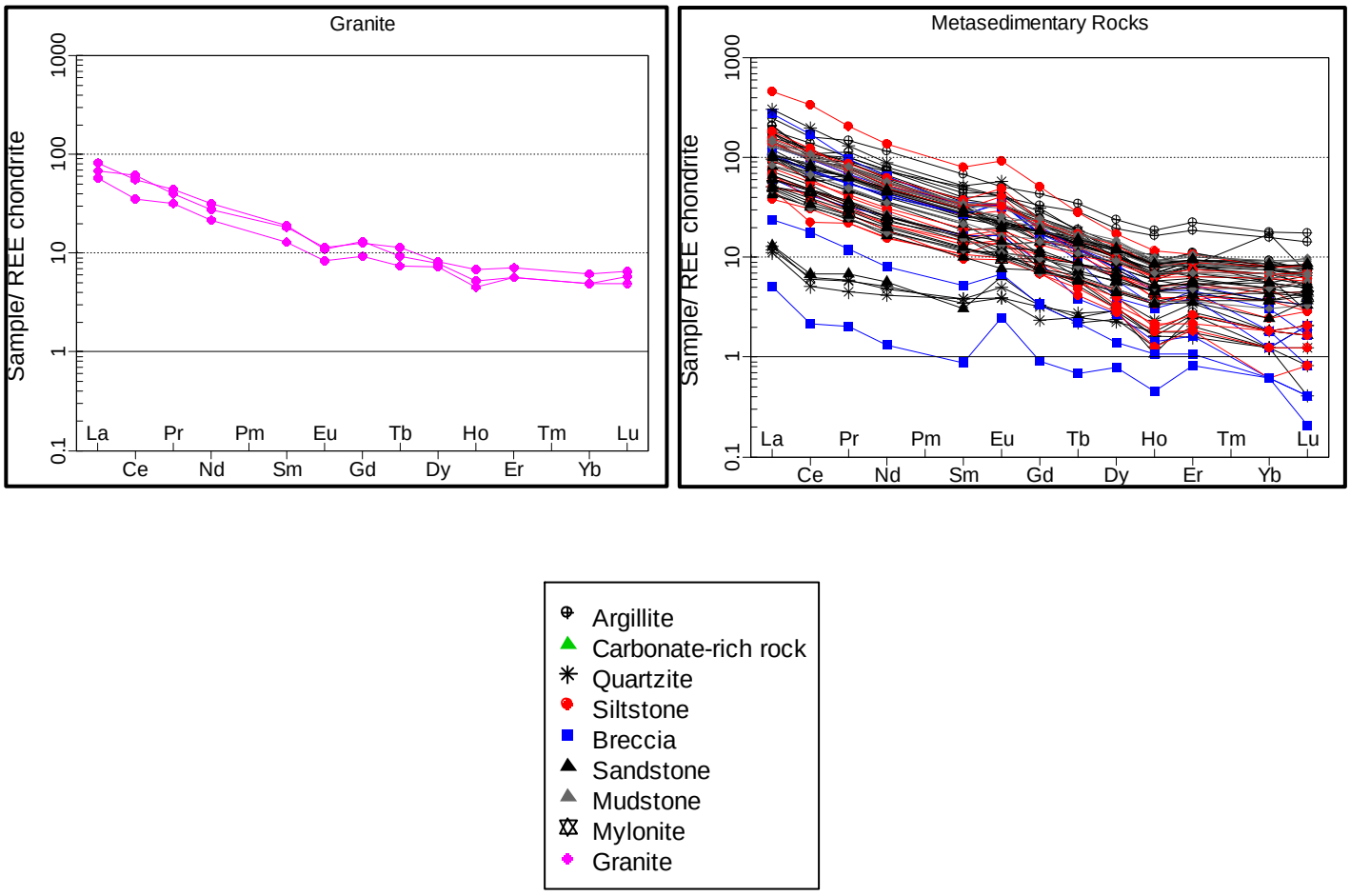


**Figure 29**: Chondrite-normalized rare earth element (REE) pattern for granitic rocks **(Left)** and metasedimentary rocks (**Right**) from borehole CHD013. Note the predominant LREE enrichment and HREE depletion diagrammatic pattern. Normalization factors were taken from Anders and Grevesse (1989).

The Cassenha Hill metasedimentary rocks (Figs. 29 and 30) exhibit slight variations in their REE pattern, with their chondrite -normalized pattern displaying LREE enrichments ($La_N/Yb_N$ ratios ranging from 3.81 to 71.16 in CHD008; 1.37 to 45.19 in CHD009; 5.83 to 25.94 in CHD011; and 7.41 to 153.26 in CHD013) and depletion in HREE ($Gd_N/Yb_N$ ratio ranging from 1.28 to 5.93 in CHD008; 1.30 to 11.38 in CHD009; 1.63 to 3.21 in CHD011; and 1.34 to 14.64 in CHD013). Moreover, the rocks have average $La_N/Lu_N$ values of 15.65 in CHD008, 14.86 in CHD009, 11.45 in CHD011, and 29.48 in CHD013. These values, together with the patterns observed in the diagrams, support a common source of origin and that not much granite was available in the source.

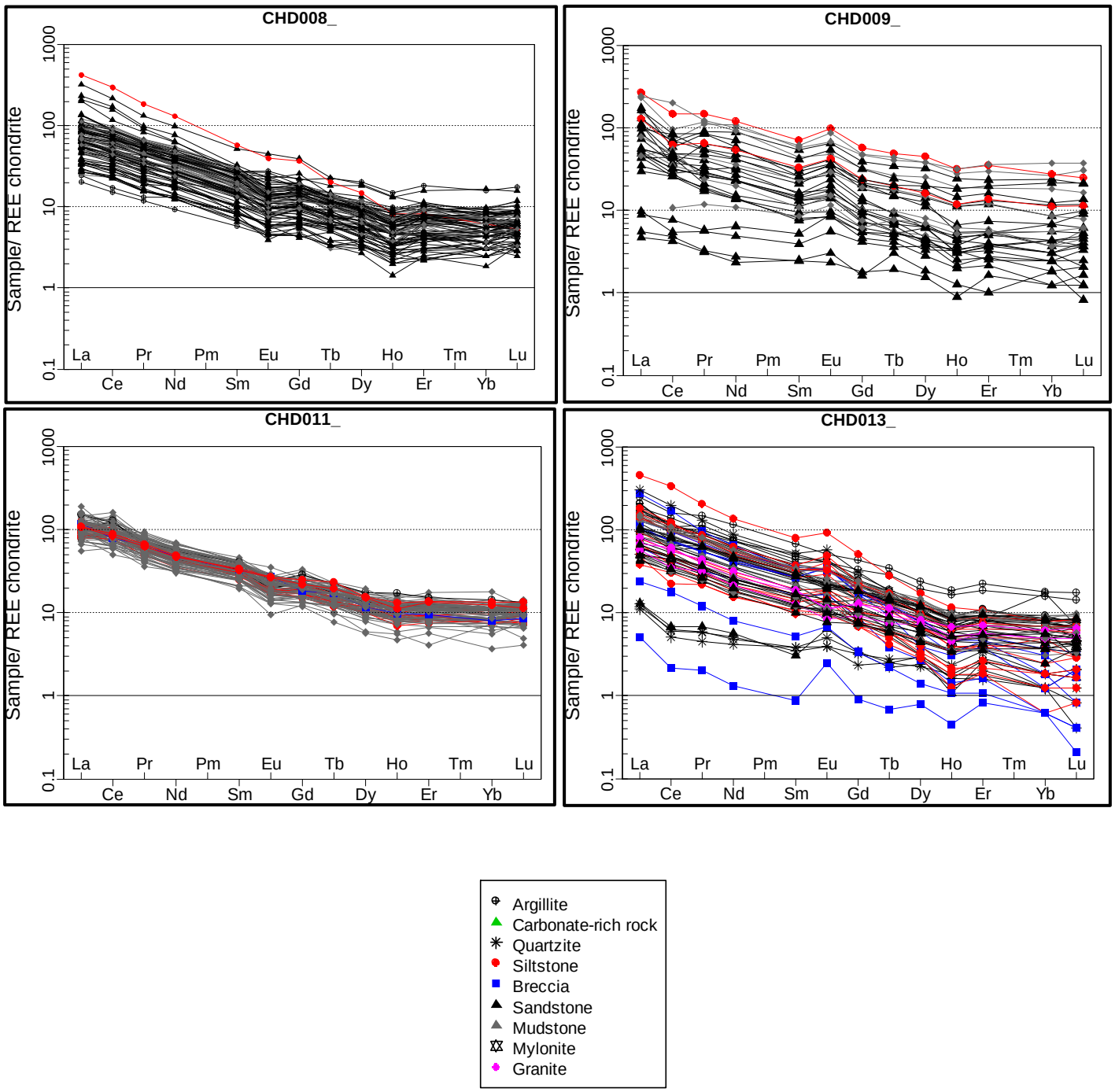


**Figure 30**: Chondrite-normalized rare earth element (REE) patterns for all of the major rocks occurring at Cassenha Hill prospect plotted by borehole. Note the predominant LREE enrichment and HREE depletion diagrammatic pattern. Normalization factors were taken from Anders and Grevesse (1989).

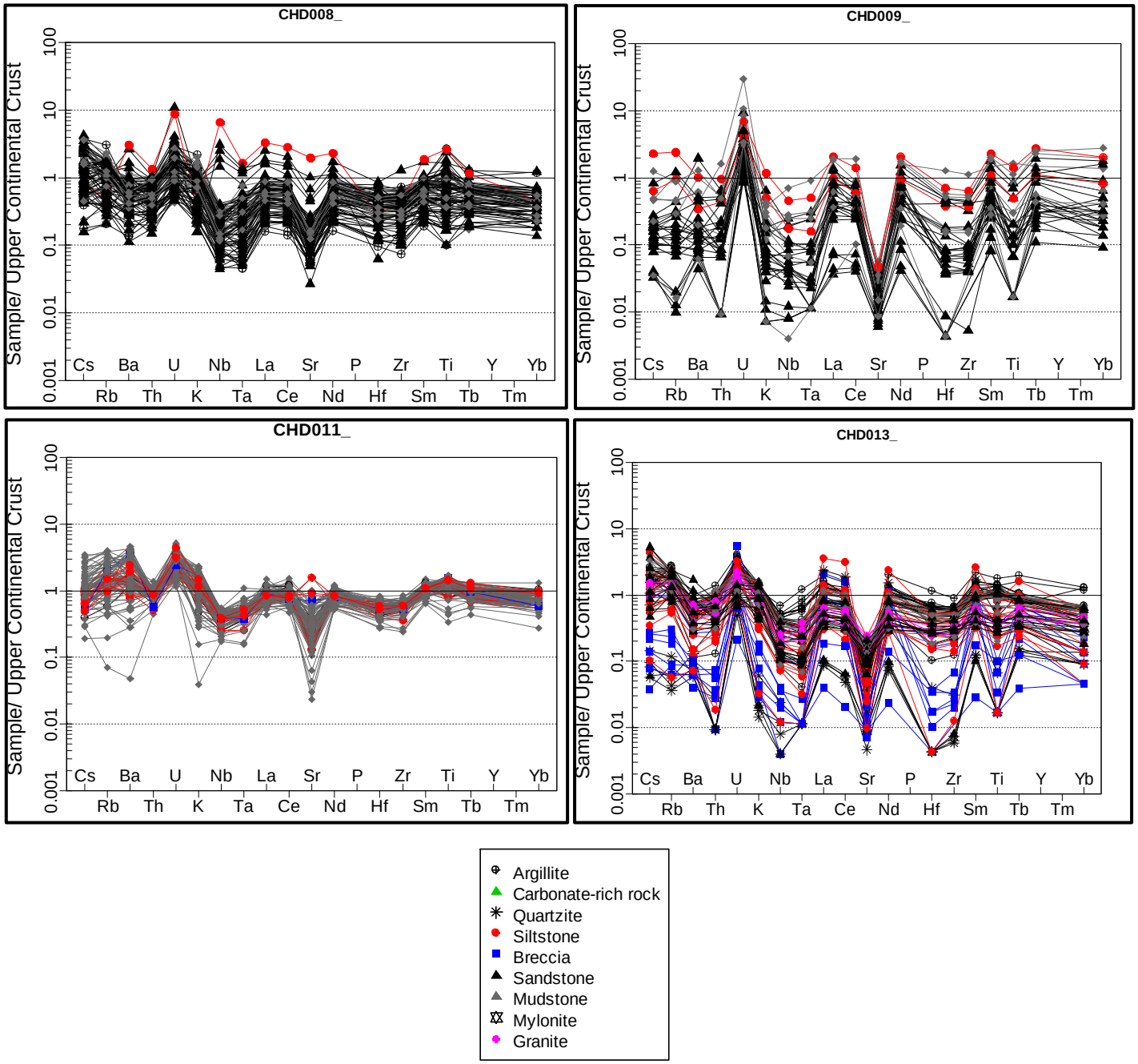


**Figure 31**: Upper continental crust-normalized trace element pattern for all major rocks occurring at Cassenha Hill prospect. Normalization factors were taken from Taylor and McLennan (1995).

All major rocks have also been investigated by using multi-element distribution patterns observed in spider diagrams. The elements have been arranged in the order proposed by Taylor and McLennan (1995) and normalized to upper continental crust (UCC) values (Fig. 31). The diagrams exhibit a predominant negative anomaly pattern in high field strength elements (HFSE) Zr, Hf, P, Ta, Ti, Th and Nb in majority of the rock types. However, Nb and Ti tend to display dual pattern of occurrence as they seem to be relatively enriched in some rocks compared to others. U represents the only HFSE element relatively enriched compared to UCC concentration. On the other hand, the rocks of the Cassenha Hill prospect are characteristically enriched in large ion lithophile elements (LILE) K, and Ba, while being strongly depleted in elemental Sr. The occurrence of Rb and Cs is highly variable as they are preferentially enriched in some rocks and depleted in others.

### **5.6.** *Tectonic Setting*

Sedimentary rocks tend to exhibit geochemical characteristics that allow them to be typified and/or associated to a specific tectonic setting in which the sedimentation processes took place (Bhatia, 1983, 1985; Roser and Korsch, 1988; McLennan and Taylor, 1991; Gonzalez et al., 2017). Major and trace elements ratios have also been widely used for distinguishing tectonic settings at which rocks are/were derived. Bhatia (1983) proposed four main tectonic settings responsible for the origin of sedimentary rocks, (1) Passive Margins (PM); (2) Active Continental Margins (ACM); (3) Continental Island Arc (CA); and (4) Oceanic Island Arc (OIA). In order to place each rock to its tectonic setting based on geochemical affinities, Bathia (1983) proposed the $TiO_2$ and the ($Fe_2O_3$ + MgO) ratios in weight percentage (Wt%). By applying these ratios to rocks collected in this study (Fig.32), it can be observed that most of rocks are likely to have been derived from passive margins tectonic settings, whereas, some of the rocks, namely, meta-mudstone, meta-siltstone and breccia, plot in between active continental margins and continental island arcs. On the other hand, rock samples from borehole CHD013, demonstrate two distinct

geochemical affinities. The majority of the rock samples plot in the passive margin tectonic field, while the other rocks samples preferentially plot on the continental island arc tectonic field, with some samples even plotting in the oceanic island arc field. As the major oxides tend to be relatively mobile during the sedimentation processes, their present-day composition might not be representative of the processes that took place at the source area (Bhatia, 1983). Therefore, in order to mitigate this uncertainty, trace elements (i.e., Th, Y, REE, Zr, Hf, and Sc) are often used to compare and/or verify the results obtained using the major element geochemistry due to their relatively lower mobility (Bhatia, 1983).

The trace element composition of the rocks from borehole CHD013 show a projection trend towards the continental island arc (CIA) and passive margins (PM) fields (Fig.32). It further suggests that there are two distinct group of rocks as mentioned earlier. One predominantly derived from passive margin tectonic setting and the other one from active continental margins-continental island arc settings.

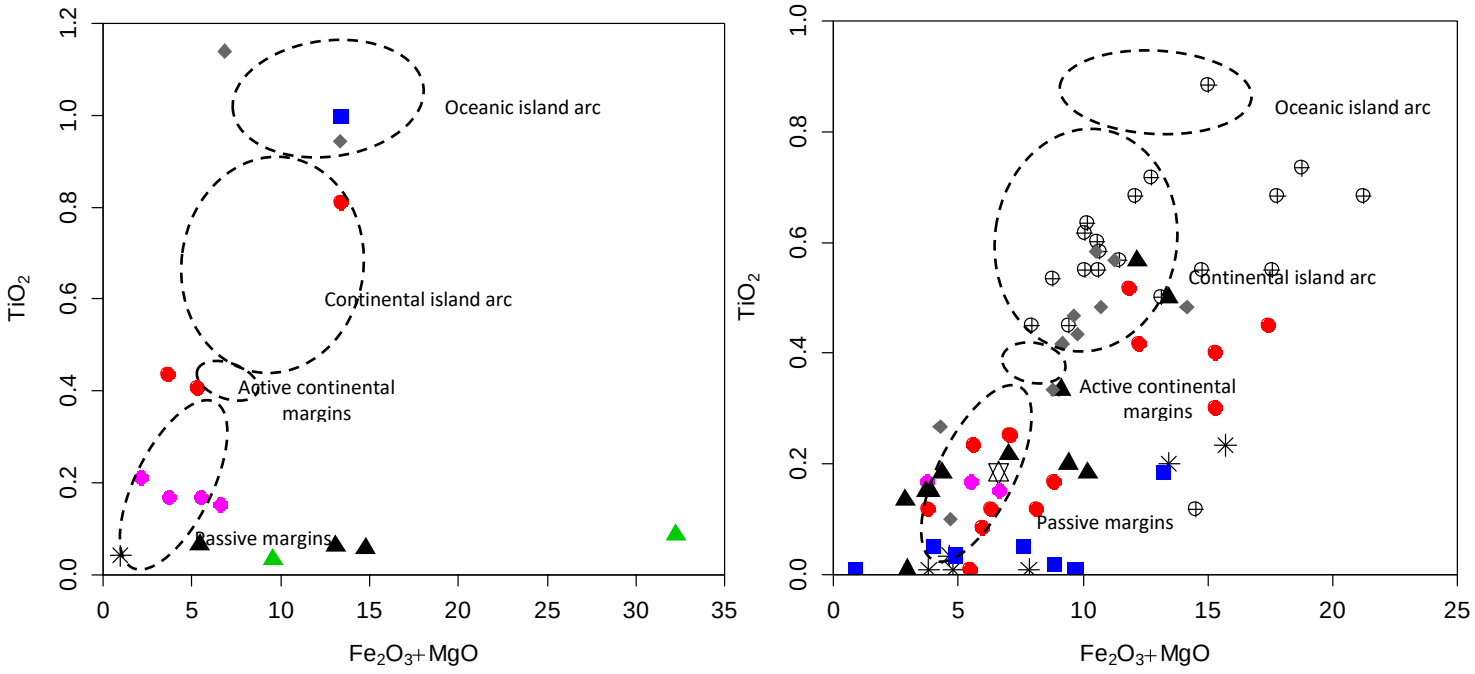

**Figure 32**: Comparative tectonic settings discriminant diagrams. **Left**: $Fe_2O_3$+MgO vs $TiO_2$ discriminant diagram using the rock samples examined in this study (after Bhatia, 1983). **Right**: $Fe_2O_3$+Mgo vs $TiO_2$ discriminant diagram using the rocks from borehole CHD013 (After Bhatia, 1983).

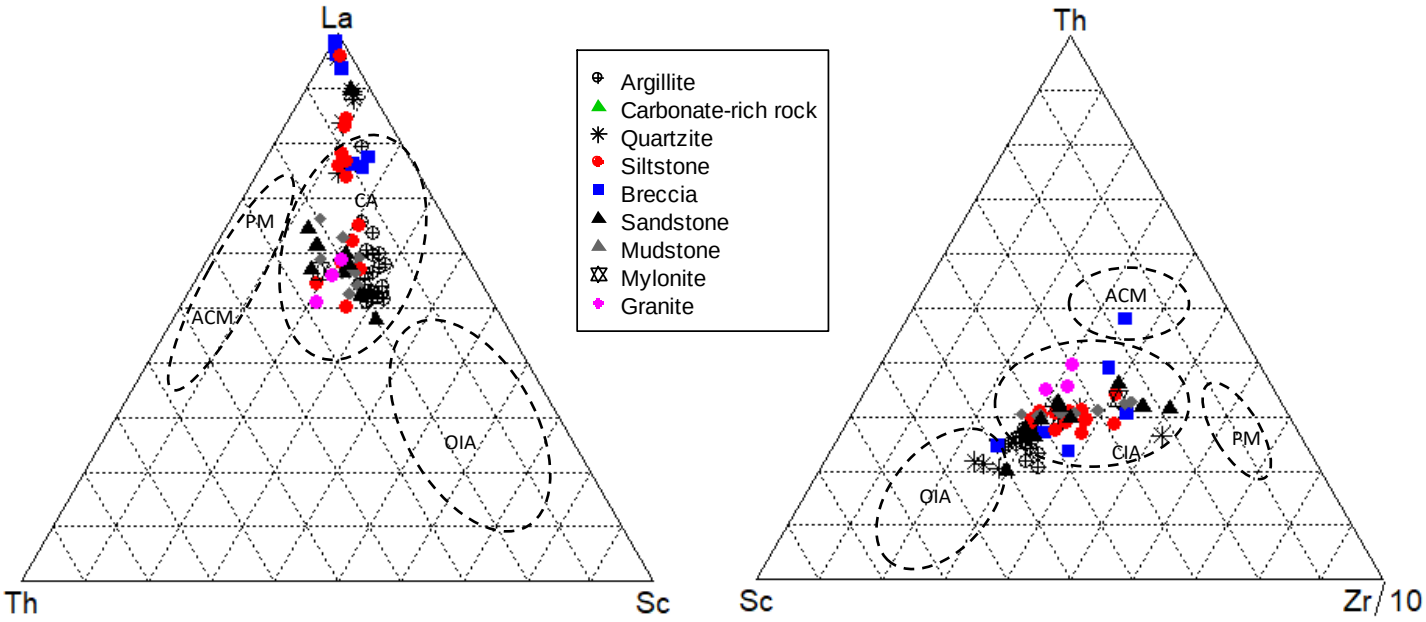


**Figure 33**: Comparative tectonic settings discriminant diagrams (Cont.) **Left**: Th-La-Sc tectonic discriminant diagram using the rocks from borehole CHD013 (after Bhatia and Crook, 1986). **Right:** Sc-Th- Zr/10 tectonic discriminant diagram using rocks from borehole CHD013 (after Bhatia and Crook, 1986).

## 5.7. Oxygen, Hydrogen, and Carbon Isotopes

### 5.7.1. Introduction

Stable isotopes have been widely used in the study of ore-forming processes. Their usefulness relies on the fact that the commonly analyzed isotope ratios are of elements (i.e., H, C, O, and S), which are major constituents of Earth reservoirs (i.e., water, air, lithosphere, and organic matter). Furthermore, variations in isotopic compositions tend to take place in elements that are stable in a wide range of temperatures, and occur in different phases such as solid, liquid and vapour phases. As a general rule, higher isotope ratios are present in the solid phase, where the molecular bond is stronger, rather than in co-existing liquid/vapour phases. The heavier isotopes are also commonly concentrated in molecules where they are at the maximum oxidation state (Hoefs, 1987). The differences in isotope ratio between co-existing substances are determined by calculating the fractionation factor of isotopes using the equation 1 below.

$$\alpha_{A-B} = R_{A/}R_B \qquad (3)$$

Where R is the isotope ratio of interest in substance A or B. The value of $\alpha$ is usually very close to 1 and, generally, has the form of 1.00XX.

In this study, O, H and C isotope analyses were conducted on whole-rock samples, quartz veins, carbonates, and chlorites with a primary goal of inferring the source and temperature of the hydrothermal fluid, the temperature of mineralization, and lastly, the extent of fluid mixing.

### 5.7.2. Oxygen and Carbon Isotopes

Oxygen isotope values are reported with reference to the Standard Mean Ocean Water (SMOW) and are calculated using the equation below:

$$\delta^{18}O\ ‰ = \left[\frac{\left[\left(\frac{^{18}O}{^{16}O}\right)sample - \left(\frac{^{18}O}{^{16}O}\right)SMOW\right]}{\left(\frac{^{18}O}{^{16}O}\right)SMOW}\right] \times 1000 \quad (4)$$

The Oxygen Isotope ($\delta^{18}O$) value of fluids in the Earth's (Fig. 35) crust varies substantially. In general, seawater has a $\delta^{18}O$ value of 0‰, fluids of magmatic origin have $\delta^{18}O$ values ranging from +5 to +8‰, and meteoric waters have $\delta^{18}O$ values ranging from -15 to 0‰ depending on geographic location. The $\delta^{18}O$ values of whole-rock of the selected samples of the Cassenha Hill Prospect and the results are shown in Table 5. The overall Isotopic composition ranges from +7‰ to +12.4‰. The meta-sandstones have $\delta^{18}O$ value ranging from +9.7‰ to +12.4‰. The meta-siltstones have $\delta^{18}O$ values ranging from +7.1‰ to +11.2‰. The carbonate-rich rock has $\delta^{18}O$ values ranging from +7.1‰ to +10.1. The meta-mudstones have yielded $\delta^{18}O$ values between +7‰ and +8.9‰. The quartzite, breccia and granite have $\delta^{18}O$ values of +12‰, +8.8‰, and +8.5‰, respectively.

The analyzed quartz veins are comprised of two separate phases, and have yielded $\delta^{18}O$ values ranging from +12.81‰ to +13.85‰, while the $\delta^{18}O$ of carbonates is +17.55‰ ($\delta^{13}C$ = -5.5). The isotopic composition of the quartz veins and carbonate are relatively similar suggesting that they formed from the same fluid and at similar temperatures.

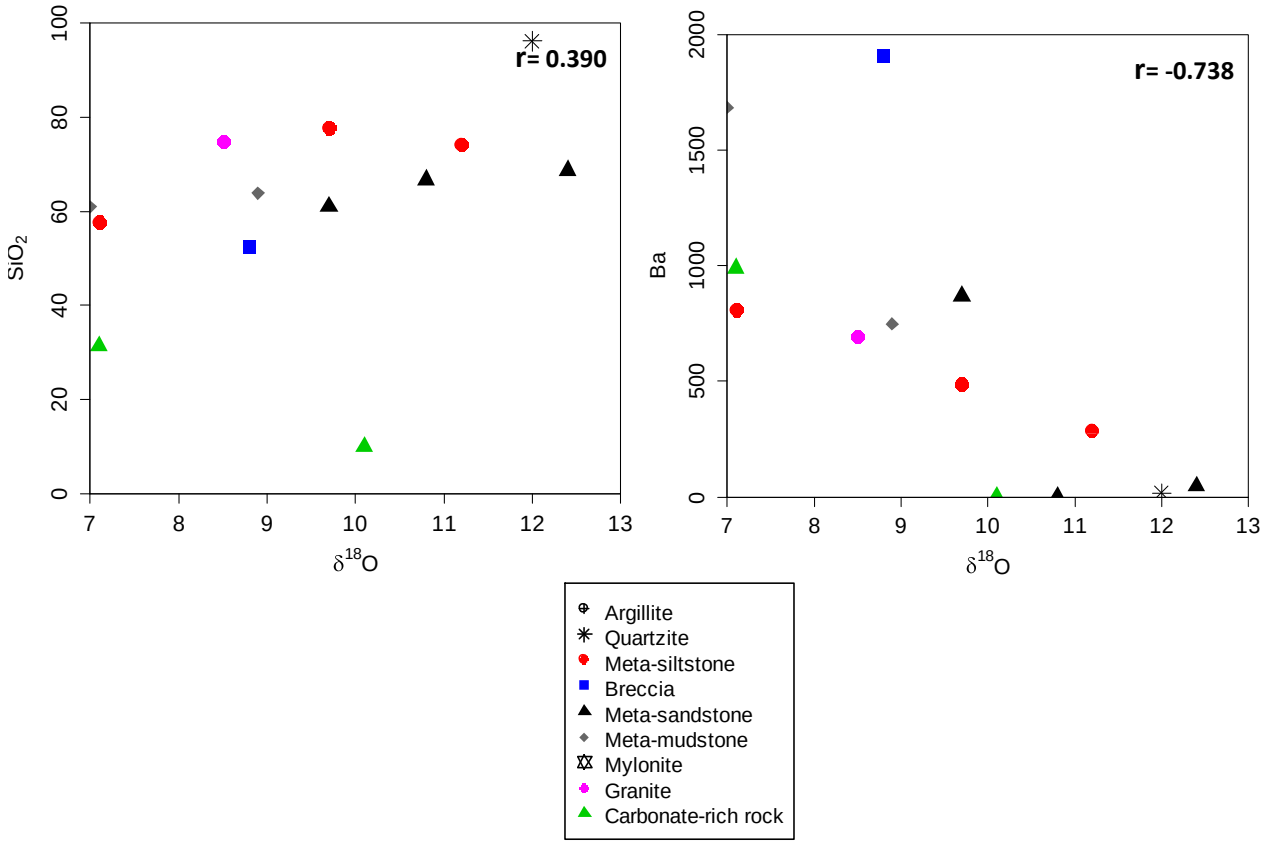


**Figure 34:** Bivariate plots of $SiO_2$ and Ba versus $\delta^{18}O$ for whole rock samples.

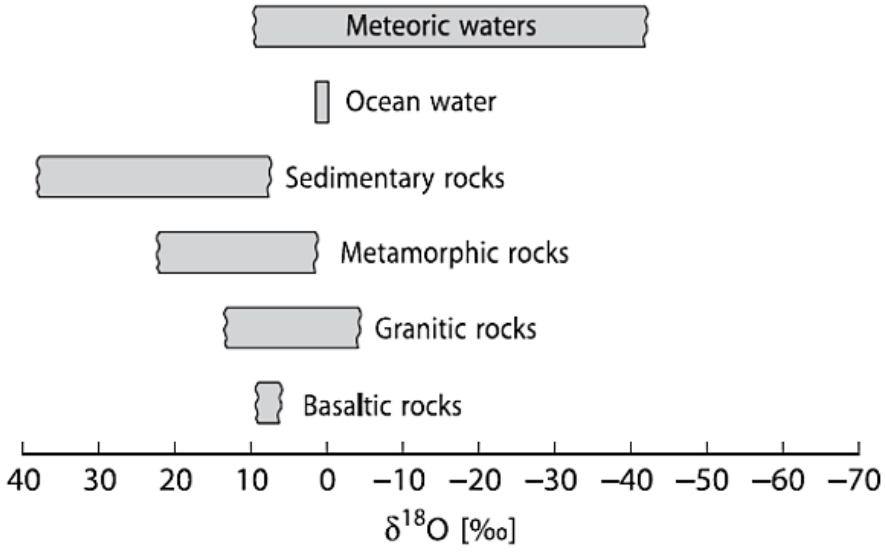


**Figure 35**: $\delta^{18}O$ values of important geological reservoirs (after Taylor 1974).

### 5.7.3. Hydrogen Isotopes

The δD values and water content of the analyzed chlorites are shown in Table 6. The chlorite grains were extracted from the meta-siltstones, meta-mudstones, and brecciated rocks occurring at near surface depths (i.e., < 87.08m). The δD values range from -56 to -45‰. The chlorite from meta-mudstone (SVS 101) has δD value of -45‰ which is slightly enriched in deuterium compared to all other analyzed chlorite minerals. The measured $H_2O^+$ concentrations vary between 2.17 – 5.39 wt.%, and occurs at its maximum on the chlorite extracted from the breccia rock. The water content is well correlated with the hydrogen isotope data (r= -0.914, n= 4) (Fig. 36).

The significance of the strong correlations between the water content and chlorite δD values is limited by the small dataset of the analyzed samples (n = 4). Therefore, additional data would be required to develop a meaningful conclusion from the dataset. However, the obtained data is used in the discussion for the assessment of the probable source of the mineralizing fluids as the 10% variation is not significant.

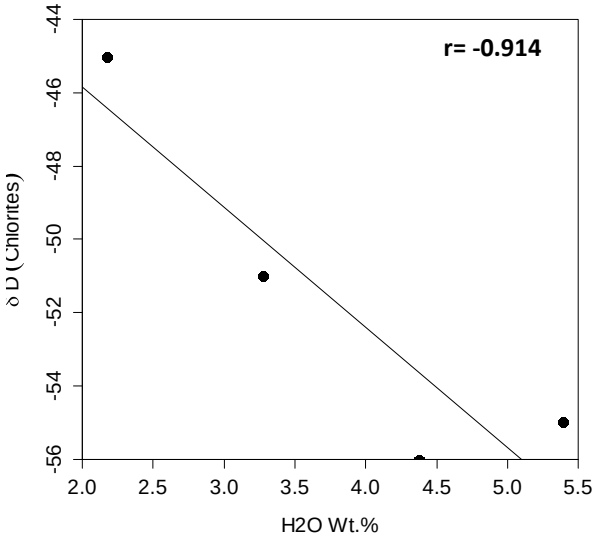


**Figure 36:** Variation of δD values vs measured water content in Wt.%. The solid line represents the best fit line among the samples.

**Table 5**: Stable isotope composition of the analyzed samples of the Cassenha Hill Prospect.

| Sample ID | Rock Type | $\delta^{18}O$ | $\delta^{13}C$ | $\delta D$ | Wt.% $H_2O$ |
|---|---|---|---|---|---|
| **SVS 814-815** | Meta-sandstone | 9.7 | | | |
| **SVS 809-810** | Meta-sandstone | 10.8 | | | |
| **SVS 812-813** | Meta-sandstone | 12.4 | | | |
| **SVS 805-806** | Meta-siltstone | 11.2 | | | |
| **SVS 811** | Meta-siltstone | 7.1 | | | |
| **SVS 801-802** | Meta-siltstone | 9.7 | | | |
| **SVS 807** | Carbonate-rich rock | 7.1 | | | |
| **SVS 808** | Carbonate-rich rock | 10.1 | | | |
| **SVS 101** | Meta-mudstone | 7 | | | |
| **SVS 102** | Meta-mudstone | 8.9 | | | |
| **SVS 803** | Quartzite | 12 | | | |
| **SVS 122** | Breccia | 8.8 | | | |
| **SVS 009** | Granite | 8.5 | | | |
| **SVS 121a** | Quartz vein | 13.25 | | | |
| **SVS 121b** | Quartz vein | 13.53 | | | |
| **SVS 814-15** | Quartz vein | 12.81 | | | |
| **SVS 808** | Carbonate | 17.66 | -5.54 | | |
| **SVS 811** | Chlorite | | | -51 | 3.27 |
| **SVS 101** | Chlorite | | | -56 | 4.38 |
| **SVS 102** | Chlorite | | | -45 | 2.17 |
| **SVS 122** | Chlorite | | | -55 | 5.39 |

- Bulk rock by conventional fluorination has one (1) decimal place.
- Quartz by laser fluorination has two (2) decimal places.

## 5.8. Source of fluids

The probable source of infiltrating fluids at the Cassenha Hill prospect has been evaluated by assessing the $^{18}O/^{16}O$ ratio of quartz veins and carbonates, and by assessing the D/H ratio of chlorites. The values obtained for each mineral separate is shown in Table 5. The $\delta^{18}O$ values (SMOW) for quartz veins range from +12.81‰ to +13.53‰, whereas the carbonates have yielded a $\delta^{18}O$ value of +17.55‰ (SMOW) ($\delta^{13}C$= -5.54‰). The δD values of chlorite range from -56‰ to -45, and the water content ranges from 2.17 to 5.39 Wt.%. The results obtained from the quartz veins and carbonates mineral separates are similar. This similarity is consistent with them forming from the same fluid at similar temperatures. Therefore, assuming fluid-rock interaction took place at ≈ 350°C, based on the presence of quartz, the fluid would have had a $\delta^{18}O_{H20}$ values of around +8‰, which are typical of magmatic waters. On the other hand, δD values of chlorite indicate a more evolved and external water source, which at a temperature of ≈ 350°C, and with the difference between chlorite and water being -33.5‰, such fluids should have had $\delta D_{H20}$ value of about -20‰. These values are similar to those observed in meteoric waters (Taylor, 1974), thus suggesting that the Cassenha Hill prospect fluid contained a significant component of meteoric water, which might explain the supergene characteristics of the mineralization at which high influx of meteoric waters is required. However, it is worth noting that the analyzed chlorite minerals were extracted from near surface metasedimentary rocks, and do not represent the earliest formed chlorite minerals (i.e., in igneous rocks), which could possibly have yielded magmatic $\delta D_{H20}$ values.

The difference between the $\delta^{18}O_{H20}$ values of fluids in quartz-carbonate (i.e., +8‰) and $\delta^{18}O_{H20}$ of chlorites (i.e., -4‰) suggests the following: (1) Two different water reservoirs, and possible interplay/mixing between them (i.e., magmatic and meteoric waters); and (2) The water is ultimately of meteoric origin but exchanged with hydrogen-poor magma/rock, so that the δD are unchanged, whereas the $\delta^{18}O$ increases due to exchange with the rock. The magmatic $\delta^{18}O$ of the ore-fluids could either reflect a direct magmatic

association or be the result of extensive high-temperature isotopic exchange between meteoric waters and surrounding rocks, possibly as response of granitoid intrusion. Such exchange may have been originated from the late stage of magma cooling and is believed to be the carrier of $Cu^{+}$, which initially precipitated as copper sulfides (i.e., chalcopyrite and chalcocite) when interacted with more predominant meteoric waters due to a drop in temperature and salinity and/or shift in pH (Norman et al., 1976). It is believed that during such interactions, the proportion of magmatic fluids was minimal and less influential when compared to the meteoric counterparts. The latter is believed to have played a major role in the genesis of the prevalent Cassenha Hill mineralization. This is supported by the occurrence of shallower depth mineralization (< 1Km) and copper oxides, which are originated by leaching of $Cu^{2+}$ from the source by circulating meteoric waters. Field characteristics suggest that these fluids have circulated throughout the system with aid of shallow to deep penetrating NW-SE trending fractures in which copper oxides have precipitated. Therefore, The Cassenha Hill prospect represents a hydrothermal system at which the influx of meteoric waters was a carrier and agent of precipitation of $Cu^{2+}$ at favorable conditions with relatively minor contribution of magmatic waters, instead, the circulation was possibly driven by the heat generated by the granitic intrusion.

# 6. CHAPTER VI

## DISCUSSION, CONCLUSIONS AND RECOMMENDATIONS

### 6.1. Discussion

#### 6.1.1. Introduction

The occurrence of Cu-Au mineralization at the Cassenha Hill prospect and the relatively poor understanding on the characteristics of the various rock types (i.e., host and barren rocks), their source/provenance, and the origin and/or type of the fluid responsible for the mineralization is the rationale of this study. Therefore, this study attempted to characterize the rocks, focusing on the determination of the host lithologies, the sources of fluids present, and propose a genetic model for the prospect by relating its characteristics to well-known deposits that exhibit similar features.

#### 6.1.2. Rock types and their characteristics

The petrographic and geochemical studies undertaken on the selected rocks of the Cassenha hill prospect enabled the identification and/or classification of seven lithologies occurring in the area. Namely, granites, breccia, meta-mudstone, meta-siltstone, meta-sandstone, carbonate-rich rock and quartzite. Among these rocks, breccia and mudstone tend to show greater association with the mineralization, and are believed to be the host of the Cassenha Hill mineralization. However, samples from borehole CHD013 indicate that the mineralization can occur in all rock types, and is controlled by the degree of fractures and alteration occurring in a rock.

*The granitoids ($\delta^{18}O$= 8.5‰)*

The granitic rocks at the Cassenha Hill prospect occur as isolated plutons or as intrusions into the metasedimentary rock sequence. Macroscopically, such granitoids exhibit textures varying from equigranular to porphyritic, are fractured, partly oxidized, reddish brown to light brown, and are mostly composed of K-feldspars, quartz, biotite, chlorite, and iron-oxides. Jordana (1950) suggested that the granitoid plutons at Cassenha Hill prospect are predominantly porphyritic, which this study partly disagrees as most the observed granites are in fact equigranular. This assumption is supported by observed field characteristics and by the petrographic study, in which, the sampled granite exhibits textures ranging from hypidiomorphic to allotriomorphic, and crystals are mostly equigranular. The major and trace elements study suggests that the granitoids from the Cassenha Hill prospect are pera-metaluminous and have a typical "granite" composition, with alkalinity ranging from Calc-alkaline to high K-Calc-alkaline series, and are enriched in LILE elements. These characteristics, together with the calculated molecular $(Al_2O_3)/(Na_2O+K_2O+CaO)$ ratio suggest that the granitic rocks occurring in the study area are/were originated from the partial melting of sedimentary rocks and can be classified as S-type granites (Table 2). However, the same granitoids exhibit isotopic signatures (i.e., $\delta^{18}O$ = +8.5‰) that are typical of I-type granites, therefore, if the Cassenha granitoids are in fact originally S-type, there may have been some exchange with meteoric fluids. The positive correlation between Zr and Y, Nb, and Rb suggest that the same granites were originated from the same source and have undergone fractional crystallization. This is further supported by the characteristic LREE enrichment, small Eu depletion, observed in the chondrite-normalized REE diagrams (Figs. 29 and 30), which are typical of granites derived from a relatively homogeneous felsic precursor, and by the positive correlation between $\delta^{18}O$ and $SiO_2$ (Fig. 34) and the negative correlation between $\delta^{18}O$ and Ba (Fig. 34) which can be attributed to effects of fractional crystallization process thus supporting patterns observed in the trace elements Harker diagrams (Fig. 25). In general, fractional crystallization of a felsic melt involves the fractionalization of feldspars, mainly plagioclase

(Chappel and White, 1974), thus increasing Rb, Ga, Cs, and contrarily, decreasing Sr, Ba, Eu, as observed in the Cassenha Hill granites (Figs. 30 and 31). The uniformity between the REE composition of the granites and the metasedimentary rocks suggests that, in fact, the source rock was similar in composition as the country rock. Therefore, a hypothesis of equilibrium batch melting can be proposed for the genesis of the Cassenha Hill granitoids. If the granites were originated from partial batch melting, it should have a representative higher content of Zr, Ti, Cs, Mg, Ca, and Ba and should have mineral composition indicative of higher temperature crystallization (Holtz and Barbey, 1991; Antunes et al., 2008).

Field relationships are consistent with Cassenha Hill granites having intruded the pre-existing metasedimentary succession; however, no lithological contact could be observed in this study. Furthermore, the petrographic studies undertaken in the sampled rocks also show little or no evidence of contact metamorphism in the area. This is possibly due to the position of the analyzed samples in respect to the granitoid intrusion-metasedimentary rocks contact. The Cu content (i.e., 18 ppm) of the sampled granitic rock is relatively low suggesting that they do not host the mineralization. However, some of the granites, logged by RVR Geologists, have FeOx-rich fractures that are infilled by copper oxides (i.e., malachite and chrysocolla), and disseminated sulfides. Therefore, the hosting capability of the Cassenha Hill granites should not be fully disregarded.

*Metasedimentary rocks*

The metasedimentary rocks were intruded by the Cassenha hill granitoids at approximately 2.1 Ga (Carvalho et al., 2000). The contact between the granite and metasedimentary rocks could not be identified in this study, however, borehole CHD013 intersected granitic rocks at a depth of 81m, for 3m. It is believed that sample position, displacement, erosion and/or upliftment are among the possible causes of absence of gradational/abrupt visible contact. The metasedimentary rocks are characterized by

being highly oxidized, weakly to strongly fractured and comprise the majority of the rocks outcropping in the prospect (Fig. 5). In fact, the macroscopic appearance of the oxidation state of the rocks is expressively high that Aurum Exploration Services Geologists termed them as Banded Iron Formation (BIF). However, the petrographic and geochemical studies undertaken in the sampled rocks indicate that their $Fe_2O_3$ content is relatively low (i.e., 0.78 to 9.91 Wt.%) when compared to typical BIFs rocks (i.e., >25 Wt.%). Prior to this study, the nomenclature and characteristics of the Cassenha Hill rocks were quite controversial and debatable, mainly due to their high degree of alteration, oxidation, fracturing, and variable mineralogy.

*Breccias ($\delta^{18}O$= 8.8‰)*

Field, petrographic, and geochemical characteristics suggest that the Cassenha Hill breccias owe their origin to processes associated with the emplacement of intrusive magmas (i.e., phreatic-phreatomagmatic brecciation) and/or tectonism (i.e., tectonic breccias). The former is originated as a result of either (1) direct interaction between magmatic body and externally derived water source, and (2) as result of exposure of a magmatic heat flux upon an external water body, without any direct contact/interaction between the magma body and water source (Sillitoe, 1985; Tamas and Milesi, 2002). The latter is formed as response to high strain rates during the movement of faults in a brittle environment (Sillitoe, 1985). In fact, the two processes tend to be analogous rather than dissimilar as hydraulic fracturing and faulting are closely related and as tectonic displacements may trigger hydraulic fracturing. Generally, brecciation resulting from granitic emplacement takes place when there is a buildup of hydrostatic pressure underneath a local barrier of relatively low permeability due to ascending fluids, magmatic heating, and transmission of deeper fluid pressures to the barrier via a compressible cap of gas that separated and accumulated during boiling, and if such fluid pressure exceeds the lithostatic pressure and tensile strength of the rock (Facca and Tonani, 1967; Henley and Thornley, 1981; Sillitoe, 1985). If that is true, then the intrusion

of the Cassenha Hill granites into the metasedimentary rocks is somehow related to the brecciation stage, which possibly occurred in a form of hydrothermal explosion as a result of hydrofracturing. The high-pressure and high-temperature ascending fluid caused decompression of the fluid-filled fissures, and the subsequent destruction of the country rock, which, with progressive hydrofracturing widened the initial fissures to generate the breccia pipes/bodies. The hypothesis of a phreatic-phreatomagmatic origin of the Cassenha Hill breccias is evidenced by the whole rock and quartz veins $\delta^{18}O$ values of the breccia rock. Those values advocate an influence of predominantly magmatic waters, with minimal contribution of external water source in the genesis of the breccia bodies. Furthermore, characteristics such as dimension (< 1000 m in width), geometry (elongated lenses, pipe-like shape), depth of formation (< 1km), fragments (shape: sub-angular to rounded; composition: monolithic, mostly quartz fragments), matrix (matrix supported, 20 – 70% matrix), breccia-country rock contact (sharp contact, well defined) observed in the Cassenha Hill breccias, are typical of phreatic-phreatomagmatic originated breccias.

On the other hand, the proposition of tectonic-derived breccias should not be disregarded. In fact, the Cassenha Hill breccias exhibit characteristics which are commonly attributed to tectonic/fault breccias. Alternatively, a continuum between the various processes/stages of brecciation should be considered. A continuum hypothesis is widely supported by the various brecciation stages observed at the prospect, which are indicative of various tectonic reactivations. Furthermore, it is worth noting that the emplacement of the Cassenha Hill granites took place in a syn-tectonic extensional regime rather than orogenic as indicated by the trace element data. Such regimes tend to occur in shear zones where fault/tectonic breccias are prone to develop. The characteristic NNW-SE, NW-SE, and W-E strike orientation of the breccia structures, which are related to NW-SE trending regional shear zone (Aurum Exploration Services, 2007), further indicates that their genesis is somehow related to tectonism and/or fault propagation, and the occurrence of predominantly quartz cement with angular fragments (i.e., 2 to 20 mm in size) indicates hydraulic brecciation of the country rock, therefore a major role of

Si-rich fluids thus supporting the continuum between phreatic-phreatomagmatic and tectonic processes as responsible for the genesis of the Cassenha Hill breccias. In summary, the textural and crosscutting relationships suggest the following: (1) Period of faulting and cataclasis as response of the regional shearing; (2) extensive silicification of the fractures; (3) Episodes of brittle fracturing concurrently with circulation of Si-rich fluids possibly originated from the granitoid intrusion causing hydrothermal hydraulic brecciation when mixing with meteoric waters (4) Various tectonic reactivations resulting in the brecciation of the country rock (late breccias). Therefore, the Cassenha Hill breccias can be genetically classified as a continuum between hydrothermal and tectonic processes.

*Other metasedimentary rocks*

The bulk rock composition of the meta-sandstones ($\delta^{18}O$= 10.96‰) and carbonate-rich rocks ($\delta^{18}O$= 8.6‰) indicate that the both are the least weathered in the study area. These results, however, contrasts with the ones obtained in the petrographic study, where, it could be observed that the carbonate-rich rocks are moderately to highly altered with carbonate and talc alteration being the main alteration behaviors. The contrast observed in meta-sandstones is possibly due to their textural and compositional maturity discrepancies. The meta-sandstones in the study area tend to be compositionally immature and texturally mature as observed in the geochemical and petrographic study, respectively. Compositionally, the meta-sandstones and carbonate-rich rocks are enriched in CaO and $Na_2O$ and depleted in $Al_2O_3$, and plot in the weakly weathered field of the A-CN-K diagram (Fig. 28).These evidences, together with the brittle characteristics observed in the petrographic study, suggest that the meta-sandstones and carbonate-rich rocks have predominantly experienced mechanical rather than chemical weathering.

The meta-siltstone ($\delta^{18}O$= 9.3‰) analyzed in this study are weakly to moderately weathered as observed in the A-CN-K diagram (Fig. 28). Petrographically, the meta-siltstones also do not display evidences of having experienced considerable weathering and are relatively poor in fractures.

As mentioned earlier, breccias and meta-mudstones *($\delta^{18}O$= 7.95‰)*, sampled in this study, are the rocks that show association with the mineralization. These rocks exhibit similar petrographic and geochemical characteristics. Petrographically, the breccias and meta-mudstones tend to be strongly fractured, moderately to highly altered (mainly chloritized), and vein-rich. The occurrence of opaque minerals, iron and copper oxides is also considerably higher in breccias and meta-mudstones (± 5-20 vol.%) when compared to other lithologies. However, due to their relatively fine grain sizes, some of the minerals could not be identified/seen microscopically. Such minerals predominantly occur within or at the edge of the fractures/veins and are in most cases associated with the occurrence of chlorite minerals. Furthermore, these minerals tend to be late and are believed to occur as replacement of pre-existing sulfides (i.e., pyrite and chalcopyrite). The replacement tends to takes place from the center to the rims. The relative higher content of $Al_2O_3$ in the breccia and mudstones indicate that these rocks have experienced a higher degree of weathering compared to other lithologies. This is further supported by the CIA and WIP alteration indices (Fig. 28), where the breccia and mudstone samples plot in the intermediate to strongly weathered compositional field. Therefore, these evidences suggest that the intensity of weathering and deformation is somehow correlated to the mineralization. Meaning that the mineralization is associated with the highly altered and fractured rocks. This characteristic association between mineralization and highly altered fracture-rich rocks and not to a specific rock type, is supported by the hosting capability demonstrated by the argillite, siltstone, and quartzite samples from borehole CHD013, which have yielded Cu concentrations values of > 10000 ppm (>1% Cu). This evidence suggests that the mineralization at Cassenha Hill is structurally rather than lithologically controlled. Furthermore, the results obtained in this study have not yielded any evidence

of gold (Au) mineralization as proposed by Jordana (1950) and Aurum Exploration Services (2007). This might be explained by either (1) the lack of Au-rich samples, (2) detection limit of the analyzing equipment, and/or (3) non-existence of considerable Au mineralization. Therefore, this study supports the hypothesis that the target mineralization at Cassenha Hill is mainly copper (Cu).

Overall, the petrographic and geochemical studies undertaken in the rocks of the Cassenha Hill prospect indicate the following: (1) The rocks are moderately to strongly fractured; (2) The rocks have experienced weak to moderate degrees of chemical weathering, however, the breccias and mudstones have been subjected to an higher degree of weathering; (3) The rocks are compositionally immature and originated from felsic precursors; (4) The rocks are sulfur-poor, and lack in sulfide minerals; (5) The rocks are enriched in LREE and LILE elements and depleted in HREE and HFSE elements; (6) The majority of the rocks have yielded results that associate them to continental island arc and/or active continental margins tectonic settings , while the minority are associated to passive margins; (7) Cu is the main target mineralization; (8) The mineralization is associated with chloritization and predominantly occurs within and/or at the edges of quartz/chlorite-rich veins/fractures and is not restricted to any rock type.

### 6.1.3. Alteration and Mineralization

***Alteration***

Alteration processes/behaviors are important indicators of mineralization as they can provide insight into the characteristics of hydrothermal systems (Mathieu, 2018). Generally, such processes/behaviors occur proximal to the ore thus providing a useful tool for vectoring towards the mineralization. The characterization of alteration enables the determination of mineralizing style (i.e., Porphyry, IOCG, Volcanic Massive Sulfide deposit, and others), while, the quantification provides an insight on the position of the sample within the hydrothermal system (Mathieu, 2018). Various methods have been devised in order to characterize the alteration processes/behaviors of hydrothermal systems. These include alteration indexes, mass-balance calculations and norms. Each of the methods have their limitations as they should take into account the composition of the protolith and mobility of elements (Mathieu, 2018).

The Cassenha hill rocks have experienced alteration of varying styles and intensities, among which, potassic alteration, sericitization, silicification, chloritization, and argillic alteration seem to be the most predominant. The geochemical studies indicate that the rocks in the study area have experienced weak-moderate to strong weathering, and that the mineralization is in fact associated with the intensely weathered/altered rocks. This section will typify and quantify the alteration processes taking place at the Cassenha Hill prospect by using the AI and Chlorite-carbonate-pyrite (CCPI) alteration indexes developed by Ishikawa et al. (1976) and Large et al. (2001), respectively. These alteration indexes, which are given in molecular proportions, consider mineralogical changes within the rock and the numbers are dimensionless and range from 0 (fresh rocks) to 100 (intensely altered rocks) (Mathieu, 2018).

$$AI = 100 \times (K_2O + MgO) / (K_2O + MgO + Na_2O + CaO) \quad (5)$$

$$CCPI = 100 \times (FeO^T + MgO) / (FeO^T + MgO + Na_2O + CaO) \quad (6)$$

Although these alteration indexes were primarily developed for Volcanic Massive Sulfide deposits (VMS) and volcanic rocks, they have demonstrated usefulness for the characterization of a variety of deposit types (Sharma, 2014).

The breccias and meta-mudstones, sampled in this study, have yielded average AI values of 97.28 and 78.57, respectively, and average CCPI values of 98.86 and 80.55, respectively. These values are typical of rocks that have been chloritized and are associated with the ore as observed in the AI-CCPI alteration boxplot (Fig. 36). These results are in agreement with the petrographic study, at which chloritization, mainly through the replacement of biotite by chlorites, shows strong association with the mineralization. This supported by the AI and CCPI values obtained from borehole CHD013 (i.e., IA ave. = 86.19 and CCPI ave. = 93.64). Furthermore, in order to properly understand the hydrothermal system, it is ideal to differentiate alteration processes/behaviors that are diagenetically originated from the hydrothermal counterparts. This is achieved by plotting the AI against the CCPI, where, one can clearly differentiate alteration originated as a result of hydrothermal fluids from the ones originated due to diagenetic processes (Fig. 36).

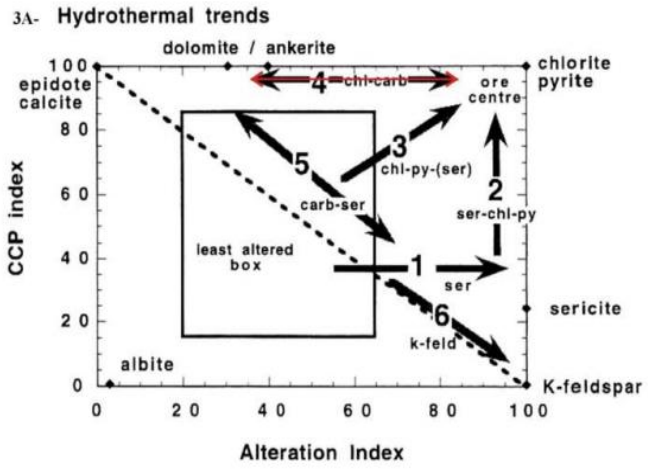


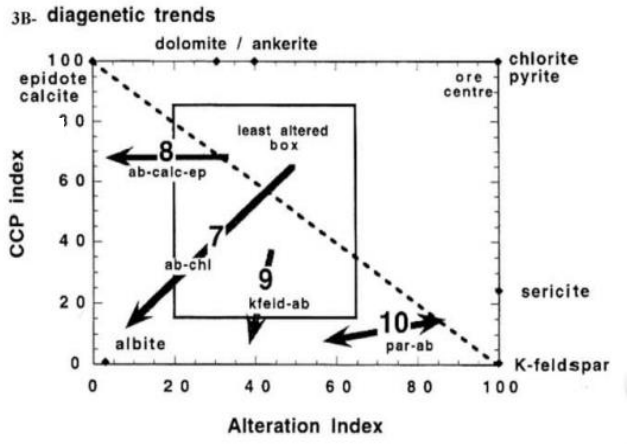

**Figure 37**: Alteration boxplot for differenciation between hydrothermally originated and diagenetically originated alteration trends (after Large et al., 2001; Sharma, 2014).

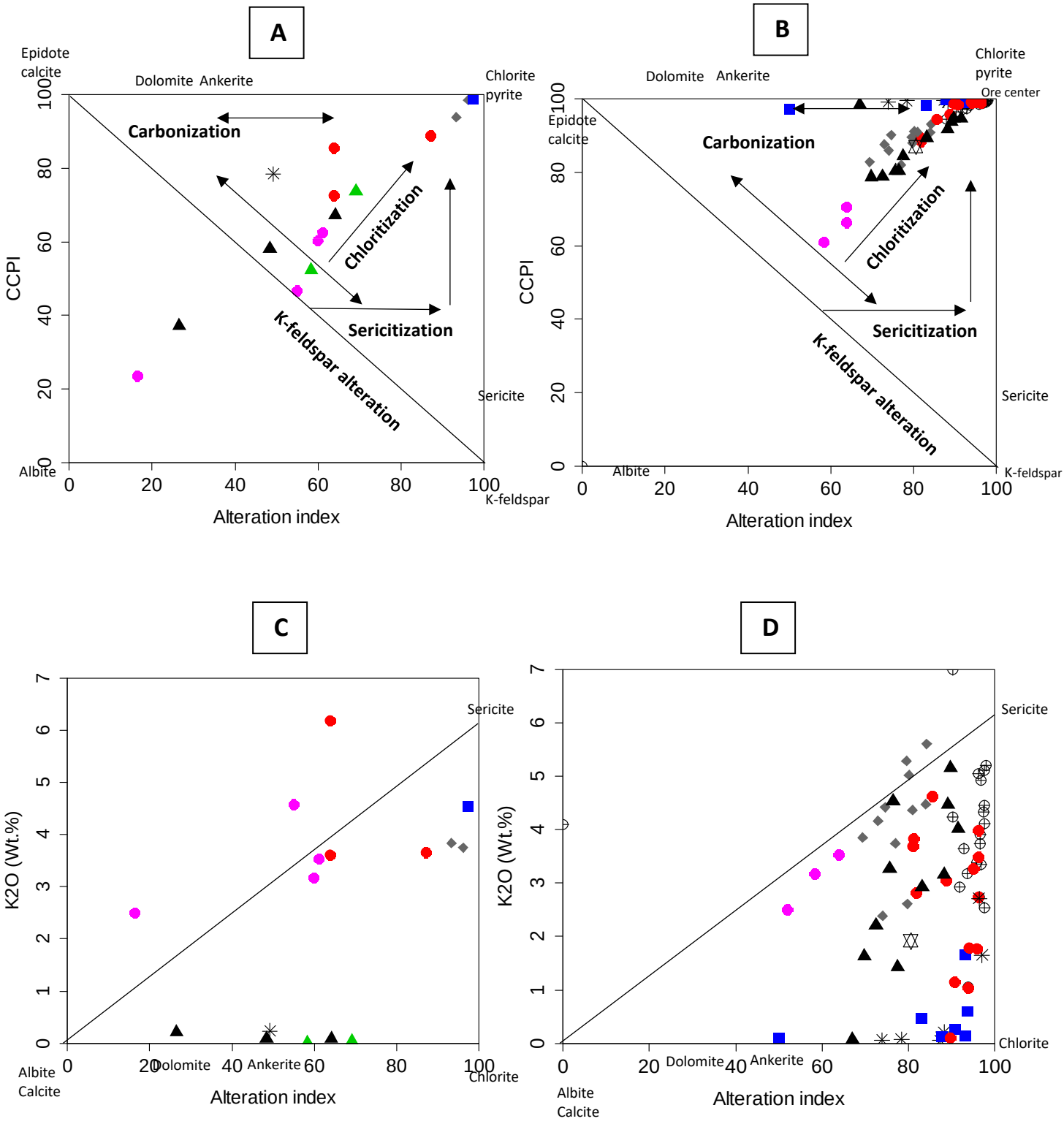

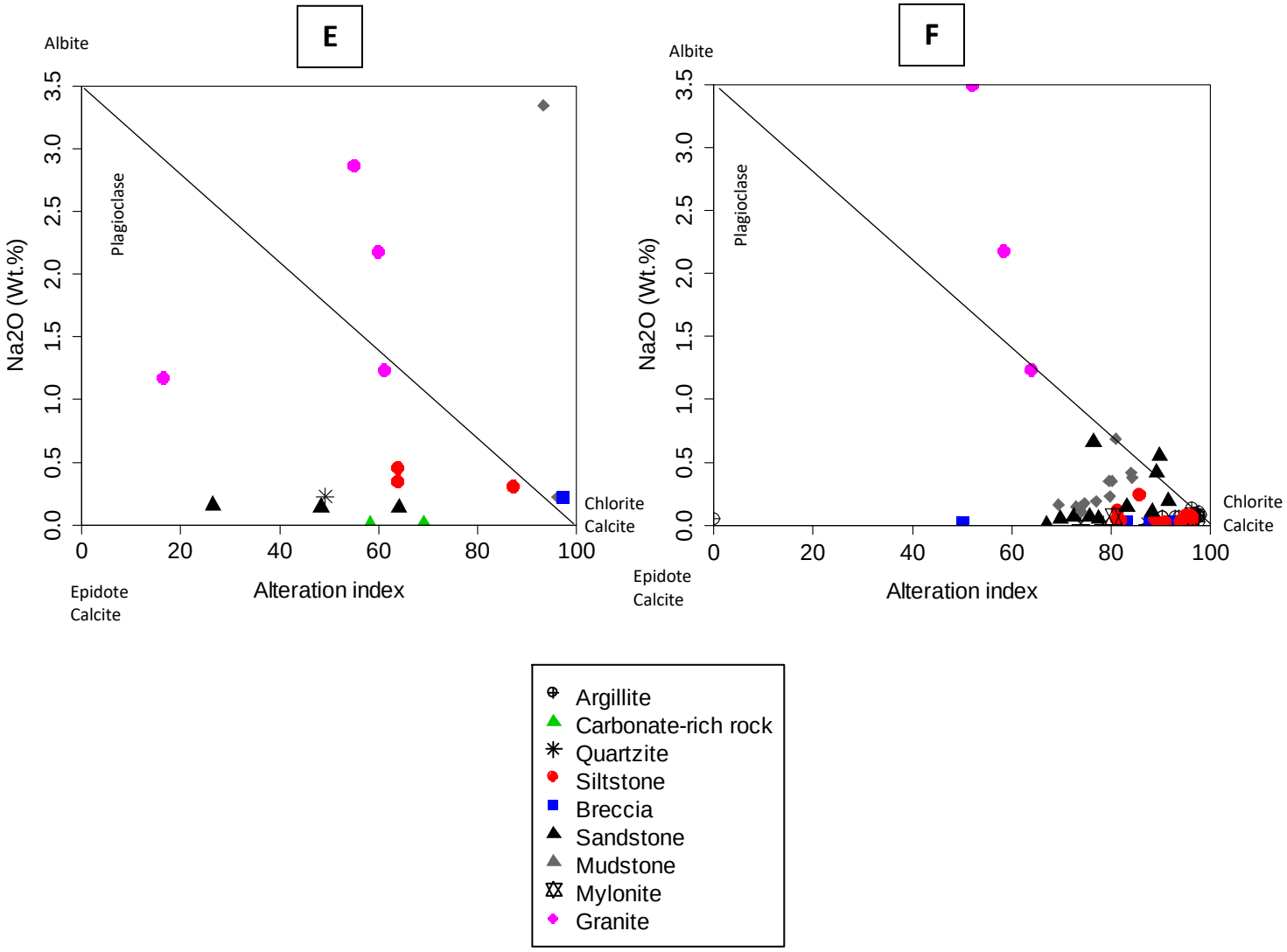


**Figure 38**: Alteration boxplots of selected rocks of the Cassenha Hill prospect and rocks from borehole CHD013. (**A**) Alteration box plot for the samples collected in this study; (**B**) Alteration boxplot for the samples in borehole CHD013; (**C**) $K_2O$ vs AI for the samples collected in this study; (**D**) $K_2O$ vs AI for the samples in borehole CHD013; (**E**) $Na_2O$ vs AI for the samples collected in this study; (**F**) $Na_2O$ vs AI for the samples in borehole CHD013

The trends obtained from the AI and CCPI indicate that all rocks occurring at Cassenha Hill prospect have been hydrothermally altered to some extent as illustrated in the AI-CCPI alteration boxplot (Figs. 36 and 37). It further suggests that diagenetic processes had little or no influence on the formation of alteration minerals as all the samples fall above the line of diagenetic field. The majority of the rocks follow the chlorite-sericite-pyrite alteration trend, thus confirming the pervasive chloritization behavior observed in the host rocks. Moreover, it can also be observed that the rocks that have experienced a higher degree of chlorite alteration plot at or near the predicted ore zone thus confirming their hosting characteristics. The chlorite-carbonate alteration trend can also be observed in some rocks of the borehole CHD013, this alteration behavior is reported to occur immediately adjacent to the ore (i.e., Massive sulfide deposits) at the footwall (Large et al., 2001). The AI vs $K_2O$ plot indicates that the host rocks are enriched in $K_2O$ and chlorite ± sericite, this suggests that K-metasomatism (replacement of Na-rich phases, primarily plagioclase, and formation of secondary minerals such as chlorite and calcite) was a predominant alteration behavior in the host rocks. K-metasomatism causes substantial modifications in the chemical composition of the hosts rocks, such as enrichment of $K_2O$ and Rb and depletion of $Na_2O$ and Sr as observed in the AI vs $Na_2O$ alteration plot and in the upper continental crust (UCC) spider diagrams (Fig. 31) (Shafiquallah et al., 1976; Ennis et al., 2000). Moreover, the occurrence of K-metasomatism is associated with downward percolating fluids. These fluids can be originated from various sources such as magmatic (Shafiquallah et al., 1976; Ennis et al., 2000), hydrogen metasomatized basement rocks from deep within a metamorphic complex (Glazner, 1988; Ennis et al., 2000), or from low temperature alkaline, saline aqueous systems within hydrologically closed basins (Ennis et al., 2000). The occurrence of hydrothermal chlorite, which is only stable at temperatures greater than 200$^{o}$c (Beaufort et., 2015), concurrently with K-metasomatism, suggests that the fluids responsible for the mineralization have temperatures > 200$^{o}$C. Such chlorites are originated by dissolution-crystallization and/or direct precipitation processes and are common in open systems, where fluid-rock interaction is considerably high (Beaufort et., 2015).

At Cassenha hill prospect, K-metasomatism is believed to have initiated in the granitoid at early stages of hydrothermal alteration, and is responsible for the replacement of plagioclase and quartz, to a lesser extent, by K-rich feldspars (microcline) and to a lesser degree of albite (Fig. 6). Moreover, it also believed that K- metasomatism has triggered the precipitation/fixing of hematite within the fractures as observed in the granitic samples. Continuous hydrolysis results in the breakdown of K-feldspars giving rise to sericite (sericitization) ± quartz, and release of $K^+$ ions, which in an open system may migrate and increase effects of K-metasomatism and silicification elsewhere. Consequently, silicification of the country rock has occurred, and is characterized by the precipitation of quartz along grain boundaries and transportation of the same to other sites of the system. Silicification is further observed as infilling of quartz within the fractures and/or in form of quartz veins. In the carbonate-rich rocks and vein-rich sandstones (Figs. 8e and 14), talc alteration (i.e., replacement of dolomite by talc) is the most predominant alteration type. The replacement occurs from the core to rims and suggests that fluids rich in silica and magnesium circulated through the rock. The alteration mineral assemblage consists of talc ± dolomite ± calcite ± quartz. Among the alteration types, chloritization, mainly through the replacement of igneous biotite in granites and hydrothermal biotite in metasedimentary rocks is the most predominant alteration style. In the granitoid, biotite is selectively replaced by chlorite (Fig. 6) and does not cause textural destruction, on the other hand, in highly chloritized rocks, the replacement it is characterized by being pervasive (Figs. 13 and 17). In fact, chlorite alteration can be observed throughout the hydrothermal system (i.e., from the granitoid intrusion to the gossan) and proportionally intensifies towards the surface (i.e., distal to the intrusion). Furthermore, chlorite alteration is more pervasive in vein/fracture-rich rocks suggesting strong association with mineralization. The chlorite alteration mineral assemblage consists of chlorite ± quartz ± sericite ± epidote ± calcite. Lastly, argillic alteration, which occurs closer to the surface, seems to be latest hydrothermal alteration assemblage to have been developed. This alteration could not be observed microscopically due to the broken and oxidized nature of the samples. However,

macroscopic and geochemical studies indicate an alteration assemblage consisting of Illite ± goethite ± hematite ± limonite ± magnetite ± chlorite ± sericite. The argillic alteration zone is characterized by the occurrence of significant Cu mineralization (i.e., 441 to 4541 ppm) that appears to be disseminated in copper-bearing clays.

### *Mineralization*

The mineralization at Cassenha Hill prospect is characterized by the occurrence of pyrite, chalcopyrite, and chalcocite as sulfides, cuprite, malachite, azurite, and chrysocolla as copper oxides, and hematite, magnetite, and goethite as Iron oxides/hydroxides (Table 6). The mineralization tends to occur within and/or at the edges of quartz/chlorite-rich veins and is hosted by any occurring metasedimentary rock type, predominantly in fracture/vein-rich and highly chloritized rocks. Although the occurrence of copper mineralization could not be identified due to the fine-grained nature of the sampled rocks, the geochemical study pointed out anomalous values of Cu in some of the rocks. Moreover, the Cassenha hill rocks are characteristically poor in sulfide minerals, and the copper oxides correspond to the most prevalent mineralization. The gangue mineralogy consists of quartz, chlorite, calcite and Iron oxides/hydroxides minerals (i.e., hematite, magnetite, and goethite).

#### *Sulfides*

Sulfide minerals are rare and consist mostly of pyrite, chalcopyrite, and chalcocite. These minerals represent the stage I of hydrothermal mineralization and are believed to be part of the hypogene ore, from which the copper oxides have possibly been originated through continuous hydrolysis and oxidation. The pyrite and chalcopyrite minerals occur predominantly as disseminated mineral grains within the fracture-rich granitoid together with hematite ± magnetite. However, remnants of pyrite can be seen in the argillic alteration zone, being replaced by goethite (Figs. 12a and 12b). Therefore, occurrence of

sulfides may well extend from the granitoids to areas just below the water table or even towards the gossans. The proportionality of abundance between sulfide minerals could not be defined in this study due to their rarity as whole in the study area. Furthermore, the absence of primary sulfides in the weathering profile suggests that they have all been oxidized to secondary supergene copper minerals such as malachite, azurite, and chrysocolla (Aurum Exploration Services, 2007). Although not observed in this study, the occurrence of other sulfide minerals such as bornite and covellite should not be disregarded, due to the oxidizing nature of the system. The paragenetic sequence of sulfide minerals can be inferred as: pyrite > chalcopyrite > chalcocite > bornite> covellite (Chavez, 2000).

*Copper oxides*

Copper oxides can be defined as copper minerals containing oxidized anions, such as copper carbonates, oxides, phosphates, silicates, and arsenates (Chavez, 2000). At Cassenha Hill, copper oxides are believed to represent the stage II and the most prevalent mineralization, and consist predominantly of malachite, azurite, and chrysocolla minerals. Among which, malachite and chrysocolla seem to be the most abundant. Copper oxides occur predominantly along fractures, thus suggesting that they have formed as a result of percolating meteoric waters. This is further evidenced by the $\delta D_{H2O}$ values of chlorites (i.e., -20‰; $\delta^{18}O_{H2O}$ = -4‰), which is characteristic of such waters. However, in some areas they occur as impregnation in the host rocks. It is evidenced by the staining of malachite in relatively fracture-poor compact siltstone rock blocks occurring in the prospect. When occurring within fractures and/or veins the copper oxides tend to be intergrown with iron oxides/hydroxides. Azurite often occurs as pseudomorph of malachite and is less abundant. The generation of copper oxides involve series of chemical reactions that will be discussed in the genetic model of the prospect.

*Iron oxides/hydroxides*

The occurrence of iron oxides/hydroxides is variable as they are associated with every stage of mineralization in the prospect. The dominant iron oxides/hydroxides are: hematite, magnetite, and goethite, however, limonitic texture (i.e., limonite ± goethite), can also be observed near the surface as the gossan (i.e., iron cap). Hematite intergrown with magnetite occur as fracture-filling in the granitoids (stage I of mineralization), and in the breccia and metasedimentary rocks (stage II of mineralization). In addition to intergrown relationship with hematite, magnetite tends to occur as NW-SE trending veins near the surface. The veins have thickness ranging from few millimeters to up to 1 meter. Goethite occurs as replacement of sulfide minerals, commonly pyrite, and occurs within the veins in the argillic alteration zone. Limonite ± goethite forms the gossan (iron cap) at Cassenha Hill prospect. The gossan is characterized by having a rust-red coloration and represent the latest stage/state of oxidation of the Cassenha Hill prospect. Furthermore, the geochemical study indicates that in, some areas, such gossans are enriched in copper (i.e., 441 to 4541 ppm) and are characterized by an increase of $Fe_2O_3$ and $Al_2O_3$ and decrease in MgO. The amount of Iron hydroxides (i.e., limonite ± goethite) diminishes with increasing depth, and hematite and magnetite become more predominant.

*Summary*

The occurrence of oxidized copper minerals such as chrysocolla, malachite, and azurite suggest that the Cassenha Hill prospect has been subjected to supergene processes at the weathering profile resulting in the oxidation of deeper sulfides, which is characteristic of deposits of porphyry-type, IOCG, Skarn affinities, and others (Fig. 38) (Chavez, 2000). On the other hand, Characteristics such as low sulfidation, shallow depth of formation, low temperature mineral assemblage, and significant influx of meteoric waters correspond, to a certain degree, to low sulfidation base metals epithermal systems (Fig. 39) (White

and Hedenquist, 1995). However, the absence of significant copper sulfides near the surface and occurrence of predominantly copper oxides, favors a supergene-style rather than epithermal.

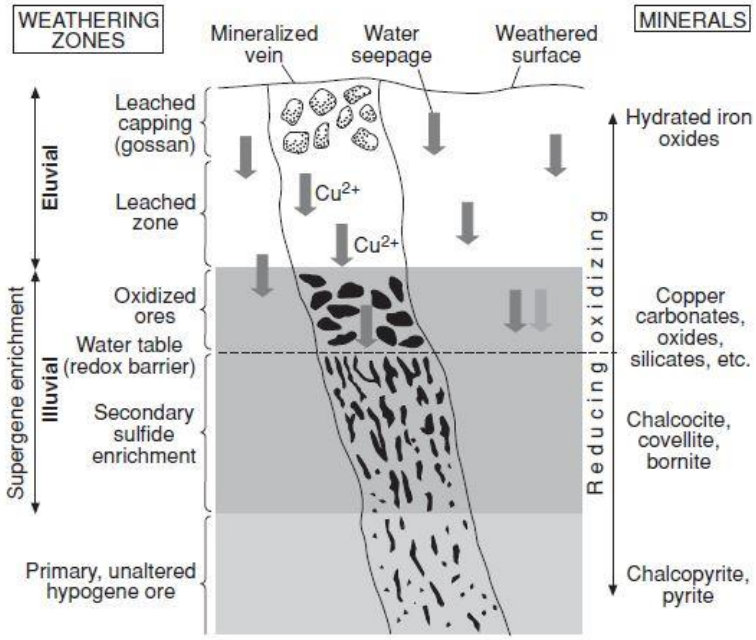


**Figure 39**: Schematic diagram illustrating the weathering profile of supergene copper oxide deposits (*Taken from Robb, 2005*).

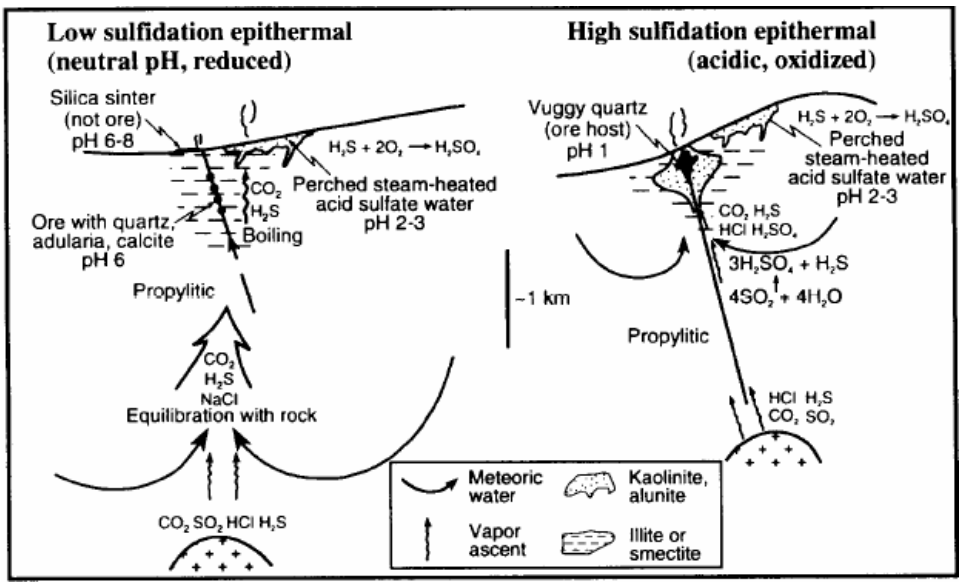

**Figure 40:** Generalized sketches showing the relationship between fluid types and alteration zoning in epithermal systems. (**a**) Low-sulfidation epithermal system, which is characterized by a near-neutral pH and reduced fluid at a depth of 1-2 Km, and is in equilibrium with the host rocks at greater depths; (**b**) High-sulfidation epithermal systems, which is characterized by the ascension of volatiles to the epithermal environment where they are absorbed by meteoric water, forming a highly acid solution that leaches the rock outward from the fluid conduit (*Taken from Hedenquist et al., 1994; White and Hedenquist, 1995).*

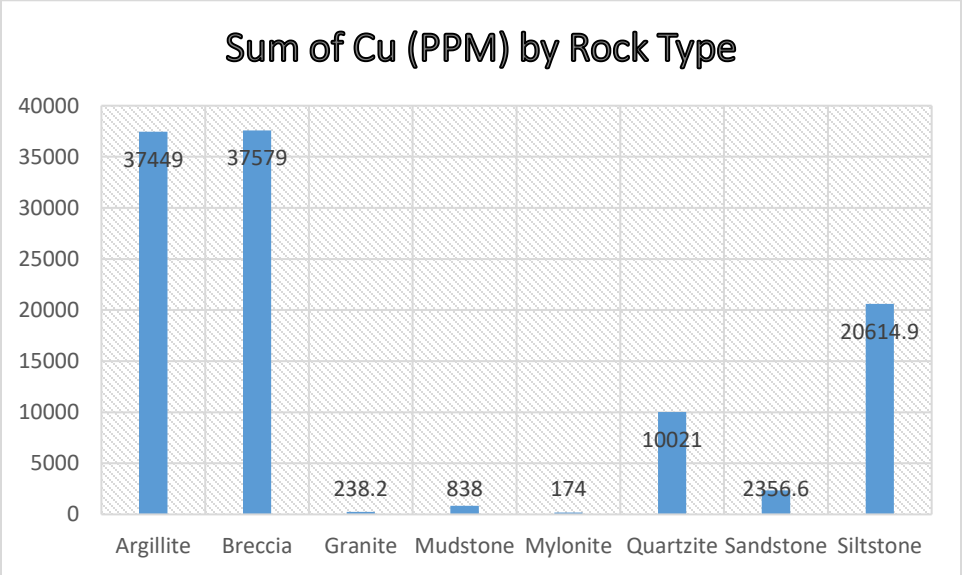


**Figure 41:** Bar graph showing the sum of Cu content (ppm) by rock type using the assay data from borehole CHD013.

**Table 6**: Inferred paragenetic sequence of magmatic, hydrothermal and supergene minerals occurring at Cassenha Hill prospect.

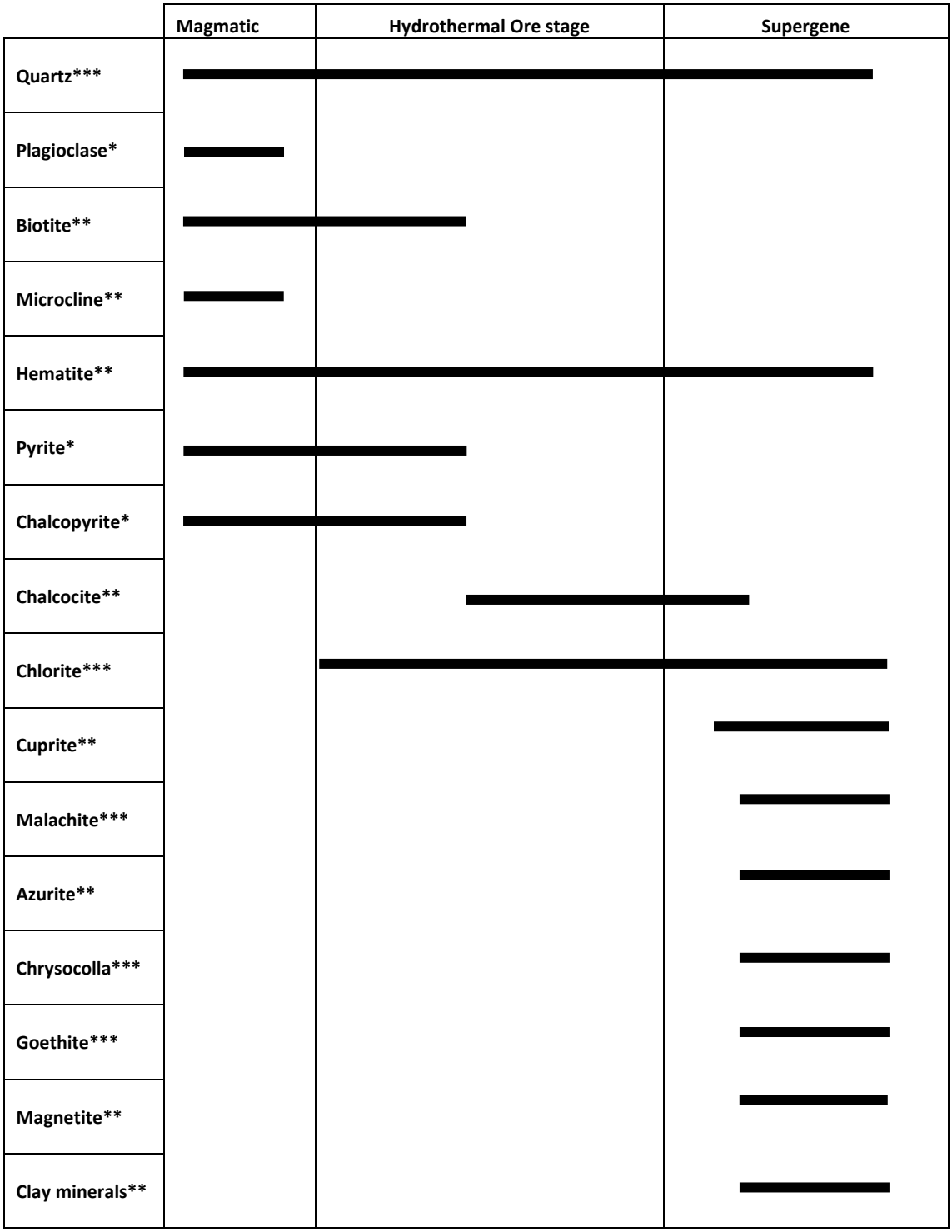


**Abundance:** * rare, ** fairly abundant, *** abundant

### 6.1.4. Genetic model for the Cassenha Hill prospect

The field, petrographic, and geochemical observations undertaken in this study suggest that the Cassenha Hill prospect has experienced several episodes of tectonic activity, brecciation, and mineralization, and that the various minerals observed are in fact products of hydrothermal alteration and weathering events that superimposed on pre-existing rocks and earlier sulfide-bearing veins. The polyphase formation of the Cassenha Hill mineralization involves the following: (1) Partial melting of pre-existing metasedimentary rocks resulting in the formation of S-type granitoids in a syn-tectonic environment. These granitoids are characteristically poor in sulfur and sulfide minerals as their protolith is poor in the same, thus explaining the low sulfidation and lack of sulfide minerals in the hydrothermal ore-stage, contrarily, these granitoids are enriched in LILE elements (i.e., Si, Rb, K, Ba) thus producing alkali earth-rich fluids; (2) At late stage of magma cooling, the intrusion of the magma body increases the temperature of the groundwater, without or with minimal contact with the magma, at a shallower depth than the magma, causing flashing and/or expansion when the lithostatic pressure of the overlain rocks is exceeded. Such phenomena possibly led to formation of the multiple stages of brecciation, and is believed to have triggered the faulting/fracturing at the prospect concurrently with circulation and precipitation of sulfide-bearing Si-rich epithermal fluids, forming the earlier sulfide mineralization (i.e., hypogene ore) within fractures and quartz veins, and the early hydrothermal alteration. (3) Thereafter, it is believed that series of tectonic reactivations occurred and were responsible for the development of additional faulting/fracturing and/or veining, resulting in the formation of late tectonic/fault breccias. Such faulting/fracturing is believed to have worked as conduit for the circulation of meteoric waters, which with continuous hydrolysis and oxidation, leached the earlier copper sulfides from the source rock and reprecipitated the same as copper oxides within the fractures and/or veins, thus forming the prevalent Cassenha Hill mineralization (i.e., supergene ore).

If the above hypothesis is true, then the hydrothermal hypogene ore-stage should be late Eburnean in age and have been generated due to the Eburnean orogenic event (≈ 2.1 – 1.8 Ga). In addition to this, the circulation of such heated fluids may be responsible for the potassic alteration observed in the granitoids, as well as for the formation of secondary minerals such as chlorite and sericite. The altered rocks and hypogene ore, possibly due to several episodes of uplift, were exhumed and subjected to supergene processes that are presumably related to the Pan African orogenic event (i.e., ≈ 900 – 500 Ma). Although the polyphased mobilization and reprecipitation of minerals during hydrothermal and supergene processes overprinted the primary characteristic of the ore, it is believed that the metals are originated from the granitoids. This is supported by the evidence of circulation of alkali earth-rich fluids (i.e., quartz veins), lack of sulfur and sulfide minerals, enrichment of LILE elements, which are signatures typical of S-type granitoids. Furthermore, similar geochemical affinities between the granitoids and hosting rocks, such as enrichment in LREE and depletion in HREE, support this hypothesis.

The sequential development of supergene copper oxides in various mineralizing systems has been well explained by Chavez (2000), Robb (2005), and Sillitoe (2005). The formation of supergene-enriched copper deposits such as the Cassenha Hill prospect, relies on the existence of a geochemical environment (Fig. 42) where the following domains are available: (1) Source rock that undergoes oxidation and mass loss – generally sulfide minerals-rich (i.e., pyrite, chalcopyrite, and chalcocite); (2) Sink region or oxide zone – where the mass lost from the source as well as the certain hypogene minerals accumulate; and (3) the protolith – the unreacted pre-oxidation sulfide mineral assemblages (Chavez, 2000). The mineralogy of the geochemical environment is strongly dependent on the characteristics of the source rock and subsequent chemical interactions with the host rock and oxidizing environment. Based on the characteristics of the source rock, copper oxide deposits can be broadly subdivided into two: “Exotic copper deposits”, which are characterized by the occurrence of a pyrite-rich source rock and non-reactive host rock (i.e., Mina Sur, Huinquintipa, El Tesoro, and La Cascada mines in Chile) and “in

situ copper deposits" which are originated from a pyrite-poor source rock and reactive host rock (i.e., El Abra, Lomas Bayas, and Radomiro Tomic mines in Chile) (Munchmeyer, 1997; Chavez, 2000).

From a supergene perspective, the Cassenha Hill prospect exhibits characteristics generally attributed to "in situ copper deposits". Such deposits are formed as direct replacement of sulfide-bearing mineral assemblages by copper oxides, due to the circulation of meteoric waters (Fig. 42), with relatively limited copper mobility. At Cassenha Hill, the source rock has a low Sulfur/metal (S/Me) which is characteristic of source rocks comprised predominantly of chalcopyrite and/or chalcocite minerals and lesser pyrite (Fig. 39) (Chavez, 2000). The interaction between percolating meteoric waters and a source rock with relatively lower pyrite content, inhibits the production of ferric sulfate and sulfuric acid solutions (i.e., $\{Fe_2(SO_4)_3\}$ and $\{H_2SO_4\}$, respectively), which are fundamental for the leaching and mobilization of copper as $Cu^{2+}$ and the subsequent precipitation as copper oxides, this explains the in situ replacement of the copper sulfides by copper oxides observed in the study area. Furthermore, the relative abundance of K-feldspars and silicates, and the occurrence of carbonates (i.e., calcite and dolomite) in the host rocks possibly caused the rock to buffer/neutralize the acidic solutions derived from the breakdown of sulfides and mafic minerals (i.e., biotite) via hydrolysis and oxidation, thus reducing the mobility of $Cu^{2+}$ and also triggering the in situ precipitation of copper oxides. The in-situ oxidation characteristic of the Cassenha Hill prospect is evidenced by the occurrence of hematite ± goethite halos, together with copper oxides that are stable at near-neutral to slightly alkaline pH range such as malachite, azurite, and chrysocolla (Fig. 42). Therefore, if the in-situ oxidation hypothesis is true for the Cassenha Hill prospect, then the copper grades observed in the supergene ore, will not differ much from the hypogene ore, as non-significant enrichment is prone to have occurred (Chavez, 2000).

In such geochemical systems, there is a distinguishable vertical zonation and paragenetic sequence that is controlled by the Eh-pH of the solution. Therefore, the occurrence of malachite and azurite closer to the surface, which are only stable at specific Eh-Ph conditions, indicate that the geochemical environment was near-neutral to slightly alkaline, and the source of acidic solutions has been consumed, and that carbonates were readily available during their precipitation, while, the occurrence of chrysocolla suggests that chloride activity was more important than the available sulfate (Arcuri and Brimhall, 1998). The reactions below exemplify the principles involved in the genesis of the supergene ore at Cassenha Hill prospect (Robb, 2005).

$$4CuFeS_2 + 17O_2 + 10\,H_2O \longrightarrow 4Fe(OH)_3 + 4Cu^{2+} + 8S0^{2-}_4 + 8H^+ \quad (7)$$

chalcopyrite goethite

Reaction (7) illustrates the destabilization of sulfides when interacting with oxidized groundwater. The oxidization is moderately acidic due to the absence of considerable pyrite and liberates the copper as $Cu^{2+}$ (aq) from the source rock and leaches downwards. A gradual increase in ph and decrease in Eh, due to reactions with country rocks results in the precipitation of CuO (tenorite), followed by $Cu_2O$ (cuprite), malachite ($Cu_2CO_3(OH)_2$, azurite ($Cu_3(CO_3)_2(OH)_2$ and chrysocolla ($Cu_2H_2Si_2O_5(OH)_4$)

$$2Cu^{2+} + CO^{2-}_3 + 2OH^- \longrightarrow Cu_2(OH)_2CO_3 \quad (8)$$

Malachite

Reaction (8) Illustrates the reaction between $Cu^{2+}$ (aq) and carbonate-rich rocks, leading to the formation of malachite and other copper carbonates.

$$CuFes_2 + 3Cu^{2+} \longrightarrow 2Cu_2S + Fe^{2+} \quad (9)$$

Chalcopyrite chalcocite

Reaction (9) illustrates the direct precipitation of supergene sulfides by replacement of primary sulfides in the oxide/sink zone.

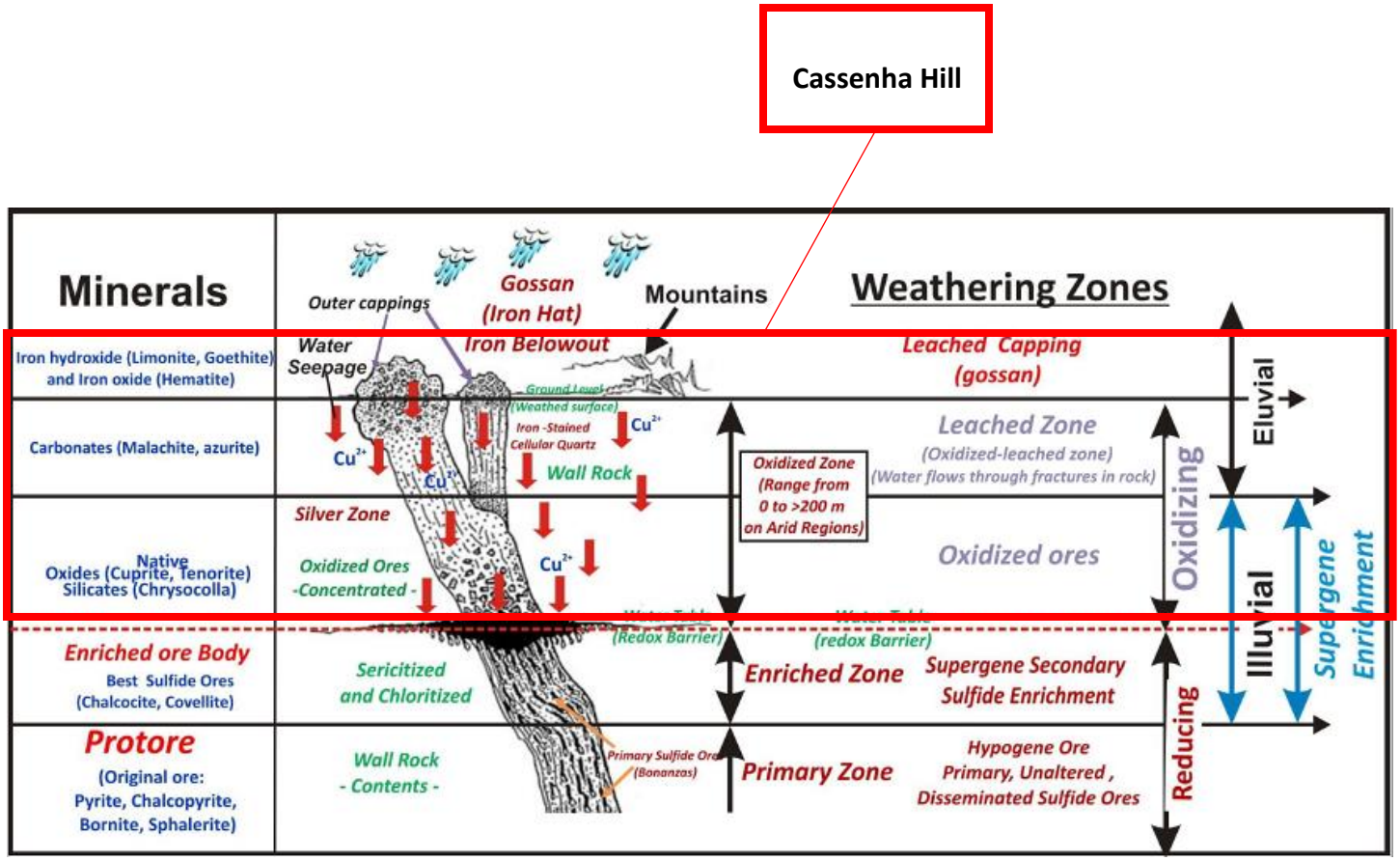


**Figure 42**: Schematic diagram illustrating the zones and the main components of supergene copper oxide deposits (*Taken from Harraz, 2013*). Red rectangle highlights the position of the Cassenha Hill prospect in respect to the schematic diagram.

Overall, the Cassenha Hill prospect exhibits characteristics/features typical of polymetallic vein-type of porphyry copper deposits that have experienced supergene enrichment and/or mineralization at the weathering profile. The features include: (1) The prospect is situated in a magmatic arc tectonic setting, in which most of the world's porphyry copper deposits are hosted (Sillitoe, 2010); (2) Occurrence of polymetallic Cu ± Au ± U ± Fe mineralization, although Au and U mineralization was not observed in this study, it is reported to occur at the prospect (Aurum Exploration Services, 2007); (3) The mineralization is hosted by metasedimentary rocks that have been intruded by a felsic pluton (Cox, 1986); (4) Chloritization, silicification and sericitization are the main alteration styles (McMillan, 1972); (5) The mineralization occurs within and/or at edges of veins and fractures, and is structurally-controlled; (6) The primary hypogene sulfides have been leached by moderately acidic meteoric waters to form the supergene ore in a oxidizing-reducing environment.

Therefore, this study allows one to, tentatively, suggest that the Cassenha Hill prospect represents an extension of a polymetallic vein-type of porphyry copper deposits that have experienced in-situ supergene mineralization at the weathering profile.

## 6.2. Conclusions

The lithogeochemical characterization of the Cassenha hill prospect with emphasis on the classification of the various rock types (i.e., host and barren rocks), determination of origin of the protoliths, spatio-temporal distribution of alteration, and general mineralization characterization were among the topics dealt with in this study. By integrating borehole core logging, petrography, and geochemistry as combined geological tools, this study has demonstrated that there are as much as seven lithological units (namely granite, breccia, meta-mudstone, meta-siltstone, meta-sandstone, quartzite, and carbonate-rich rocks) occurring at the Cassenha Hill prospect. In addition to this, this study has demonstrated that the majority of the Cassenha Hill rocks have been hydrothermally altered by low temperatures waters (i.e., 200$^{o}$c to 350$^{o}$c), at which chloritization is the most predominant resulting alteration style. Petrologically, all of the Cassenha Hill rocks demonstrate geochemical affinities typical of rocks originated from sources of intermediate to felsic composition and are possibly originated from the same source.

The Cassenha Hill mineralization is hosted by any occurring rock type and seems to be controlled by the NW-SE trending shear structures occurring at the local scale. This study also suggests that the mineralization is associated with rocks that have experienced the highest degree of chloritization. Two ore stages could be identified, namely, hypogene ore (stage I) consisting of pyrite ± chalcopyrite ± other copper sulfides, and supergene ore (stage II) consisting of malachite ± azurite ± chrysocolla, which represent the prevalent mineralization at the prospect (Fig. 39 and Table 6). This study suggests that the downward circulation of predominantly meteoric waters within the fracture system is responsible for the genesis of the stage II mineralization, and is also possibly highly influential in the formation of the hypogene ore.

Lastly, this study indicates that the logged exploration boreholes have not substantially reached neither the hypogene ore nor the supergene sulfide zone, and that the current understanding of the Cassenha Hill mineralization has been solely based on the information gathered from the oxidized-transition zones.

## 6.3. Recommendations and future work

There are several outstanding questions that still need to be addressed at the Cassenha hill prospect. These include but are not limited to: (1) The age of the granitoid emplacement and its geochronological and spatial relationship with the country rocks; (2) The …depth boundaries between various zones (i.e., From the hypogene ore to the gossan zone); and (3) The exact age of the stage I mineralization and its evolution to the stage II; (4) Fluid inclusion studies on various quartz generations; and (5) The role of tectonism on the generation of the various fractures/fault systems.

Furthermore, for a clearer and fully understanding on the characteristics of the Cassenha Hill mineralization and its subsequent economic viability, significant number of additional deeper (i.e., +200m) exploration boreholes should be drilled along the Cassenha Main zone and surrounding areas. Although this study only focused on Zone 1 (Fig. 4) of the Cassenha Hill prospect, the geological relationship between the Cassenha Hill Zone 1 and Cassenha Hill Zone 2 should not be disregarded, consequently, the exploration program should encompass these two Zones.

## 7. References

Allsopp, H. (1975). Summary of age determinations on the Kunene Complex. Witwatersrand Geological Department, Johannesburg. Geological Survey of Namibia, Unpublished report, 4 pp.

Andrade, F. (1954). Rochas graníticas de Angola, Mem. Junta Missão de Investigação do Ultramar, Lisboa, vol. 4, 464 pp.

Antunes, I., Neiva, A., Silva, M., Corfu, F. (2008). Geochemistry of S-type granitic rocks from the reversely zoned Castelo Branco Pluton, Central Portugal. Lithos, vol.103, 445-465.

Arcuri, T., Brimhall, G. (2003), The chloride source for atacamite mineralization at the Radomiro Tomic porphyry copper deposit, northern Chile: Economic Geology, vol. 98, 1667–1681.

Aurum Exploration Services. (2007). August field progress report. Retrieved from https://www.asx.com.au/asxpdf/20070803/pdf/313sw1g4kwtswc.pdf.

Barton, P. (1991). Ore textures: Problems and opportunities. Mineralogical magazine, vol. 55, 303-315.

Bassot, P., Pascal, M., Vialette, Y. (1980/1981). Données novelles sur la stratigraphie, la géochimie et la géomorphologie des formations précambriennes de la partie méridionale du Haut Plateau angolais, Bulletin du Bureau de Recherches Géologiques et Minieres. (2 Série), Sect. 4, nº 4, 285- 309.

Beaufort, D., Rigault, C., Billon, S., Billault, V., Inoue, A., Inoue, S., Patrier, P. (2015). Chlorite and chloritization processes through mixed-layer mineral series in low-temperature geological systems – a review. Clay Minerals, vol. 50, 497-523.

Bhatia, R. (1983). Plate tectonics and geochemical composition of sandstones. Journal of Geology, vol. 91, 611-627.

Bhatia, M. (1985). Rare earth element geochemistry of Australian Paleozoic graywackes and mudrocks: provenance and tectonic control. Sedimentary Geology, vol. 45, 97-113.

Bhatia, M., Crook, K. (1986). Trace element characteristics of graywackes and tectonic setting discrimination of sedimentary basins. Contributions to Mineralogy and Petrology, vol. 92, 181-193.

Bokana, R. (2015). The lithogeochemical characterization of the Hondekloof nickel mineralization, Kliprand area, Garies Terrane, Namaqualand, South Africa (Master's thesis, University of the Western Cape, Cape Town, South Africa). Retrieved from https://etd.uwc.ac.za/xmlui/handle/11394/5024.

Carvalho, H., 1984. Estratigrafia do Precambrico de Angola. Garcia de Orta, Serie Geologia, Instituto de Investigação Científica Tropical, vol. 7 (l-2), l-66.

Carvalho, H., Tassinari, C., Alves, P., Guimarães, F., Simões, M. (2000). Geochronogical review of the Precambrian in western Angola: Links with Brazil. Journal of African Earth Sciences, vol. 31, 383–402.

Chappell B., White A. (1974). Two contrasting granite types. Pacific Geology, vol. 8, 173–174.

Chavez, W. (2000). Supergene oxidization of copper deposits: Zoning and distribution of copper oxide minerals. SEG Newsletter, vol. 41, 10 – 21

Cox, D. (1986). Descriptive model of polymetallic veins, in Cox, D.P., and Singer, D.A., eds., Mineral deposit models. U.S. Geological Survey Bulletin 1693, p. 125.

Cox, R., Lowe, D., Cullers, R., (1995). The influence of sediment recycling and basement composition on evolution of mudrock chemistry in the southwestern United States. Geochimica et Cosmochimica Acta, vol. 59, 2919–2940.

Craig, J. (2001). Ore-mineral textures and the tales they tell. The Canadian Mineralogist, vol. 39, 937-956.

Cullers, R. (2002). Implications of elemental concentrations for provenance, redox conditions, and metamorphic studies of shales and limestones near Pueblo, CO, USA. Chemical Geology, vol. 191, 305-327

Da Silva, A. (2005). A Geologia da República de Angola desde o Paleoarcaico ao Paleozoico Inferior. Instituto Nacional de Engenharia, Tecnologia e Inovação. Retrieved from https://core.ac.uk/download/pdf/70660747.pdf

Ennis, D., Dunbar, N., Campbell, A., Chapin, C. (2000). The effects of K-metasomatism on the mineralogy and geochemistry of silicic ignimbrites near Socorro, New Mexico. Chemical Geology, vol. 167, 285-312.

Facca, G., Tonani, F. (1967). The self-sealing geothermal field. Bulletin of Volcanology, vol. 30, 271-273.

Fedo, C., Nesbitt, H., Young, G. (1995): Unraveling the effects of potassium metasomatism in sedimentary rocks and paleosols, with implications for paleoweathering conditions and provenance. Geology, vol. 23, 921–924.

Garcia, D., Coelho, J., Perrin, M. (1991). Fractionation between $TiO_2$ and Zr as a measure of sorting within shale and sandstone series, northern Portugal. European Journal of Mineralogy, vol. 3, 401-414.

Garcia, D., Fonteilles, M., Moutte, J. (1994). Sedimentary Fractionations between Al, Ti, and Zr and the Genesis of Strongly Peraluminous Granites. The Journal of Geology, vol. 102, 411-422.

Girty, G., Ridge, D., Knaack, C., Johnson, D., Al-Riyami, R. (1996). Provenance and depositional setting of Paleozoic chert and argillite, Sierra Nevada, California. Journal of Sedimentary Research, vol. 66, 107–118.

Glazner, A. (1988). Stratigraphy, structure, and potassic alteration of miocene volcanic rocks in the sleeping beauty area, central Mojave Desert, California. Geological Society of America, Bulletin 100, 424–435.

Gonzalez, P., Garban, G., Hauser, N., Gigena, L. (2017). Geochemistry of metasedimentary rocks from the Puncoviscana Complex in the Mojotoro Range, NW Argentina: Implications for provenance and tectonic setting. Journal of South American Earth Sciences, vol. 78, 250-263.

Harris, C., Erlank., A. J. (1992). The production of large-volume, low δ18O rhyolites during the rifting of Africa and Antarctica: The Lebombo Monocline, southern Africa. Geochimica et Cosmochimica Acta, vol. 56, 3561-3570.

Harris, C., Ashwal, L. (2002). The origin of low $\delta^{18}O$ granites and related rocks from the Seychelles. Contributions to Mineralogy and Petrology, vol. 143, 366-376. doi:10.1007/s00410-002-0349-6.

Harris, C., Vogeli., J. (2010). Oxygen composition of garnet in the peninsula granite, Cape Granite Suite, South Africa: constraints of melting and emplacement mechanisms. South African Journal of Geology, vol. 113, 401-412.

Harnois, L. (1988). The CIW index: a new chemical index of weathering. Sedimentary Geology, vol. 55, 319–322.

Hedenquist, J., Matsuhisa, Y., Izawa, E., White, N., Giggenbach, W., Aoki, M. (1994). Geology, geochemistry, and origin of high sulfidation Cu-Au mineralization in the Nansatsu District, Japan. Economic Geology, vol. 89, 1-30.

Henley, R., Thornley, P. (1981). Low grade metamorphism and the geothermal environment of massive sulphide ore formation, Buchans, Newfoundland. Geological Association of Canada, vol. 22, 205-228.

Hoefs, J. (1987). Stable isotope geochemistry 3rd ed. Minerals and Rocks, Vol. 9, p241.

Holtz, F., Barbey, P. (1991). Genesis of peraluminous granites. In Mineralogy and chemistry of the Tourem Complex (north Portugal) sequential melting vs restite unmixing. Journal of Petrology, vol. 32, 959–978.

Ishikawa, Y., Sawaguchi, T., Iwaya, S., Horiuchi, M. (1976). Delineation of prospecting targets for Kuroko deposits, based on models of volcanism of underlying dacite and alteration haloes. Mining Geology, vol.26, 105-117 (in Japanese with English abstract).

Jelsma, H., Perritt, S., Armstrong, R., Ferreira, H. (2011). SHRIMP U–Pb zircon geochronology of basement rocks of the Angolan Shield, western Angola. In: Proceedings of the 23rd CAG, Johannesburg. Council for Geoscience, Pretoria, p 203.

Jelsma, H., McCourt, S., Perrit, S., Armstrong, R. (2018). The geology and evolution of the Angolan Shield, Congo Craton: in S. Siegesmund et al. (eds.). Geology of Southwest Gondwana, Regional Geology Reviews. https://doi.org/10.1007/978-3-319-68920-3_9.

John, D., Ayuso, R., Barton, M., Blakely, R., Bodnar, R., Dilles, J., Gray, F., Mars, J., McPhee, D., Seal, R., Taylor, R., and Vikre, P. (2010). Porphyry copper deposit model, chap. B of Mineral deposit models for resource assessment. U.S. Geological Survey Scientific Investigations Report 2010–5070–B, 169 p.

Jordana, J. (1950). Geological – Mining study on the region of Ucuma (Caquete). Geological report.

Khider, K., McQueen., K. (2005). Geochemical discrimination of weathered bedrock in the Hermidale-Byrock Region of Western NSW. In book: Regolith 2005 – Ten Years of CRC LEME. CRC LEME, 170-175.

Korpershoek, H. (1984). The geology of the Cassinga district (Angola) and its potential as compared to that of the Serra dos Carajás (Brazil). In: 33° Congresso Brasileiro de Geologia, Rio de Janeiro, Brasil.

Large, R., Gemmoll, B., Paulick, H. (2001). The alteration box plot, a simple approach to understanding the relationship between alteration mineralogy and lithogeochemistry associated with volcanic hosted massive sulphides deposits. Economic Geology, vol. 96, 957-971.

Li, S., Zhang, X., Gao, L. (2019). Ore Genesis at the Jinchang gold-copper deposit in Heilongjiang Province, northeastern China: Evidence from geology, fluid inclusions, and H-O-S isotopes. Minerals, vol. 9, 99. doi:10.3390/min9020099

Lima, M., Silva, T., Ferreira, V., Silva., J. (2014). Metasedimentary rocks of the northern portion of the Macurure Domain, Sergipano Belt, northeastern Brazil: Geochemical characterization of their protoliths and Tectonic implications. Estudos Geologicos, vol. 24 (2), 89-107.doi: 10.18190/1980-8208/estudosgeologicos.v24n2p89-107

Mathieu, L. (2018). Quantifying hydrothermal alteration: A review of methods. Geosciences, vol. 8, 245. doi:10.3390/geosciences8070245.

McCourt, S., Armstrong, R., Jelsma, H., Mapeo, R. (2013). New U − Pb SHRIMP ages from the Lubango region, SW Angola: insights into the Palaeoproterozoic evolution of the Angolan Shield, southern Congo Craton, Africa. Journal of Geological Sciences, vol. 170, 353-363.

McCrea, J.M., 1950. On the isotopic chemistry of carbonates and a paleotemperature scale. The Journal of Chemical Physics, vol. 18, 849-857.

McLennan, S., Taylor, S. (1991). Sedimentary rocks and crustal evolution: tectonic setting and secular trends. Journal of Geology, vol. 99, 1-21.

McMillan, W. (1972). OK (Alwin) mine: in Geology, Exploration and Mining in British Columbia. British Columbia Department of Mines and Petroleum Resources, 153-157.

McLennan, S., Taylor, S. (1991). Sedimentary rocks and crustal evolution: tectonic setting and secular trends. Journal of Geology, vol. 99, 1-21.

Middlemost, E.A.K. (1975). The basalt clan. Earth Science Reviews, 11, 337-364.

Moine, B., Gavoille, B., Thiebaut, J. (1982). Geochimie des transformations metasomatiques a l'origine du gisement de talc et chlorite de TrIMOUNS (Luzenac, Ariege, France), L. Mobilite des elements et zonalites: Bulletin de Mineralogie, vol. 105, 62-75.

Münchmeyer, C. (1997). Exotic deposits—products of lateral migration of supergene solutions from porphyry copper deposits, in Camus, F., Sillitoe, R.H., and Petersen, R., eds., Andean copper deposits: New discoveries, mineralization, styles, and metallogeny. Society of Economic Geologists Special Publication, vol. 5, 43–58.

Nesbitt, H., Markovics, G., Price, R. (1980). Chemical processes affecting alkalis and alkali earths during continental weathering. Geochimica et Cosmochimica Acta, vol. 44, 1659–1666.

Nesbitt, H., Young, G. (1984). Prediction of some weathering trends of plutonic and volcanic rocks based on thermodynamic and kinetic considerations. Geochimica et Cosmochimica Acta, vol. 48, 1523-1534.

Nickel, E., Allchurch, P., Mason, M., Wilmshrust, J. (1977). Supergene alteration at the Perseverance nickel deposit, Agnew, Western Australia. Economic Geology, vol. 72, 184-203.

Norman, D., Landis, G., Sawkins, F. (1976). $H_2S$ and $SO_2$ detected in fluid inclusions [abs.]: Geological Society of America. Abstracts with Programs, vol. 8, p. 1051.

Oliveira, T. (1980/1981). O Precâmbrico vulcano-sedimentar da região de Chipindo, Angola. Considerações sobre a estratigrafia e tectónica. Boletim da Sociedade Geológica de Portugal, vol. 22, 315-325.

Pariona, A. (2017, October 10). Top 10 Oil producing countries in Africa. WorldAtlas. Retrieved January 25, 2018, from http:// worldatlas.com/articles/top-10-oil-producing-countries-in-africa.html.

Parker, A. (1970): An index of weathering for silicate rocks. Geological Magazine, vol. 107, 501-504.

Piispanen, R. (1977). Major element geochemistry of the granitic rocks. Bulletin of Geological Science of Finland, vol. 49(2), 73-78.

Potter, P., Maynard, J., Depetris, P. (2005). Mud and Mudstones Introduction and Overview. Springer Science and Business Media, New York, p. 296.

Raith, M., Raase, P., Reinhardt. (2012). Guide to Thin Section Microscopy, 2nd Edition, ISBN 978-3-00-37671-9.

Robb, L. (2005). Introduction to ore-forming processes. Oxford, England: Blackwell publishing.

Roser, B., Korsch, R. (1988). Provenance signatures of sandstone mudstone suites determined using discriminant function analysis of major-element data. Chemical Geology, vol. 67, 119-139.

Sawyer, E. (1986). The influence of source rock type, chemical weathering and sorting on the geochemistry of clastic sediments from the Quetico Metasedimentary Belt, Superior Province. Chemical Geology, vol. 55, 77-95.

Shafiquallah, M., Lynch, D., Damon, P., Peirce, H. (1976). Geology, geochronology and geochemistry of the Picacho Peak area, Pinal County, Arizona. Arizona Geological Society Digest vol. 10, 305–324.

Sharma, R. (2014). Hydrothermal alteration associated with copper-gold mineralization at Dhani Basri, Bausi District, Rajasthan. Journal Geological Society of India, vol. 84, 709-726.

Sharp, Z. (1991). Determination of oxygen diffusion rates in magnetite from natural isotopic variations. Geology, vol. 19, 653-656. doi: 10.1130/0091-7613(1991)019.

Sillitoe, H. (1985). Ore-related breccias in volcanoplutonic arcs. Economic Geology, vol. 80, 1467−1514.

Sillitoe, R. (2010). Porphyry systems. Economic Geology, vol. 105, 3-41.

Silva, A., Pereira, E., Nunes, A. (1972) – Carta Geológica de Angola na escala 1/100.000. Notícia Explicativa da Folha 147 (Munenga-Dala Cachibo). Serviços Geológicos e Mineiros de Angola, Luanda, 40 pp.

Silva, A., Fernandes, N. (1978) – Geologia da região do Cariango (Angola), Boletim da Sociedade Geológica de Portugal, Lisboa, vol. 21, 27-59.

Silva, A., Kawashita, K. (1978). A evolução geológica da Faixa Dobrada Cela-Cariango (Angola), Boletim da Sociedade Geológica de Portugal, Lisboa, vol. 21, 61-82.

Tamas, C., Milesi, J. (2002). Hydrovolcanic breccia pipe structures – General features and genetic criteria – I. Phreatomagmatic breccias. Studia Universitatis Babes-Bolyai, Geologia, vol. 1, 127-147.

Taylor, S., McLennan, S. (1985). The Continental Crust: Its Composition and Evolution. Blackwell, Oxford, 312 pp.

Taylor, S., McLennan, S. (1995) The geochemical evolution of the continental crust. Review of Geophysics, Vol. 33, 241–265.

Torquato, R., Oliveira, T. (1977). Sobre a idade dos granitos e do grupo vulcano-sedimentar da região de Chipindo, Angola. Comissão de Serviços Geológicos de Portugal, Lisboa, 61, 223-238.

Torquato, R., Silva, F., Cordani, G., Kawashita, K. (1979). A evolução geológica do Cinturão Móvel do Quipungo no ocidente de Angola. Anais da Academia Brasileira de Ciências, Rio de Janeiro, vol. 51(1), 133-144.

Van de Kamp, P.C., Leake, B.E. (1985). Petrography and geochemistry of feldspathic and mafic sediments of the northeastern Pacific margin. Transactions of the Royal Society of Edinburgh, Earth Sciences 76, 411–449.

Vennemann, T., O'Neil, J. (1993). A simple and inexpensive method of hydrogen isotope and water analyses of minerals and rocks based on zinc reagent. Chemical Geology, vol. 103, 227-234. doi:10.1016/0009-2541(93)90303-Z.

Weaver, C. (1989). Clays, Muds, and Shales. Elsevier, Amsterdam, 819 pp.

White, N., Hedenquist, W. (1995). Epithermal gold deposits: Styles, characteristics and exploration. SEG Newsletter, vol. 23, 9-13.

# 8. Appendices

## Appendix A: Geological map of the Cassenha Hill prospect

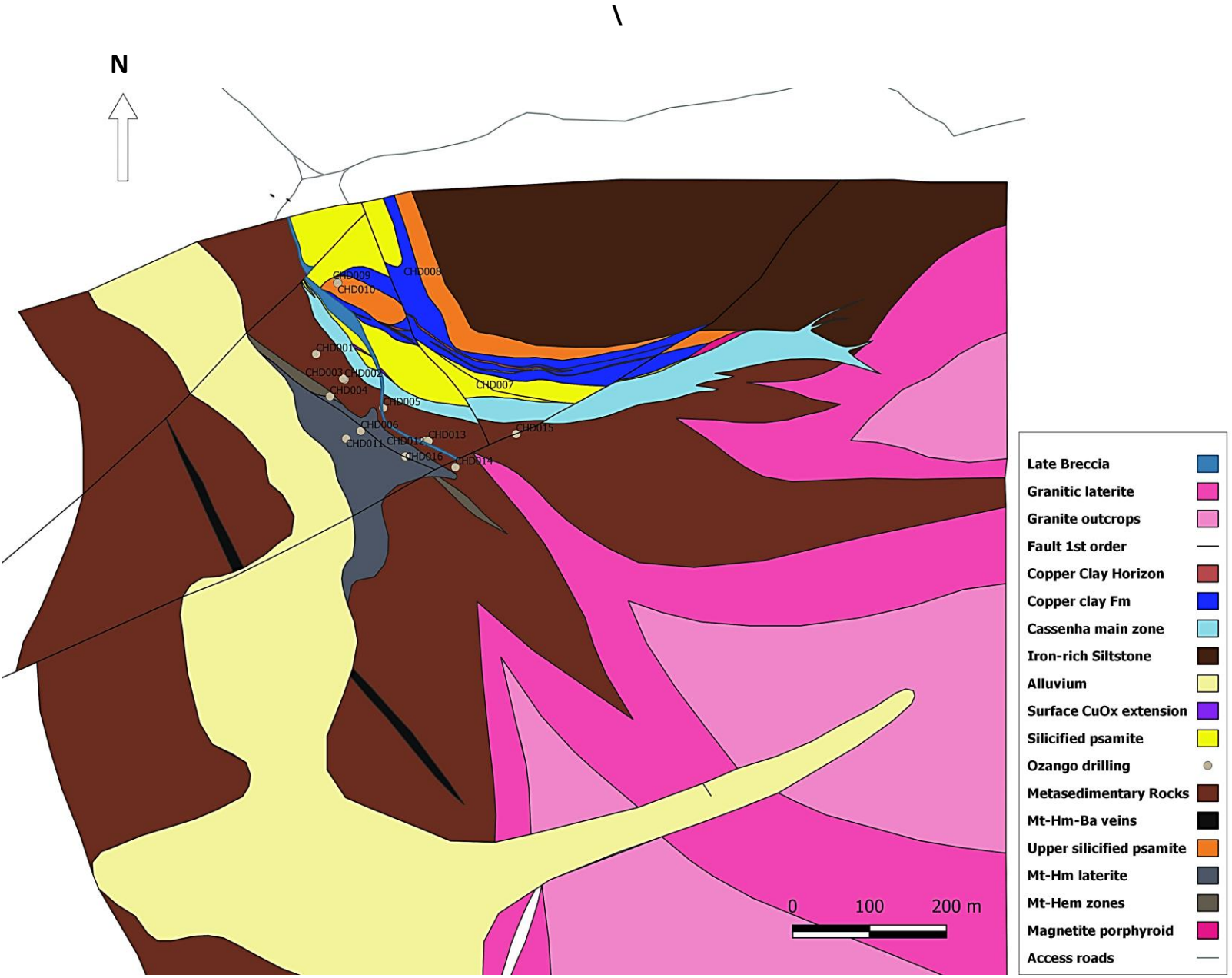
N
CHD009
CHD010
CHD008
CHD001
CHD003
CHD002
CHD004
CHD007
CHD005
CHD006
CHD011
CHD012
CHD013
CHD015
CHD016
CHD014
0
100
200 m
Late Breccia
Granitic laterite
Granite outcrops
Fault 1st order
Copper Clay Horizon
Copper clay Fm
Cassenha main zone
Iron-rich Siltstone
Alluvium
Surface CuOx extension
Silicified psamite
Ozango drilling
Metasedimentary Rocks
Mt-Hm-Ba veins
Upper silicified psamite
Mt-Hm laterite
Mt-Hem zones
Magnetite porphyroid
Access roads

**Appendix 2: Drill Logs of the exploration boreholes logged by the Author as part of this study**

Cassenha Hill Cu Prospect

Huambo - Angola

| | |
|---|---|
| Northing: | 8550704 |
| Easting: | 506895 |
| Elevation: | 1648 |
| Azimuth: | 0° |
| Total Depth: | 150 m. |

# CHD008

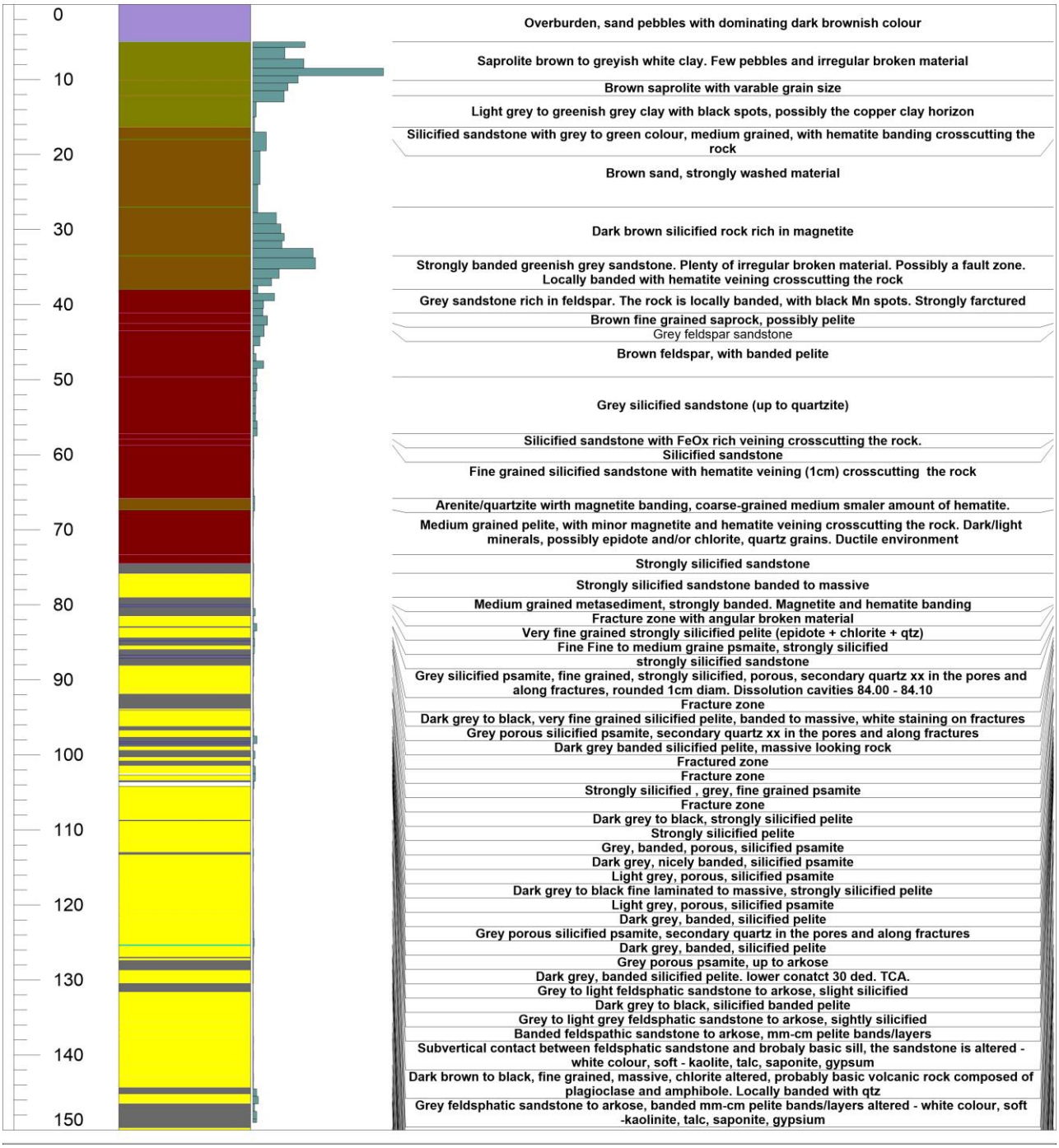


Legend Title

- Argillite
- Breccia
- Granite
- Mudstone
- Mylonite
- Quartzite
- Sandstone
- Siltstone
- Colluvium
- Fault
- Quartz Vein
- Quartz Veins
- Quartz veins
- TSOIL
- Laterite
- Saprolite
- Sand

Cassenha Hill Cu Prospect

Huambo - Angola

| | |
|---|---|
| Northing: | 8550699 |
| Easting: | 506809 |
| Elevation: | 1643 |
| Azimuth: | 225° |
| Total Depth: | 48 m. |

**CHD009**


Legend Title

- Argillite
- Breccia
- Granite
- Mudstone
- Mylonite
- Quartzite
- Sandstone
- Siltstone
- Colluvium
- Fault
- Quartz Vein
- Quartz Veins
- Quartz veins
- TSOIL
- Laterite
- Saprolite
- Sand

Cassenha Hill Cu Prospect

Huambo - Angola

Northing: 8550495
Easting: 506820
Elevation: 1536
Azimuth: 45°
Total Depth: 133.15 m.

**CHD011**

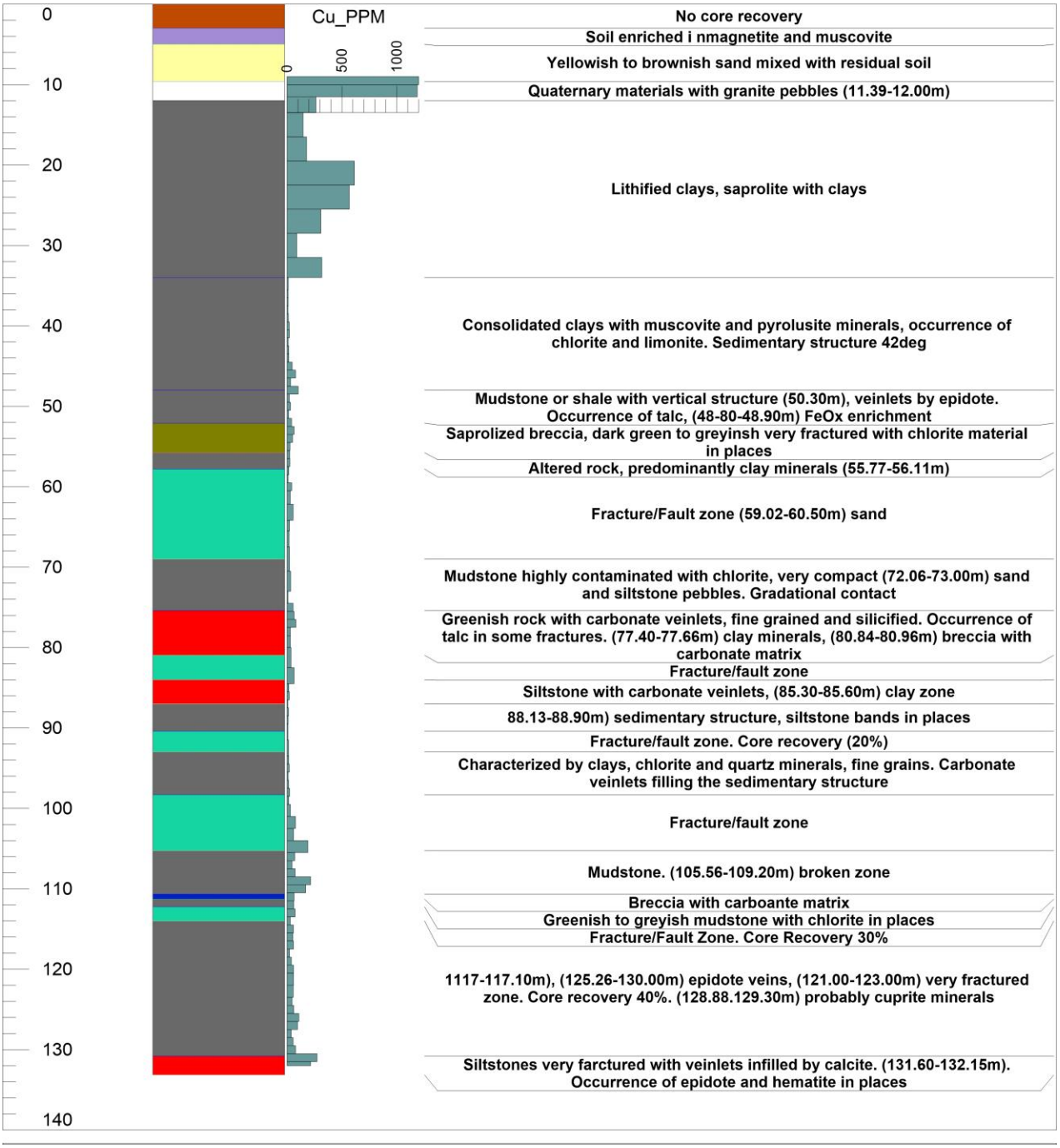


Legend Title
- Argillite
- Breccia
- Granite
- Mudstone
- Mylonite
- Quartzite
- Sandstone
- Siltstone
- Colluvium
- Fault
- Quartz Vein
- Quartz Veins
- Quartz veins
- TSOIL
- Laterite
- Saprolite
- Sand

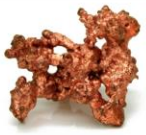

Cassenha Hill Cu Prospect

Huambo - Angola

| | |
|---|---|
| Northing: | 8550492 |
| Easting: | 506927 |
| Elevation: | 1592 |
| Azimuth: | 45° |
| Total Depth: | 90 m. |

# CHD013

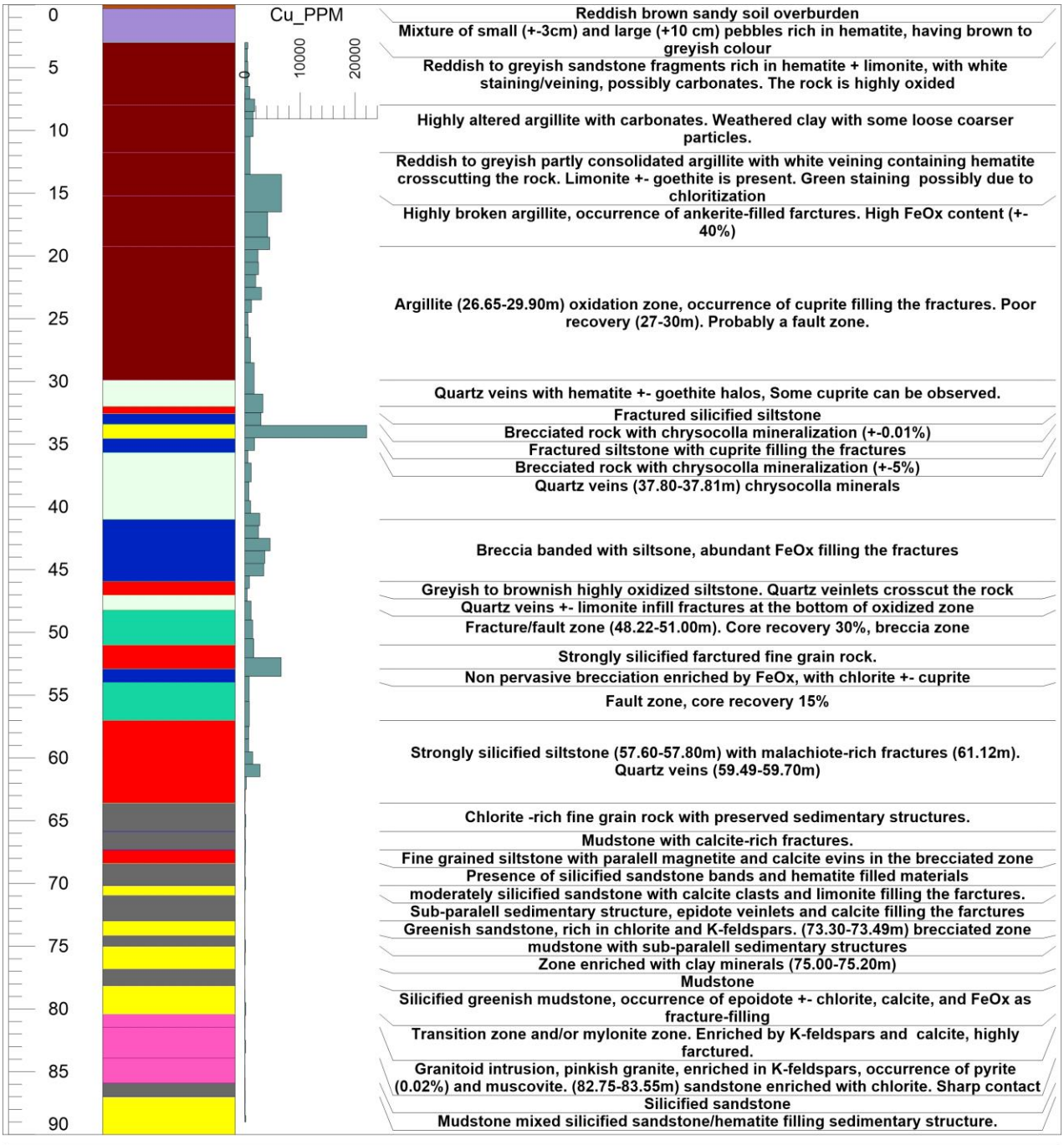


Legend Title

- Argillite
- Breccia
- Granite
- Mudstone
- Mylonite
- Quartzite
- Sandstone
- Siltstone
- Colluvium
- Fault
- Quartz Vein
- Quartz Veins
- Quartz veins
- TSOIL
- Laterite
- Saprolite
- Sand